NAVAL POSTGRADUATE SCHOOL

MONTEREY, CALIFORNIA

THESIS

INVESTIGATION OF PROPAGATION IN FOLIAGE USING SIMULATION TECHNIQUES

by

Chung Wei Chan

December 2011

Thesis Advisor:	David C. Jenn
Second Reader:	Ric Romero

Approved for public release; distribution is unlimited

THIS PAGE INTENTIONALLY LEFT BLANK

REPORT DOCUMENTATION PAGE			Form Approved OMB No. 0704-0188
Public reporting burden for this collection of information is estimated to average 1 hour per response, including the time for reviewing instruction, searching existing data sources, gathering and maintaining the data needed, and completing and reviewing the collection of information. Send comments regarding this burden estimate or any other aspect of this collection of information, including suggestions for reducing this burden, to Washington headquarters Services, Directorate for Information Operations and Reports, 1215 Jefferson Davis Highway, Suite 1204, Arlington, VA 22202-4302, and to the Office of Management and Budget, Paperwork Reduction Project (0704-0188) Washington DC 20503.			
1. AGENCY USE ONLY *(Leave blank)*	**2. REPORT DATE** December 2011	**3. REPORT TYPE AND DATES COVERED** Master's Thesis	
4. TITLE AND SUBTITLE Investigation of Propagation in Foliage using Simulation Techniques		**5. FUNDING NUMBERS**	
6. AUTHOR(S) Chung Wei Chan			
7. PERFORMING ORGANIZATION NAME(S) AND ADDRESS(ES) Naval Postgraduate School Monterey, CA 93943-5000		**8. PERFORMING ORGANIZATION REPORT NUMBER**	
9. SPONSORING /MONITORING AGENCY NAME(S) AND ADDRESS(ES) N/A		**10. SPONSORING/MONITORING AGENCY REPORT NUMBER**	
11. SUPPLEMENTARY NOTES The views expressed in this thesis are those of the author and do not reflect the official policy or position of the Department of Defense or the U.S. Government. IRB Protocol number _____N/A_____.			
12a. DISTRIBUTION / AVAILABILITY STATEMENT Approved for public release; distribution is unlimited		**12b. DISTRIBUTION CODE** A	

13. ABSTRACT (maximum 200 words)

In a foliage environment, radio wave propagation is subjected to fading on both large-scales and small-scales that impair the quality and reliability of data link transmission. This has implications in many military applications. An example is the performance of communications links and unmanned aerial vehicle radio links when the ground forces are operating in foliage environments.

The purpose of this research is to evaluate some simple models for propagation of radio waves in foliage using an electromagnetic field simulation application.

The three dimensional (3D) electromagnetic field simulation application, CST Studio Suite, was used in the modeling and simulation process. Specifically, the CST Microwave Studio module was used to model the forest using dielectric blocks. Various combinations of forest dimensions, material dielectric parameters and antenna placements were simulated to obtain propagation models of radio waves in foliage environment.

The simulation models are compared to three empirical models presented in the literature for propagation in foliage environment. Using the simulation model, we examined the coverage diagram for a transmitter antenna immersed in foliage. The results show that the proposed simulation models provide a rough approximation to radiowave propagation in an actual rainforest environment. Based on the simulated results, the path loss in foliage is affected by the forest's electrical characteristics, the height of the transmitter and the height of receiver.

14. SUBJECT TERMS Radio wave propagation, Foliage, Forest, EM wave simulation			**15. NUMBER OF PAGES** 115
			16. PRICE CODE
17. SECURITY CLASSIFICATION OF REPORT Unclassified	**18. SECURITY CLASSIFICATION OF THIS PAGE** Unclassified	**19. SECURITY CLASSIFICATION OF ABSTRACT** Unclassified	**20. LIMITATION OF ABSTRACT** UU

NSN 7540-01-280-5500

Standard Form 298 (Rev. 2-89)
Prescribed by ANSI Std. 239-18

THIS PAGE INTENTIONALLY LEFT BLANK

Approved for public release; distribution is unlimited

INVESTIGATION OF PROPAGATION IN FOLIAGE USING SIMULATION TECHNIQUES

Chung Wei Chan
Lieutenant Commander, Republic of Singapore Navy
B.Eng(EE), National University of Singapore, 1998

Submitted in partial fulfillment of the
requirements for the degree of

MASTER OF SCIENCE IN ELECTRICAL ENGINEERING

from the

NAVAL POSTGRADUATE SCHOOL
December 2011

Author: Chung Wei Chan

Approved by: David C. Jenn
Thesis Advisor

Ric Romero
Second Reader

R. Clark Robertson
Chair, Department of Electrical and Computer Engineering

THIS PAGE INTENTIONALLY LEFT BLANK

ABSTRACT

In a foliage environment, radio wave propagation is subjected to fading on both large-scales and small-scales that impair the quality and reliability of data link transmission. This has implications in many military applications. An example is the performance of communications links and unmanned aerial vehicle radio links when the ground forces are operating in foliage environments.

The purpose of this research is to evaluate some simple models for propagation of radio waves in foliage using an electromagnetic field simulation application.

The three dimensional (3D) electromagnetic field simulation application, CST Studio Suite, was used in the modeling and simulation process. Specifically, the CST Microwave Studio module was used to model the forest using dielectric blocks. Various combinations of forest dimensions, material dielectric parameters and antenna placements were simulated to obtain propagation models of radio waves in foliage environment.

The simulation models are compared to three empirical models presented in the literature for propagation in foliage environment. Using the simulation model, we examined the coverage diagram for a transmitter antenna immersed in foliage. The results show that the proposed simulation models provide a rough approximation to radiowave propagation in an actual rainforest environment. Based on the simulated results, the path loss in foliage is affected by the forest's electrical characteristics, the height of the transmitter and the height of receiver.

THIS PAGE INTENTIONALLY LEFT BLANK

TABLE OF CONTENTS

LIST OF FIGURES

LIST OF TABLES

THIS PAGE INTENTIONALLY LEFT BLANK

LIST OF ACRONYMS AND ABBREVIATIONS

3D	Three Dimensional
CAD	Computer Aided Design
CST	Computer Simulation Technology
E-field	Electric Field
EM	Electromagnetic
GO	Geometric-Optical
GUI	Graphics User Interface
HF	High Frequency
LITU-R	Lateral ITU-R
MWS	Microwave Studio
PC	Personal Computer
PEC	Perfect Electrically Conducting
PGF	Path Gain Factor
UAV	Unmanned Aerial Vehicle
UHF	Ultra High Frequency
VHF	Very High Frequency

THIS PAGE INTENTIONALLY LEFT BLANK

EXECUTIVE SUMMARY

The objective of this thesis is to investigate various simulation models for radiowave propagation in foliage environments. There are relatively few attempts to conduct simulation studies on radiowave propagation in foliage. The possibility of reliable simulation techniques bridges the gap between theoretical and field studies for propagation studies in a foliage environment. As an alternative to conducting field measurements, simulation provides a means to validate performance of communications and radar systems during their design phase.

It has been postulated in [1] that the forest can be represented by dielectric blocks for a frequency up to 100 MHz. These dielectric forest blocks are characterized by the quantities of relative permittivity ε_r and conductivity σ. Based on [2], the value of the relative permittivity ε_r ranges between 1.01 and 1.065. The value of σ ranges between 10^{-4} S/m to 10^{-3} S/m. This established a basis for studying propagation through forest via understanding the wave mechanism in the actual propagation process. Hence, the simulation models are constructed based on a single dielectric slab to represent the forest. A vertical dipole antenna is used to as a transmitter in the simulations.

Three theoretical propagation mechanisms in the transmitting–receiving path in a forest environment are described in [1]. The three mechanisms are the forest geometric optical (GO) components (consisting of direct and reflected rays), the sky wave and the lateral wave. For distances larger than 0.5 km, the GO components are largely attenuated. For short distances (i.e. much less than 100 km), the sky wave component is neglected. Hence, lateral waves are the predominant propagation mechanism in a forest environment over relatively short distances. The GO components and lateral wave are depicted in Figure 1.

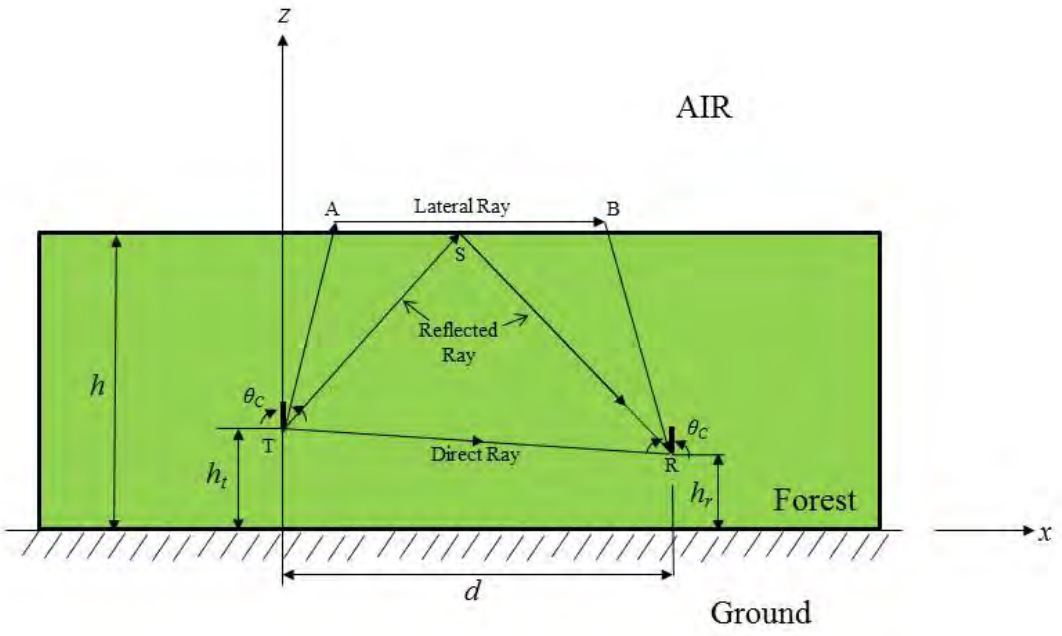

Figure 1. Propagation mechanisms in a forest (From [1]).

In this thesis, the simulation results are compared against three empirical models to determine the accuracy of the simulation models. The models are Tewari's model [3], the Jansky and Bailey model [4] and the LITU-R model [5]. The models were developed using experimental data obtained from actual measurements carried out in forests. The models are applicable for the high frequency (HF) and very high frequency (VHF) bands and vertically (v) polarized radiowave transmission. The effect of the forest on the coverage diagrams of a transmitter antenna immersed in foliage is also examined. Compared to free space, the electric field (E-field) for propagation through foliage has additional components of foliage attenuation and phase delay in foliage. Due to the constructive and destructive interference of the ground reflected wave with the direct wave, the typical maxima and nulls of the fields in a coverage diagram are still present when transmitting in a foliage environment. The reflections from the air–foliage interface can be neglected.

CST Studio Suite™, which is an electromagnetic (EM) simulation application, is used in this thesis. Specifically, the CST Microwave Studio (MWS) module is used to simulate the radiowave propagation in the dielectric forest block. The dielectric forest block and dipole antenna are constructed in CST. Several parameters, such as ε_r, σ and

the height of the transmitter antenna h_t, are varied in the simulation to examine their effects on the path loss in foliage.

From the various simulations, it is observed that the simulated results for sparse foliage (i.e., $\varepsilon_r = 1.01$ and $\sigma = 10^{-5}$ S/m) do not closely follow the three empirical models. Generally, for denser foliage (i.e., $\varepsilon_r \geq 1.05$ and $\sigma \geq 10^{-5}$ S/m), both Tewari's model and the Jansky and Bailey model are better approximations to the simulation results than the LITU-R empirical model for receiver situated at greater heights. Generally, the LITU-R model gives a better approximation to the simulation results for both transmitter and receiver situated near the ground. While the simulated results do not exactly match those given by the three empirical models, the difference between the simulated result and empirical result is approximately 10 dB in most cases. Given the lack of knowledge of the electrical properties (ε_r and σ) of the actual foliage, assumed values of the electrical properties are used in the simulations. Hence, it is expected that there will be differences between the simulated and empirical results. Nevertheless, given the observed difference, the simulation models can only be considered as a rough approximation to actual foliage propagation.

The effects of the forest on the coverage diagram of a transmitting antenna immersed in foliage are also examined using simulation. The coverage diagram for a transmitting antenna can be obtained from the electric field plots of a CST simulation. The height of the transmitter in foliage and the forest's electrical properties are varied in the simulation in order to examine their effect on the coverage diagram. From the simulation, it is observed that an increase in the height of the transmitter inside foliage results in more maxima (or lobes). In addition, the angular difference between the maxima and nulls becomes smaller as the antenna height is increased until near the canopy of the foliage. As the transmitter is sited higher up in the foliage, the path length of the reflected wave in foliage becomes longer and results in a lower E-field strength. For a transmitter sited inside a denser forest with higher ε_r and σ values, the lobes are shortened as compared to ones sited in a less dense forest. This is due to the increased attenuation in denser foliage, which is a result of higher ε_r and σ values.

During the conduct of the various simulation runs, we made several observations on the limitations of CST with respect to foliage simulation. The simulations are run on a personal computer equipped with Intel Xeon Quad-Core 2.53 GHz processor and 4 GB RAM memory. One main limitation on the simulation with respect to total simulation time is the maximum frequency used. An increase in the maximum frequency results in an exponential increase in number of mesh cells generated by CST. This leads to a significant increase in simulation time. In order for a simulation run to be completed within 12 hours, the frequency used should not exceed 75 MHz for a dielectric block of size 200 m by 100 m by 25 m.

It has been shown that it is feasible to model foliage using EM simulation applications. Using the simulation technique proposed in this thesis, a radio frequency (RF) engineer can model an RF system (especially the antenna) that is being developed for operations in foliage using CST. The performance of the system can then be examined during the design phase. This allows the designer to change the design before the actual system is built and is available for actual field tests.

LIST OF REFERENCES FOR EXECUTIVE SUMMARY

[1] Theodor Tamir, "On radio-wave propagation in forest environments," *IEEE Transactions on Antennas and Propagation*, vol. AP-15, No. 6, pp. 806–817, Nov. 1967.

[2] R.K.Tewari, S. Swarup and M. N. Roy, "Evaluation of relative permittivity and conductivity of forest slab from experimentally measured data on lateral wave attenuation constant," *International Journal of Electronics*, vol. 61, pp. 597–605, Nov. 1996.

[3] R.K.Tewari, S. Swarup and Manujendra N. Roy, "Radio wave propagation through rain forests of India," *IEEE Transactions on Antennas and Propagation*, vol. 38, pp. 433–449, April l990.

[4] Mark A. Weissberger, "An initial critical summary of models for predicting the attenuation of radio waves by trees," Electromagnetic Compatibility Analysis Center, Annapolis, Maryland, Rep. ESD-TR-81-101, July 1982.

[5] Yu Song Meng, Yee Hui Lee and Boon Chong Ng, "Empirical near ground path loss modeling in a forest at VHF and UHF bands," *IEEE Transactions on Antennas and Propagation*, vol. 57, no. 5, pp. 1461–1468, May 2009.

THIS PAGE INTENTIONALLY LEFT BLANK

ACKNOWLEDGMENTS

I would like to gratefully thank Professor David Jenn for his patience, support, and generosity with his time and instructions.

I would also like to thank Professor Ric Romero for his valuable time and support as the second reader.

Finally, thank you to my wonderful and beautiful wife for her patience and continuous support.

THIS PAGE INTENTIONALLY LEFT BLANK

I. INTRODUCTION

A. MILITARY OPERATIONS IN THE TROPICS

Tropical rainforests dominate large land masses in the equatorial region. An example is Southeast Asia. Thus, military forces of countries in these regions are trained to operate in such forest environments. In the modern battlefield, network centric operations, as well as the utility of unmanned vehicles are key enablers for mission success. Hence, the ability to find reliable communications channels for radio networks and unmanned aerial vehicle (UAV) datalinks underpins the successful execution of a mission.

When operating in tropical rainforest, the foliage provides a natural camouflage for ground forces. In order not to break cover and potentially expose one's own location to the opposing force, the military hardware, including antennas, are kept hidden under foliage cover. Military forces thus have to transmit their communications signals from under the foliage cover. At the other end of the channel, the receiving party could be an UAV operating in the airspace above a forest or a friendly unit operating either outside or within the forest. A typical scenario of military units operating in a forest environment is shown in Figure 1. The implication of such an operational scenario is that the transmission path taken will be through the forest medium. Likewise, any signal received by forces operating under foliage has to travel through the same environment. The ability to understand propagation mechanisms in forest conditions will lead to the design of better systems for operations in a forest environment.

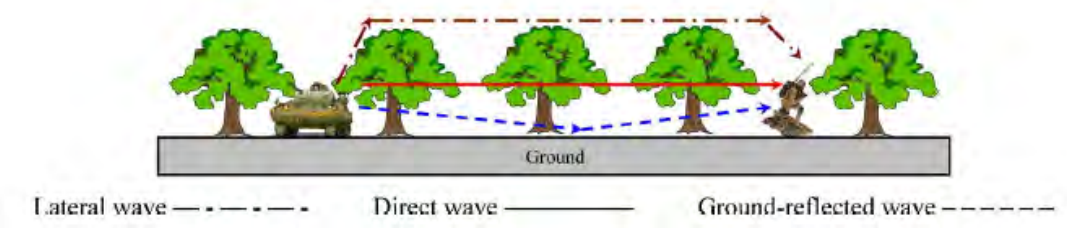

Figure 1. An example of battlefield communications application in forest environment (From [1]).

1. Physical Characteristics of Tropical Rainforest

The physical structure of a typical tropical rainforest is described in this section. A rainforest is divided into five different layers [2]. A graphical depiction of the rainforest profile is shown in Figure 2. The emergent layer contains a small number of very large trees which grow above the canopy layer, reaching heights of 45–55 m. The canopy is the primary layer of the forest and consists of the leafy top of tall trees, which forms a roof over the remaining layers. Shorter trees and tall shrubs form the understory layer. The plants in this area seldom grow to 3 m. The shrub layer and forest floor are very dark. Few plants grow in this area as a result. Hence, vegetation under the canopy layer is relatively sparse.

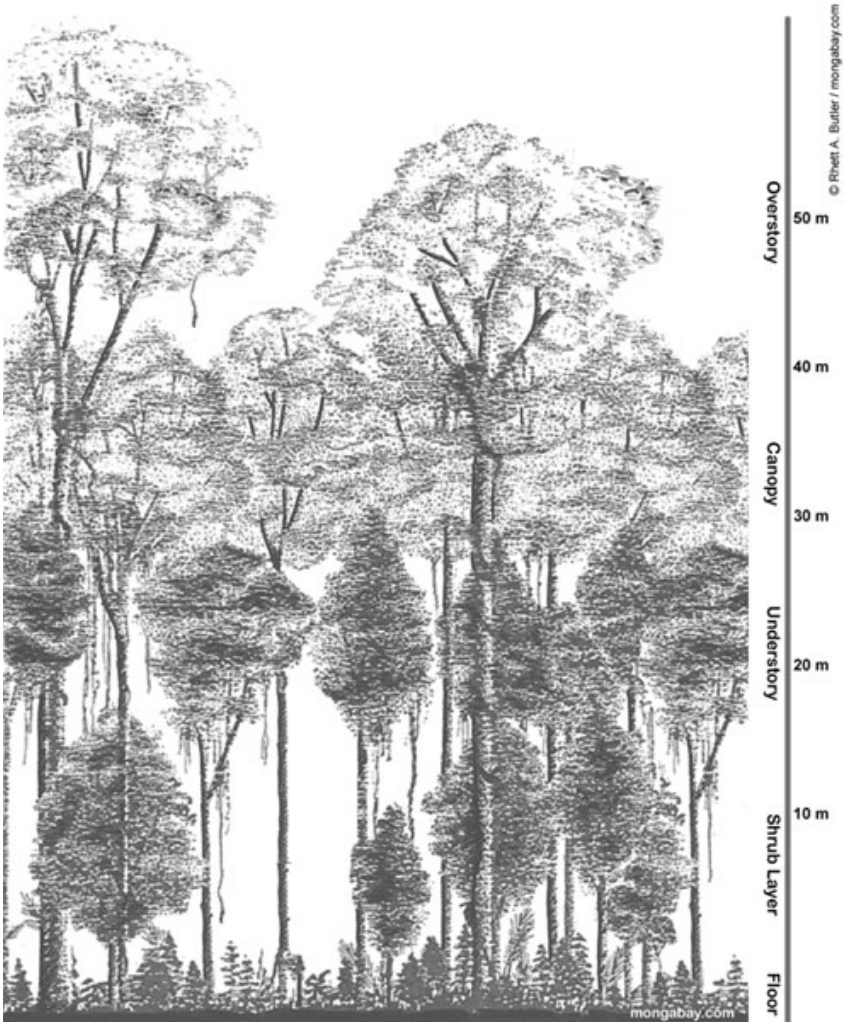

Figure 2. Profile of a tropical rainforest (From [3]).

As its name implies, the rainforest experiences rainfall throughout the year. In equatorial regions, rainfall may be year round without apparent "wet" or "dry" seasons; although, many forests do have seasonal rains. Even in seasonal forests, the period between rains is usually not long enough for the leaf litter to dry out completely. Forests farther from the equator, like those of Thailand, Sri Lanka, and Central America, where rainy seasons are more pronounced, can only be considered "semi-evergreen" since some species of trees may shed all of their leaves at the beginning of the dry season [3]. The seasonal change in the physical make-up of the forest impacts the electrical properties of a forest and, consequently, how electromagnetic (EM) waves propagate.

2. Electrical Properties of a Forest

Electrical properties of a medium are specified by its constitutive parameters, i.e., permeability, permittivity and conductivity [4]. Permeability μ and permittivity ε are expressed by the following complex quantities

$$\mu = \mu_o \mu_{r_C} \tag{1}$$

$$\varepsilon = \varepsilon_o \varepsilon_{r_C} \tag{2}$$

where $\mu_o = 4\pi \times 10^{-7}$ H/m and $\varepsilon_o = 8.85 \times 10^{-12}$ F/m.

The constant μ_{r_C} is called the relative permeability and has a value of one for lossless, non-magnetic materials. The constant ε_{r_C} is called the relative dielectric constant or relative permittivity [5]. The imaginary terms in (1) and (2) give rise to propagation losses due to attenuation and absorption. (The time convention used here is $e^{+j\omega t}$.)

Tamir proposed in [6] that the forest could be represented by dielectric blocks. This established a basis for studying propagation through forest via understanding the wave mechanism in the actual propagation process. This was in contrast to propagation studies that are based on empirically or statistically derived models. However, one main challenge in using dielectric models is the need for prior knowledge of the forest's electrical properties.

The forest's electrical properties are related to characteristics of the forest's physical structure, such as density of canopy, vegetation type and size of trees. Given the diverse composition of tropical rainforest, the electrical properties differ for each rainforest. In some cases, the electrical properties for a given forest changes according to seasonal variations that affect the canopy's leaf density. Hence, radiowave propagation in a forest medium can be explained via a simple propagation mechanism that is dependent on the electrical properties of the forest.

B. OBJECTIVES OF THESIS

Current and past research on radiowave propagation in foliage environments is largely centered on either theoretical or field studies. While there are numerous simulation studies on propagation in other environments such as urban terrain, there are relatively few attempts to conduct simulation studies on radiowave propagation in foliage. This can be attributed to the lack of information on the electrical properties of actual forests, which makes it difficult to build an accurate model to replicate actual field results in a simulation.

The objective of this thesis is to investigate various simulation models for radiowave propagation in foliage environments. The simulation results are compared with empirical results to determine the accuracy of the simulation models. The possibility of reliable simulation techniques bridges the gap between theoretical and field studies for propagation studies in a foliage environment. As an alternative to conducting field measurements, simulation provides a means to validate theoretical models of propagation and aid in the design of communications and radar systems.

C. THESIS OUTLINE

There are five chapters in this thesis. In Chapter I, the background, objectives and scope of the thesis are presented. The theoretical models of propagation in foliage and the various factors affecting performance of radiowave propagation in foliage environment are discussed in Chapter II.

In Chapter III, various EM field simulation applications which can be used to model and simulate radiowave propagation in foliage environment are presented. The construction of the model is also presented here. In Chapter IV, the simulation parameters and simulation results are presented. In Chapter V, a conclusion to the work performed in this thesis and recommendations for future work are presented.

THIS PAGE INTENTIONALLY LEFT BLANK

II. RADIOWAVE PROPAGATION IN FOLIAGE

There are three possible scenarios involving a transmitter-receiver pair in a forest operating environment. In the first scenario, both the transmitter and receiver are sited within the forest. In the second scenario, the transmitter is sited within the forest, and the receiver is sited outside the forest. The third scenario is similar to the second scenario, except that the locations for the transmitter and receiver are switched. For scenarios two and three, the propagation process can be broken into two parts. One part involves propagation in the absence of vegetation, while the other part involves propagation inside a forest environment.

In this chapter, the propagation mechanism of radiowaves in a forest environment as well as several empirical propagation models for foliage are presented and discussed.

A. RADIOWAVE PROGATION MECHANISM IN FOLIAGE

1. Representing the Forest as a Slab

In order to understand the EM wave mechanism in an actual propagation process, it has been proposed that the forest could be viewed as a dissipative dielectric slab [6]. The basic slab structure is shown in Figure 3. The dissipative dielectric slab is assumed to represent a forest with an average tree height of h. The transmitter is located at a height z_o above ground. The forest is characterized by the complex dielectric constant given by [6]

$$\varepsilon_{r_C} = \varepsilon_r - j\frac{\sigma}{\omega\varepsilon_o} = \varepsilon_r - j60\sigma\lambda_o \tag{3}$$

where ε_r denotes the average relative permittivity, σ denotes the averages conductivity of the forest and λ_o is the wavelength of a wave with frequency f. The wavelength λ_o must be sufficiently large for the representation of the forest as a uniform, continuous medium to be valid [6]. Based on a reasonably assumed average separation between trees of 1–5 m and that the intervening space is usually filled with foliage and other vegetation, an

upper frequency of f equals to 100 MHz (or a minimum wavelength λ_0 of 3 m) seems reasonable [6].

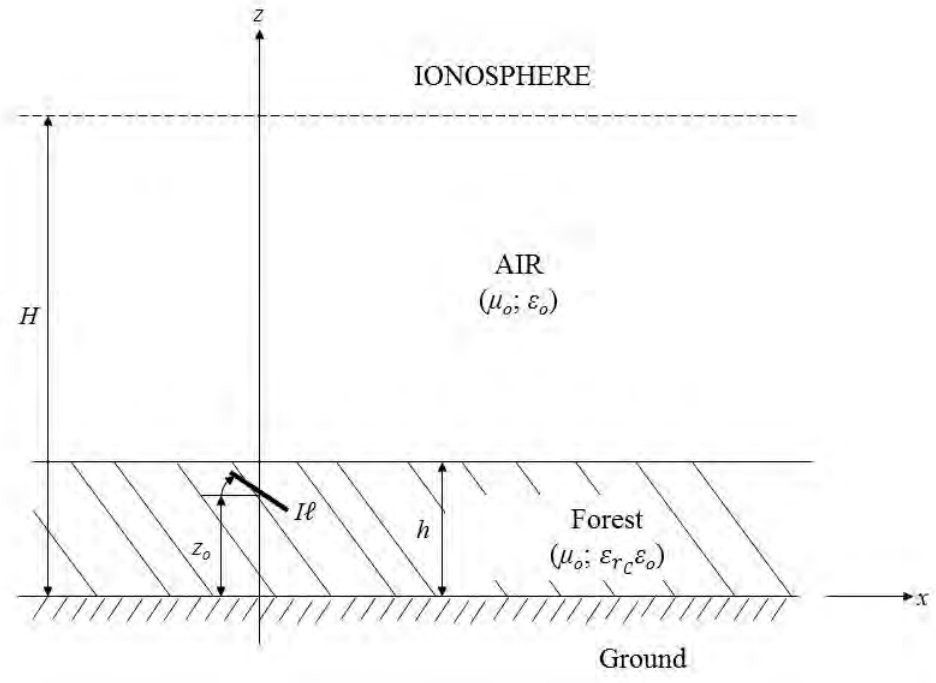

Figure 3. Basic geometry of a forest dissipative dielectric slab (From [6]).

The forests' electrical parameters ε_r and σ are critical in describing the EM propagation [7]. Unfortunately, there is very little data for these two parameters. Based on [8], the value of ε_r, which was derived from field measurements, ranges between 1.01 and 1.065. The value for σ ranges from 0.01 to 0.160 mmho/m (equivalent to 10^{-5} S/m to 1.6 x 10^{-4} S/m). It was also observed in [8] that a larger ε_r corresponds to a larger σ. In [6], the range of ε_r considered is from 1.01 to 1.5, and the range of σ considered is from 10^{-5} S/m to 10^{-3} S/m. A dense forest exhibits larger values for ε_r and σ, while a thin forest exhibits smaller values. Hence, it is expected that the lower limits (i.e., ε_r = 1.01 and $\sigma = 10^{-5}$ S/m) and the upper limits (i.e., ε_r = 1.5 and $\sigma = 10^{-3}$ S/m) occur together.

From [4], for a $\hat{z}$ polarized plane wave propagating in the *x*-direction,

$$\vec{E}(x) = \hat{z}E_o e^{-\gamma x} \tag{4}$$

where E_o is a complex constant, and γ is the propagation constant and can be expressed as

$$\gamma = \alpha + j\beta \tag{5}$$

where α is the attenuation constant (Np/m) and β is the phase constant (rad/m):

$$\alpha = \omega \left\{ \frac{\mu\varepsilon}{2} \left[\sqrt{1 + \left(\frac{\sigma}{\omega\varepsilon} \right)^2} - 1 \right] \right\}^{\frac{1}{2}} \tag{6}$$

$$\beta = \omega \left\{ \frac{\mu\varepsilon}{2} \left[\sqrt{1 + \left(\frac{\sigma}{\omega\varepsilon} \right)^2} + 1 \right] \right\}^{\frac{1}{2}} . \tag{7}$$

The attenuation constant α affects the rate of decay of the wave travelling in the dielectric media.

Three theoretical propagation mechanisms in the transmitting–receiving path in a forest environment are described in [6]. The three components are the forest geometric optical (GO) components (direct and reflected rays), the sky wave (or ionospheric wave) component and the lateral wave component. For distances larger than 0.5 km from the antenna, the forest GO components are largely attenuated. The sky wave component is only significant for distances larger than the one-hop distance. In [6], a practical distance of over 100 km is required for the sky wave to be significant. Hence, lateral waves are the predominant propagation mechanism in a forest environment over relatively short distances. The discussion in the following section focuses on the GO and lateral wave components, which are depicted in Figure 4.

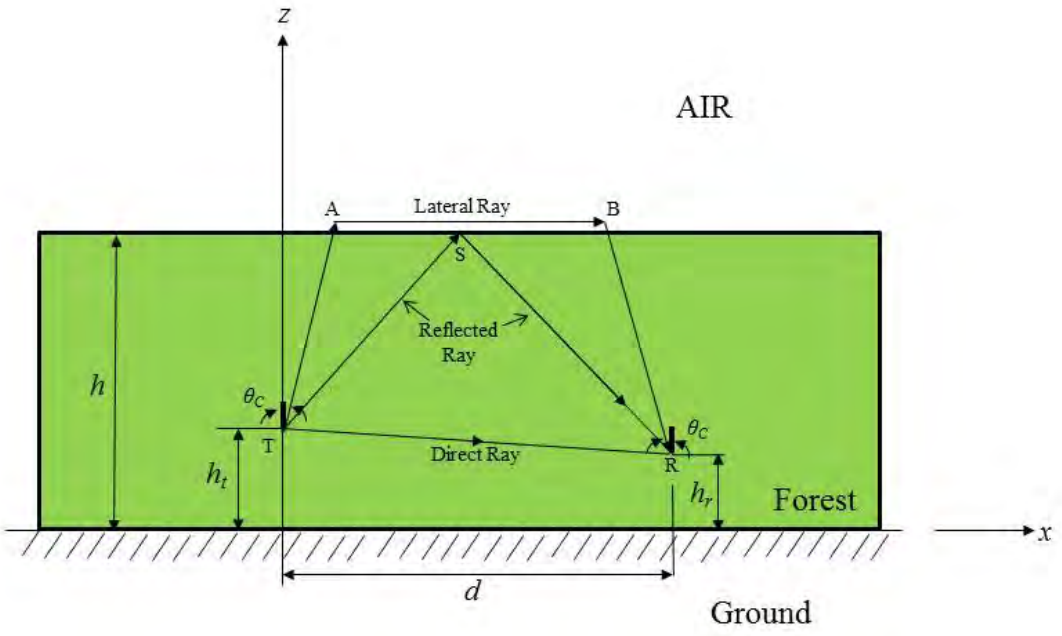

Figure 4. Propagation mechanisms in a forest (From [6]).

2. Forest GO Contribution

From [6], in the absence of the ionosphere, the first scenario reduces to that of a single half-space problem (Figure 4). The basic waves, which appear as a direct ray and a reflected ray, shown by the trajectories TR and TSR, respectively, constitute the GO contribution for this scenario. The electric field (E-field) E_F corresponding to these waves may be cast in the form [6]

$$E_F = 30I\ell\left(f_d \frac{e^{-jk_o\sqrt{\varepsilon_{rC}}r_d}}{r_d} + f_r \frac{e^{-jk_o\sqrt{\varepsilon_r}r_r}}{r_r} \right) \tag{8}$$

where I is the current in the transmitting antenna, ℓ is the length of the transmitting antenna, r_d is the distance travelled by the direct wave, r_d is the distance travelled by the reflected wave, and k_o is the wavenumber of air (vacuum) and can be expressed as

$$k_o = \omega\sqrt{\mu_o\varepsilon_o}\,. \tag{9}$$

From (8), it can be seen that E_F is inversely proportional to r_d and r_r, i.e., the field strength is dependent on r_d^{-1} and r_r^{-1}. The reflection from the ground is neglected.

3. Lateral Wave Contribution

If the forest is a lossless medium, the additional diffraction fields would be negligible compared to the GO contributions. However, given that the forest is a dissipative medium, the diffraction component has a significant contribution to the field [6].

The lateral wave is represented by the trajectory TABR in Figure 4. This wave corresponds to the radiation emitted at the critical angle of total reflection θ_c given by

$$\sin\theta_c = \frac{1}{\sqrt{\varepsilon_{r_C}}}. \tag{10}$$

The lateral wave appears when radiation occurs from a denser medium to a less dense one [6]. From (10), it can be seen that the angle θ_c is defined for ε_{r_C} real only. However, the physical interpretations are still valid if the losses are small (i.e., $\mathrm{Im}(\varepsilon_{r_C}) << |\varepsilon_{r_C}|$), and the real part of ε_{r_C} is implied in (10) [6].

When the ray of the lateral wave from the source hits the air-forest boundary (path TA in Figure 4), it is refracted into the air medium, where the ray travels tangentially along the boundary (path AB in Figure 4) while leaking energy back into the forest medium along the direction of θ_c [6]. Therefore, some of this leaked energy reaches the observation point in the forest (path BR in Figure 4). From [6], it is shown that the lateral wave has the form

$$E_z^{(L)} \propto E_L(\sqrt{\varepsilon_r - 1}\cos\phi\cos\gamma + \sin\gamma) \tag{11}$$

$$E_\rho^{(L)} \propto E_L[(\varepsilon_r - 1)\cos\phi\cos\gamma + \sqrt{\varepsilon_r - 1}\sin\gamma] \tag{12}$$

$$E_\phi^{(L)} \propto E_L \sin\phi\cos\gamma \tag{13}$$

where ϕ is the angle measured from the x–axis, γ is the angle of incline of the transmitting dipole antenna with respect to the x–axis and E_L is given by

$$E_L = \frac{60I\ell}{\varepsilon_r - 1} \cdot \frac{e^{-jk_o(r_L + \sqrt{\sqrt{\varepsilon_r} - 1}s)}}{r_L^2} \tag{14}$$

where r_L is the distance travelled by the lateral wave and s is the total separation of the source and observation points from the forest–air interface given by

$$s = 2h - h_t - h_r \cdot \tag{15}$$

From (14), it can be seen that the electric field strength of the lateral wave is dependent r_L^{-2} as compared to r^{-1} for the GO waves. This is due to the continuous leakage of energy back into the forest medium by the lateral wave across its path AB [6].

Both the GO and lateral wave contributions to the field observed in a forest environment have been explained. Other diffraction components are ignored since they are of lower order [6].

B. EMPIRICAL PROPAGATION MODELS IN FOLIAGE ENVIRONMENT

Some empirical propagation models for foliage environment are explained in this section. These models were developed using experimental data obtained from actual measurements carried out in forests. While there are many empirical foliage propagation models that have been proposed in the past thirty years, the models being discussed here apply to the high frequency (HF) and very high frequency (VHF) bands and vertically (v) polarized radiowave transmission.

1. Tewari's Basic Transmission Loss Model (Tewari)

In [9], an empirical propagation model based on experimental data obtained in the rainforests of India yields a predicted basic transmission loss L_b expressed as

$$L_b = -27.57 + 20\log f - 20\log\left(\frac{Ae^{-\alpha d}}{d} + \frac{B}{d^2}\right) \tag{16}$$

where f is the frequency (MHz), d is the separation distance (m), α is the rate of attenuation constant (dB/m), and A and B are constants evaluated from the measured data.

For vertically polarized transmission, the values of α, A and B were determined using the experimentally observed data given in Table 1.

Table 1. Values of α, A and B (From [9]).

Frequency (MHz)	α (dB/m)	A	B
50	-	0	1.9170
200	0.0125	0.4989	1.8358
500	0.0135	0.3658	0.9040
800	0.0140	0.2661	0.5331

A plot of the basic transmission loss L_b versus separation distance d curve for vertically polarized transmission is generated using MATLAB and is shown in Figure 5. The MATLAB code is given in the Appendix.

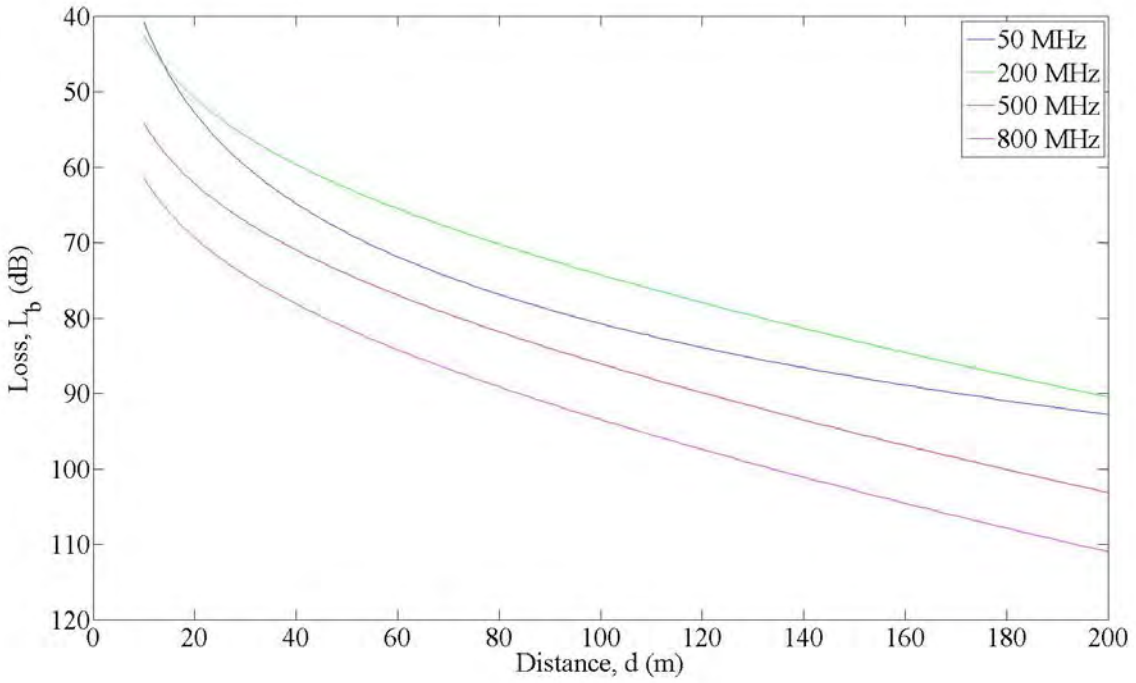

Figure 5. Plot of basic transmission loss versus separation distance for vertically polarized transmission.

From Figure 5, it can be observed that, for a given separation distance, path loss increases with higher frequency in a forest environment. This is expected, since at higher frequencies, the wavelength is comparable to the dimensions of the forest's constituents such as leaves and branches.

2. Jansky and Bailey Model

From [10], the Jansky and Bailey empirical model was developed using measured data obtained in the tropical forest of Thailand. The model is valid for cases in which both transmitting and receiving antennas are immersed in foliage and are separated by distances between 8 to 1600 meters. The model could be used for both horizontal and vertical polarization. The frequency range is between 25 and 400 MHz. The loss L_b is given by

$$L_b = 36.57 + 20\log f - 20\log\left(\frac{Ae^{-1609\alpha d}}{d} + \frac{B}{d^2}\right) \tag{17}$$

where f is the frequency in MHz, d is the separation distance in statute miles, and A, B and α are empirical constants given in Table 2.

Table 2. Constants for the Jansky and Bailey empirical model (From [10]).

Frequency (MHz)	Polarization	α (dB/m)	A	B
25	V	0.0	0.0	0.00212
50	V	0.0	0.0	0.00106
100	V	0.045	0.615	0.000529
250	V	0.050	0.759	0.000443
400	V	0.055	1.02	0.000523

Comparing (17) with (16), we observe that both empirical formulas have the same form. However, their constants are different since the measured data on which the models are based are taken from forests in dissimilar locations.

A plot of the basic transmission loss L_b versus separation distance d curve for vertically polarized transmission was generated using MATLAB and is shown in Figure 6. The MATLAB code is given in the Appendix.

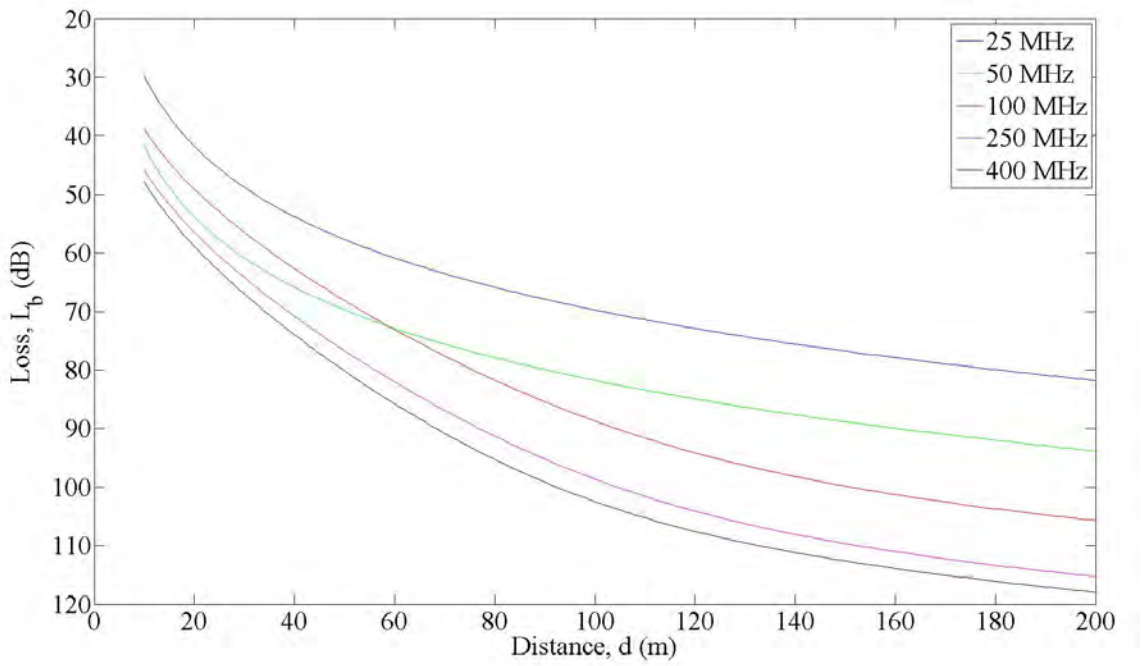

Figure 6. Plot of loss versus separation distance for Jansky and Bailey empirical model.

From Figure 6, it can be observed that, for a given separation distance, path loss increases with higher frequency in a forest environment. This is similar to that observed in Tewari's model.

3. Lateral ITU-R (LITU-R) Model

In [1], an empirical model that accounts for the excess foliage loss for lateral waves is proposed. The model was modified from ITU-R's model for VHF transmission in a small forest. The VHF frequency band is from 30 to 300 MHz. The modified LITU-R model is valid for VHF band transmission over a foliage depth of up to 5 km. The expression for the LITU-R model is

$$L_{LITU-R}(dB) \cong 0.48 f^{0.43} d^{0.13} \tag{18}$$

where f is the frequency in MHz and d is the separation distance in meters.

The path loss is obtained by including the effect of foliage loss $L_{LITU\text{-}R}$ in the plane earth path loss model [1]. Hence, the total pass loss in a foliage environment can be expressed as

$$L(dB) = 40\log_{10}(d) - 20\log_{10}(h_t) - 20\log_{10}(h_r) + L_{LITU-R} \tag{19}$$

where d is the separation distance in meters, h_t is the transmitting antenna height in meters and h_r is the receiving antenna height in meters. From (19), it can be seen that path loss is also affected by the antenna height. By increasing the transmitting or receiving antenna height, path loss is reduced.

A plot of the path loss versus separation distance based on the LITU-R model is generated using MATLAB and is shown in Figure 7. The MATLAB code is given in the Appendix. Both the transmitting and receiving antenna heights are at 5 m.

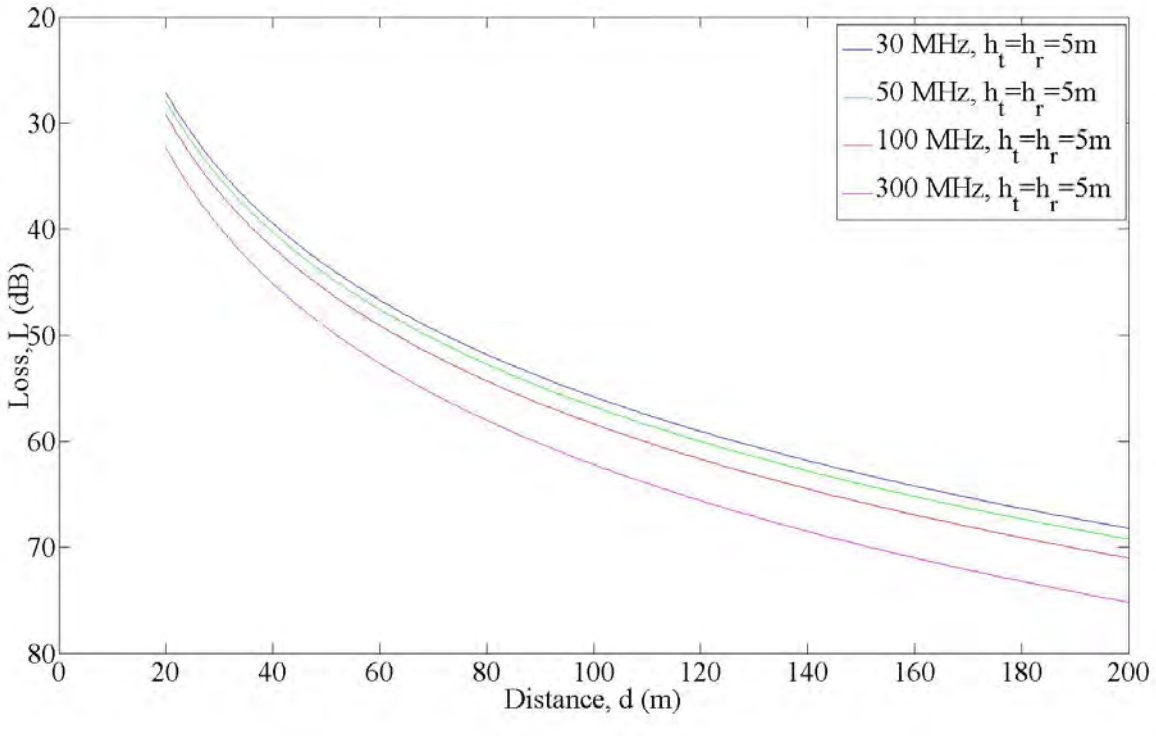

Figure 7. Plot of path loss versus separation distance based on LITU-R model.

From Figure 7, it can be observed that, for a given separation distance, path loss increases with higher frequency.

D. COVERAGE DIAGRAMS WITH TRANSMISSION THROUGH FOLIAGE

In a foliage environment, it is highly likely for both the transmitter and receiver to be operating near the surface of the earth. In such a situation, multipath or multiple reflections can cause fading of the signal [4]. A flat earth is assumed in this discussion. The geometry of the reflections from the ground in a foliage environment is shown in Figure 8. Reflections from the boundary between the foliage and air are neglected.

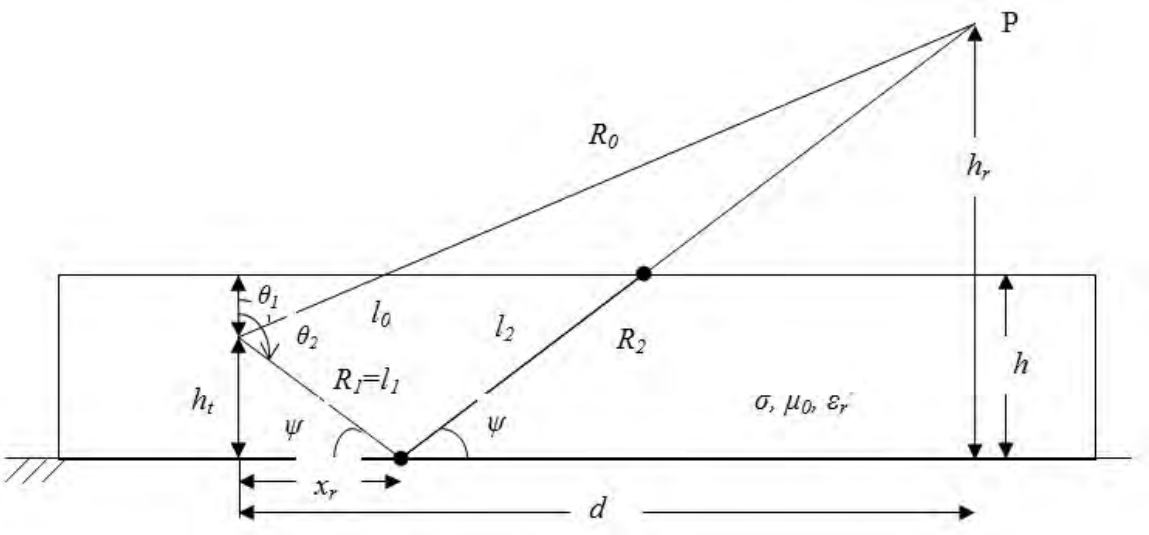

Figure 8. Mutipath effects from a flat earth in foliage.

In Figure 8, the transmitter antenna is low gain and assumed to be pointing at the horizon. The receiver is located in free space outside of the foliage. Hence, the transmitter's height h_t is less than the forest's height h, while the receiver's height h_r is greater than h. If the transmitter is very near to the ground, the angle ψ is both the grazing angle and the elevation angle. The path lengths of the rays in foliage are given by l_o, l_1 and l_2.

The foliage attenuation α and phase constant in foliage β are given by (6) and (7), respectively. The phase constant in free space can be expressed as

$$\beta_0 = \omega\sqrt{\mu_o\varepsilon_o} = \frac{\omega}{c} = \frac{2\pi}{\lambda_0}. \tag{20}$$

The reference field (or direct path in free space) can be expressed as

$$E_0 = \frac{\sqrt{G(\theta_1)}}{R_0} e^{-j\beta_0 R_0} \tag{21}$$

where $G(\theta_1)$ is the gain of the transmit antenna. Hence, the path gain factor (PGF) F is given by

$$F = \frac{E(P)}{E_0} \tag{22}$$

where $E(P)$, which is the field at point P, is expressed as (for the case of point P outside the foliage, i.e., $h_r \geq$ h)

$$E(P) = \frac{\sqrt{G(\theta_1)}}{R_0} e^{-\alpha l_0} e^{-j\beta_0 (R_0 - l_0)} e^{-j\beta l_0} + \Gamma \frac{\sqrt{G(\theta_2)}}{R_{12}} e^{-\alpha l_{12}} e^{-j\beta l_{12}} e^{-j\beta_0 (R_{12} - l_{12})} \tag{23}$$

where Γ is the reflection coefficient, $R_{12} = R_1 + R_2$ and $l_{12} = l_1 + l_2$. If the ground is assumed to be perfect electrically conducting (PEC), Γ has a value of -1. For the case where point P is inside the foliage (i.e., $h_r <$ h), $E(P)$ is expressed as

$$E(P) = \frac{\sqrt{G(\theta_1)}}{R_0} e^{-j\beta R_0} e^{-\alpha R_0} + \Gamma \frac{\sqrt{G(\theta_2)}}{R_{12}} e^{-j\beta R_{12}} e^{-\alpha R_{12}} \,. \tag{24}$$

A coverage diagram can be plotted with F shown as contours in relation to d and h_r. An example of a coverage diagram is shown in Figure 9. The diagram is plotted for a vertical $\lambda_o/2$ dipole located at height 20 m above ground in 25 m high foliage. The frequency is 50 MHz, $\varepsilon_r = 1.01$, $\sigma = 10^{-4}$ S/m and the reference distance is 1000 m.

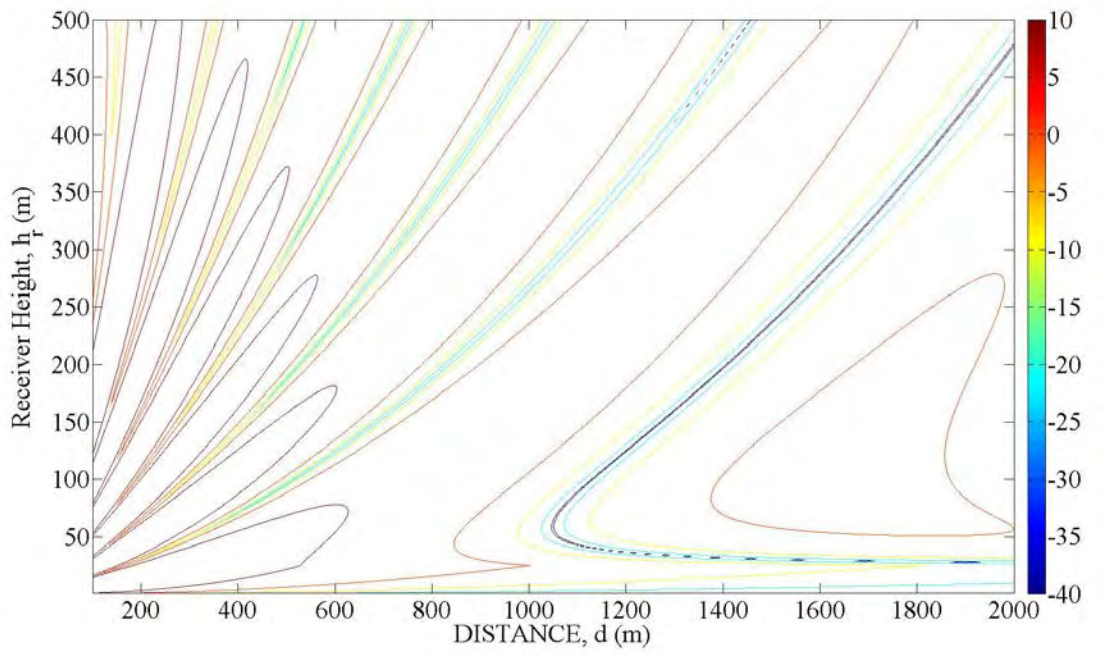

Figure 9. Example of a coverage diagram for a transmitter located inside foliage.

In Figure 9, the contours represent the PGF for 10 dB, 0 dB, −10 dB, −20 dB and −40 dB relative to free space at the reference distance. From the diagram, the maxima and nulls of the fields can be observed. This phenomenon is due to the constructive and destructive interference of the reflected wave with the direct wave.

C. SUMMARY

In this chapter, the mechanism of EM wave propagation through foliage was examined. Three empirical propagation models for foliage environment are also discussed in this chapter. The effect of a dielectric forest block on the coverage diagram of a transmitter in foliage was also examined. In the next chapter, the simulation results are analyzed with respect to the theory discussed in this chapter.

THIS PAGE INTENTIONALLY LEFT BLANK

III. EM FIELD SIMULATION APPLICATION

In this chapter, various EM field simulation applications which can be used to model and simulate radiowave propagation in foliage environment are presented. In addition, the method to construct the foliage model and set-up the simulation using CST Studio Suite™ is also presented.

A. REVIEW OF SIMULATION APPLICATION

There are many EM simulation applications in the market to aid in the study of electromagnetic related problems. The CST Studio Suite ™ was selected for this problem. The CST Studio Suite™ (CST) is developed by Computer Simulation Technology AG. The electromagnetic simulation software CST STUDIO SUITE™ comprises CST's tools for the design and optimization of devices operating over a wide range of frequencies. CST consists of several modules. The module that is useful for simulating radiowave propagation in foliage is CST Microwave Studio® (CST MWS). CST MWS is a specialist tool for fast and accurate three dimensional (3D) EM simulation of high frequency problems [10]. CST MWS enables the fast and accurate analysis of high frequency devices such as antennas, filters, couplers, planar and multi-layer structures [10].

For creation of the computer aided design (CAD) models, CST Studio Suite™ supports both options of drawing the model within CST or importing from an external file. There is a wide range of primitives available to create complex structures.

B. APPLICATION OF CST STUDIO TO SIMULATION OF RADIOWAVE PROPAGATION IN FOLIAGE

The CST MWS module is used to simulate radiowave propagation through foliage. The transient solver in CST is used for the simulation in this thesis. The transient solver is a general purpose 3D simulator. The solver can be used to study the fields propagating through a component. It can also deliver broadband frequency domain results such as scattering parameters (*S*-parameters) [10].

1. General CST MWS Studio® Set-up

a. General Simulation Settings

In order to optimize the simulation in CST, there are several settings to configure so that the results are sufficiently accurate for analysis. At the same time, these settings also ensure that the simulation does not consume too many computing resources.

The mesh is set to *Hexahedral* type. Under the mesh properties (Figure 10), the *Lines per wavelength* is set to 10, which provides a good compromise between calculation time and achievable accuracy. The *Mesh line ratio limit* is set to the default value of 10.

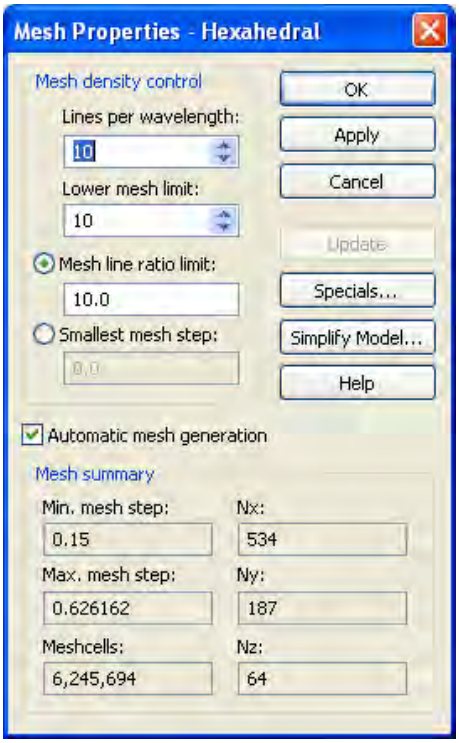

Figure 10. Mesh properties settings in CST.

The boundary conditions are configured using the selections shown Figure 11. The *Xmin*, *Xmax*, *Ymin*, *Ymax* and *Zmax* boundaries are configured as "*open (add space)*", which acts as free space and waves can pass through the boundary with minimal reflections. The *Zmin* boundary is configured as a ground plane using "*electric (Et = 0)*".

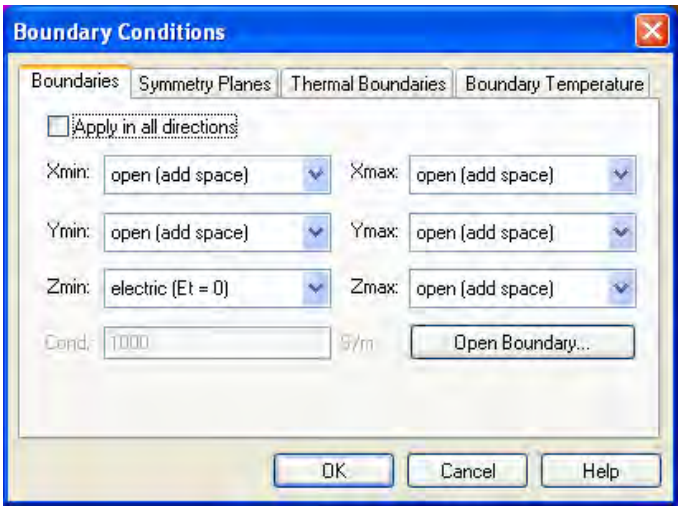

Figure 11. Properties of the boundary conditions.

For the units used in the simulation (Figure 12), dimensions are defined in meters and frequency is defined in MHz.

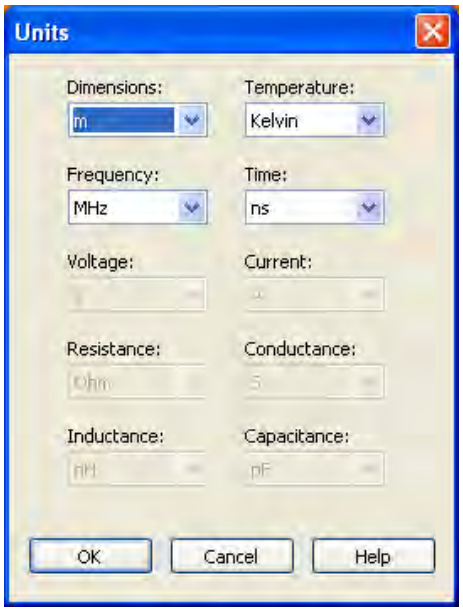

Figure 12. Configuration of units used in CST.

The range of frequencies (i.e., minimum frequency *Fmin* to maximum frequency *Fmax*) to be used in the simulation is defined using the *frequency Range Settings* shown in Figure 13.

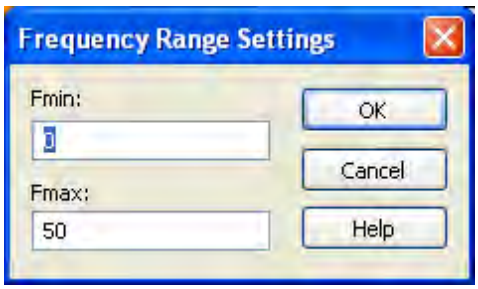

Figure 13. Frequency Range Setting window.

b. Definition of Variables

In CST, parameters can be defined for use in the simulation model. The parameters are defined in the parameter list table on the graphic user interface (GUI). The parameters shown in Table 3 are defined for the model used in CST to simulate radiowave propagation through foliage.

Table 3. List of parameters defined in CST.

	Parameter	Value	Description	Units
1	H	varies according to simulation run	Height of dielectric block	meters
2	L	varies according to simulation run	Length of dielectric block	meters
3	W	varies according to simulation run	Width of dielectric block	meters
4	c	3×10^8	Speed of light	meters/second
5	f	varies according to simulation run	Transmission frequency	MHz
6	lamda	$c/(f \cdot 10^6)$	Wavelength	meters
7	$\ell 2$	varies according to simulation run	Dipole length	meters
8	r	$0.0005 \cdot$lamda	Dipole radius	meters
9	xd	varies according to simulation run	X-coordinate of dipole	meters
10	yd	varies according to simulation run	Y-coordinate of dipole	meters
11	zd	varies according to simulation run	Z-coordinate of dipole and represents the transmitter height, h_t	meters
12	d	$0.025 \cdot$lamda	For mating discrete port to dipole	meters

2. Physical Construction

Based on [6], the forest can be modeled as a single homogeneous dielectric block to represent the entire vegetation for frequency up to 100 MHz. A half-wave ($\lambda_o/2$) dipole is used as the transmitting antenna.

a. One Layer Dielectric Block

A single homogenous dielectric block with length (L), width (W) and height (H) is constructed to represent the forest. The dielectric block is constructed using a *Brick* object in CST with the properties shown in Figure 14. The variables used to construct the dielectric block are obtained from the variable list in Table 3.

Figure 14. Properties of dielectric forest block.

The dielectric block is configured as a dielectric material, which has the properties shown in Figure 15 and 16. The material type is set as *Normal*. The value for *Epsilon* (relative permittivity ε_r) is set according to the test case in each simulation run. Since the forest is considered a non-magnetic structure, the value of *Mue* (relative

permeability μ_r) is set to a value of one. The electrical conductivity σ is set accordingly for each simulation run.

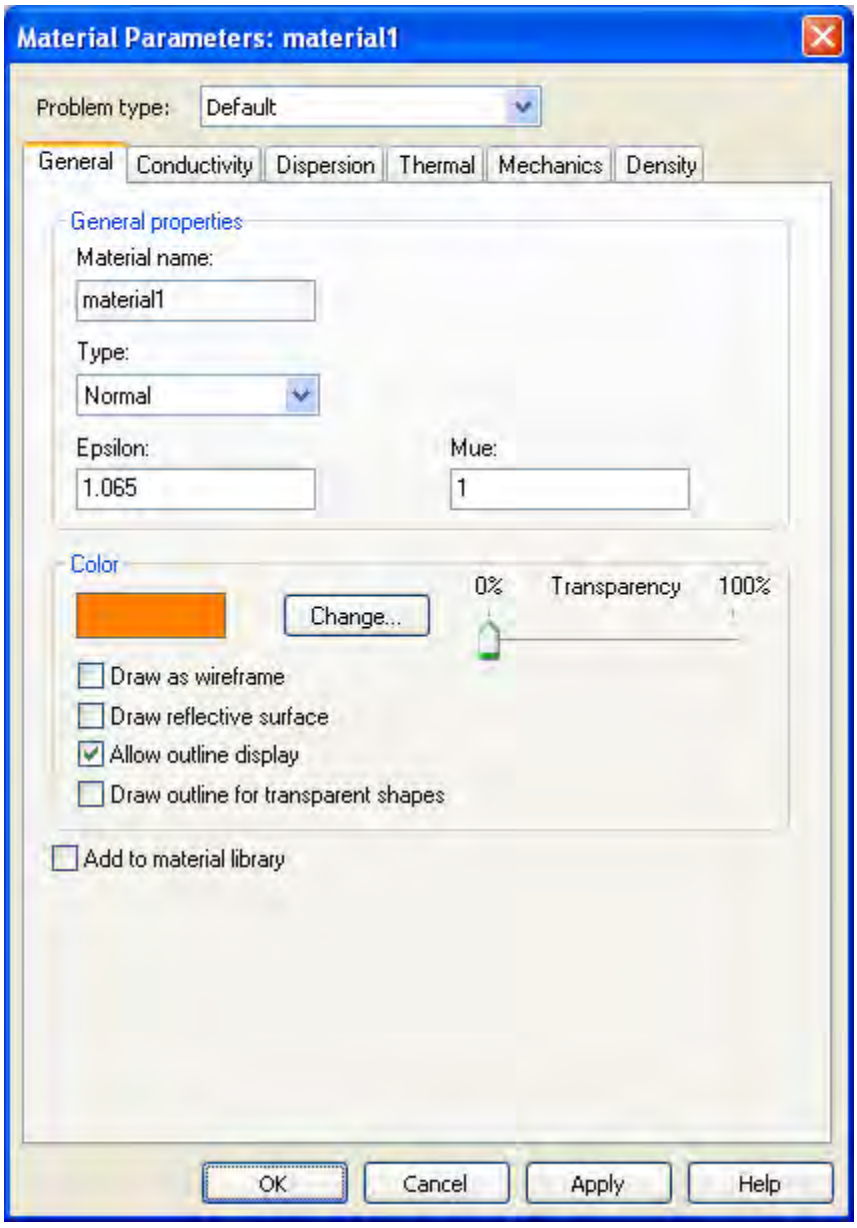

Figure 15. Parameters for material property of dielectric block.

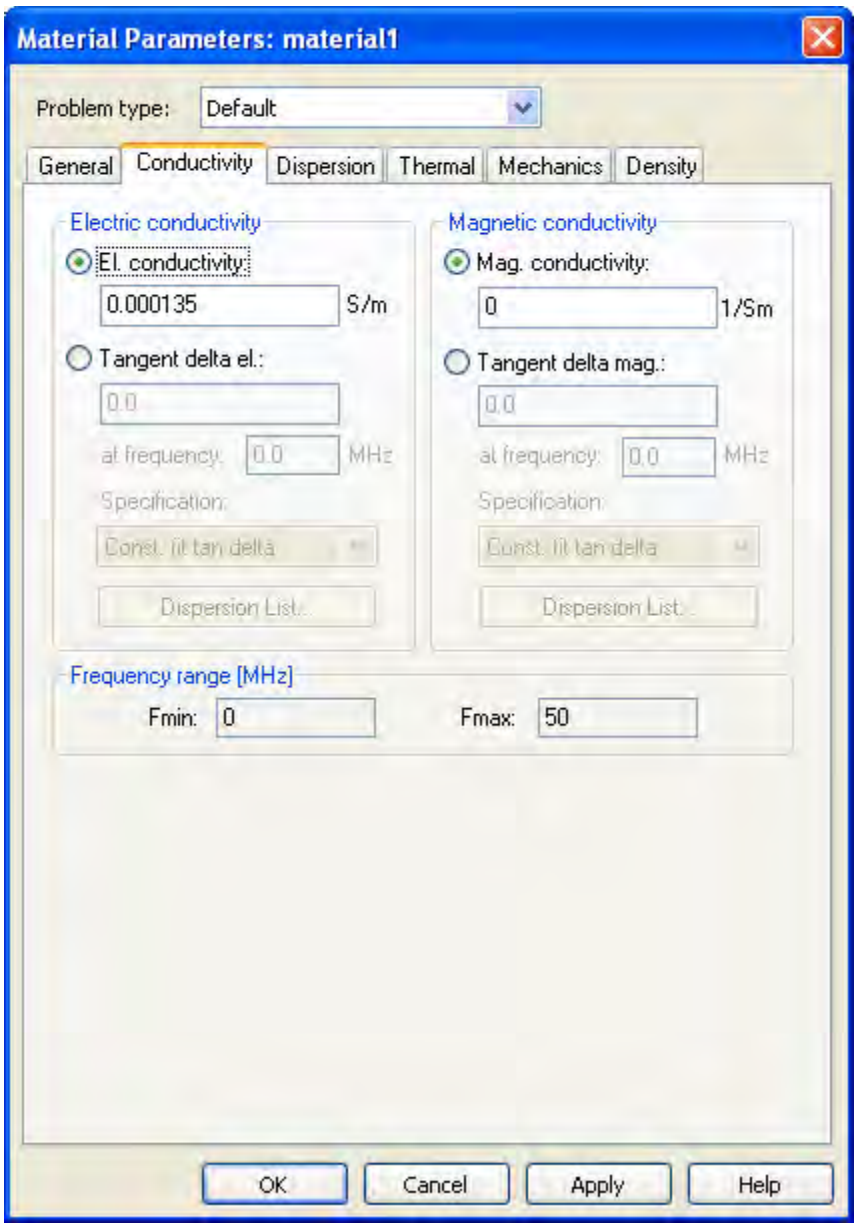

Figure 16. Parameters for material property of dielectric block.

From the settings in Figures 14, 15 and 16, the forest block is constructed in CST and is shown in Figure 17.

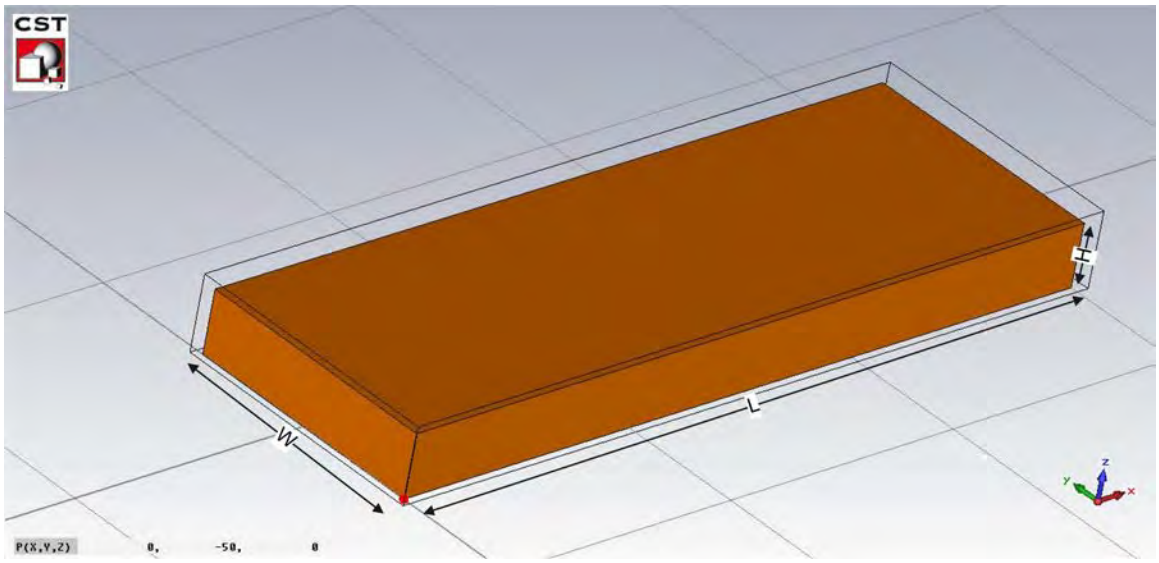

Figure 17. Forest dielectric block constructed in CST.

b. Half –Wave Dipole Antenna

The dipole antenna is modeled as a long thin rod with an impedance of 73 Ω. The length of the rod $\ell 2$ is set to slightly less than half a wavelength. The rod's length affects the matching of antenna. The length, which provides the optimum transmitted power (i.e., least reflected power), is set during each simulation run. The method for obtaining the matched length is described at the end of this section. The radius of the rod is set to $0.0005\lambda_o$. A discrete port is inserted at the rod's center to act as the excitation source. In order to construct the dipole antenna, a *Cylinder* object with the properties shown in Figure 18 is used. A small *Brick* object with properties shown in Figure 19 is also defined. The gap space for inserting the discrete port is created by subtracting the *Brick* object from the *Cylinder* object via a *Boolean subtract* operation in CST. The variables defined in Table 3 are used to construct the dipole antenna. The material of the dipole antenna is set as PEC with the properties shown in Figure 20.

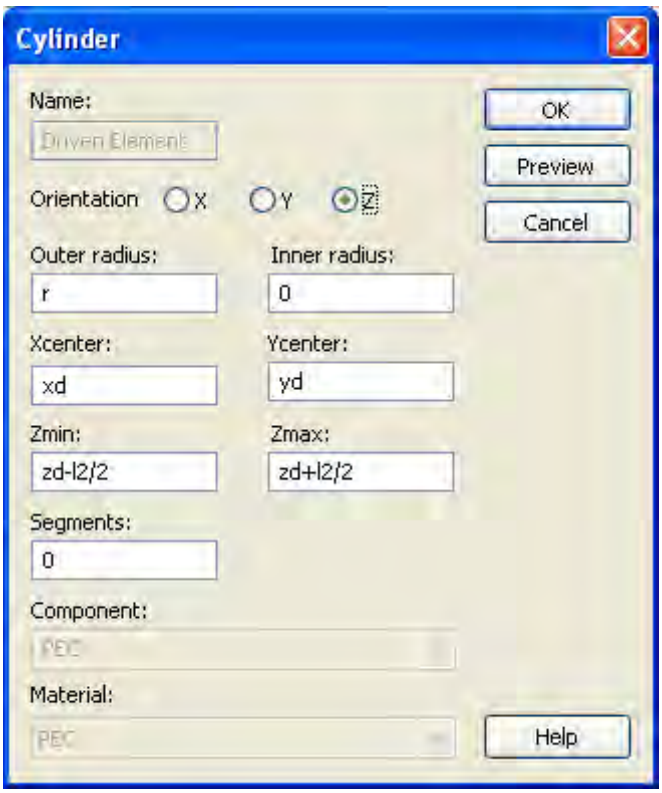

Figure 18. Properties of *Cylinder* object used to construct dipole antenna.

Figure 19. Properties of *Brick* object used to create space needed for discrete port.

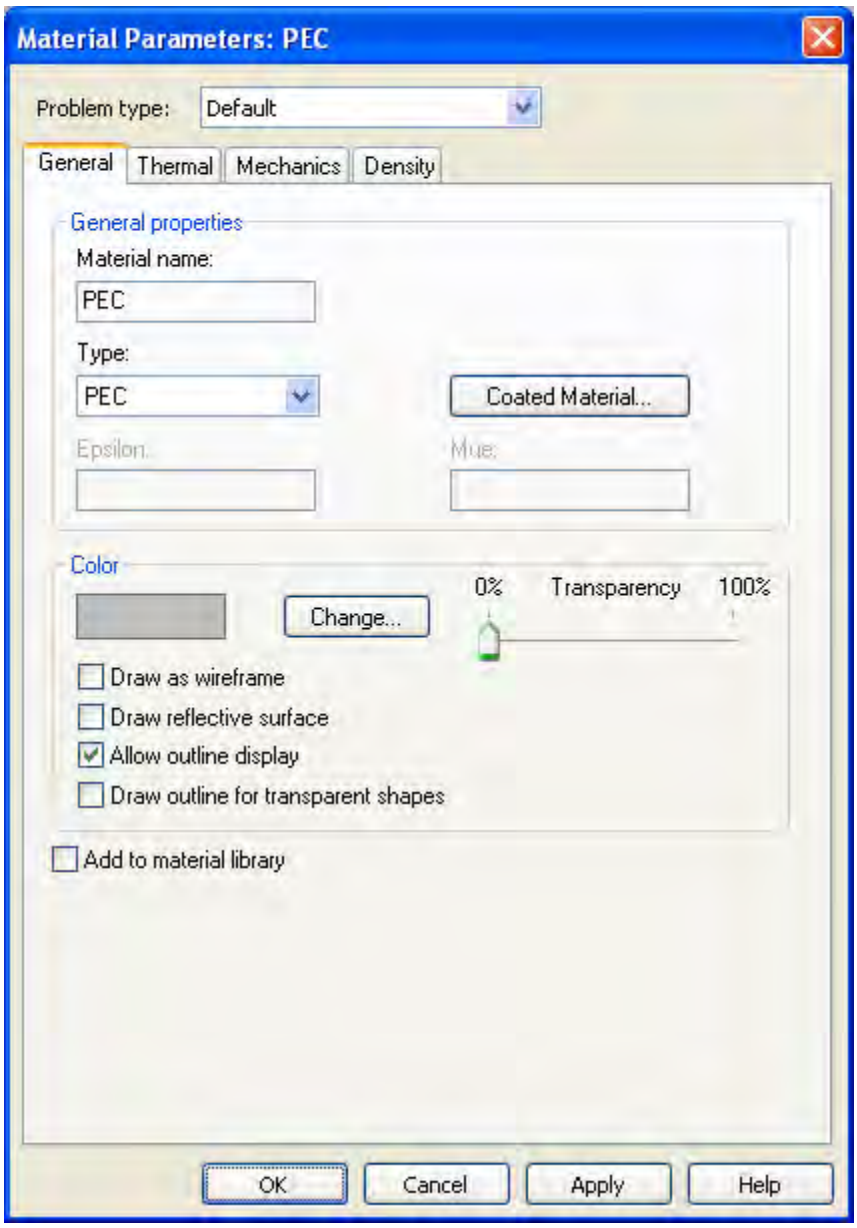

Figure 20. Properties of PEC material for dipole antenna.

A discrete port is required to feed the dipole antenna with power for the simulation. In CST, the radiated power from the antenna is normalized to 1 W or 0 dBW. A *Discrete Edge Port* is defined with the properties shown in Figure 21.

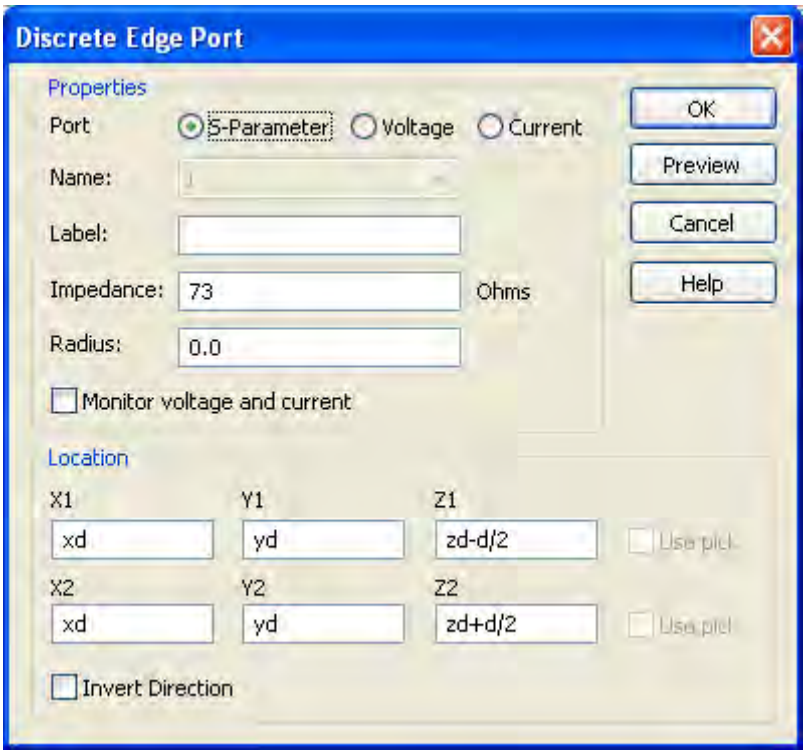

Figure 21. Properties of *Discrete Edge Port* used to provide power to dipole antenna.

From the settings in Figures 18, 19, 20 and 21, the dipole antenna of length $\ell 2$ is constructed and shown in Figure 22.

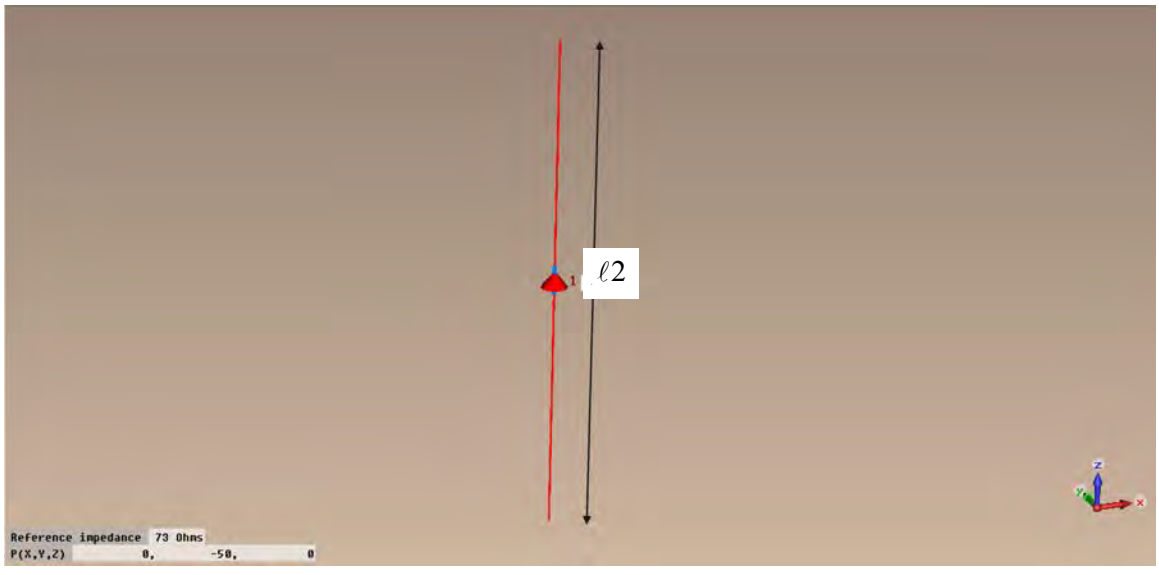

Figure 22. Dipole antenna constructed in CST.

The dipole antenna has to be matched to ensure that most of the energy is transmitted. When the antenna is matched, the reflection coefficient or scattering parameter (S_{11}) is the lowest at the frequency of interest. In order to match the antenna, a suitable dipole length has to be obtained for use in the simulation. This is achieved by using the parameter sweep functionality in CST. In the parameter sweep dialog box, the range of values to sweep and number of steps are defined. The parameter sweep function produces a series of *S*-parameter curves corresponding to different antenna lengths. The most appropriate length is chosen based on the curve whose minima coincides with the frequency of interest. This means that S_{11} is lowest at the transmission frequency for the given length. Using Figure 23 as an example, we see that a dipole length $\ell 2$ of 2.52 m gives the smallest S_{11} at a frequency of 50 MHz. The selected length is then used as the length of the dipole antenna for the simulation to produce the EM fields in the dielectric block.

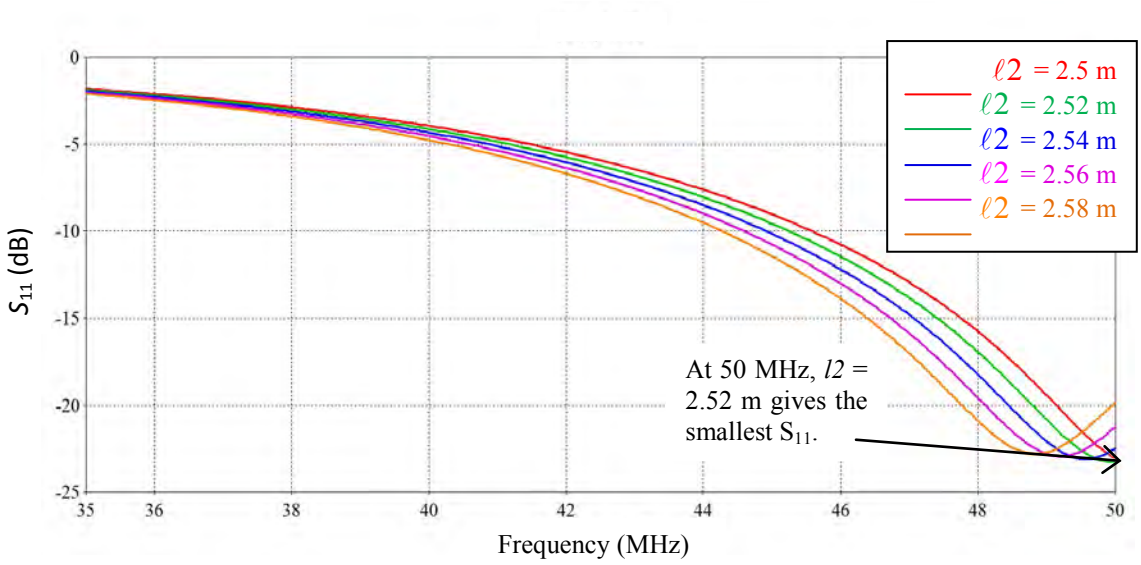

Figure 23. S_{11} results for different dipole antenna lengths.

3. Fields Monitors

In order to monitor the fields produced by the simulation, *E–field* and *Powerflow* monitors are used. In CST, the *E–field* monitor stores the electric field vectors, while the *Powerflow* monitor stores the Poynting vector of the EM field. For each frequency to be monitored, one *E–field* monitor and one *Powerflow* monitor has to be defined. A typical property window for a field monitor is shown in Figure 24.

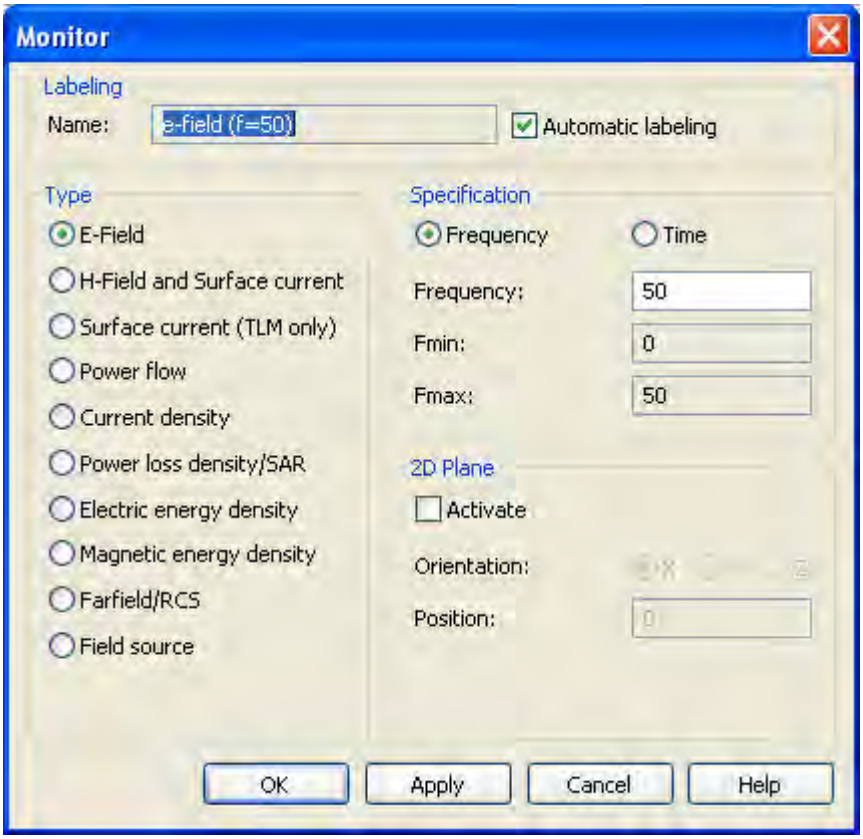

Figure 24. Property window for a field monitor.

The generated electric fields and Poynting vector can be exported to an ASCII file. When exporting the generated field data, a resolution of step size one is selected for the *x*, *y* and *z* components. This is shown in Figure 25. By exporting the data to ASCII, the generated field data can be manipulated in MATLAB for analysis purposes.

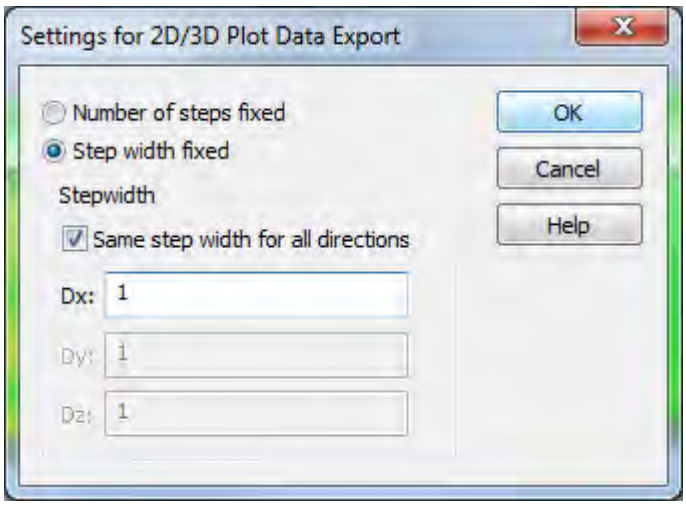

Figure 25. Setting the resolution of field data to be exported in CST.

C. SUMMARY

In summary, the steps for setting up CST to perform the simulation for radiowave propagation in foliage were covered in this chapter. The steps for constructing the forest dielectric block and the dipole antenna were also covered. The results and analysis of the simulation runs are presented in the next chapter.

IV. SIMULATION AND ANALYSIS

The various simulation runs performed in CST to model the radiowave propagation in foliage are presented in this chapter. The analysis of the simulation runs is also discussed and presented in this chapter.

A. COMPARISON WITH EMPIRICAL MODELS

In this section, the objective is to validate the results of the simulation model against empirical models. In this simulation model, the forest is represented as a single dielectric block. The transmitter is a dipole antenna that is immersed inside the forest. The generated Poynting vector data is then processed in MATLAB to obtain a loss versus distance curve. The steps to construct the model were described in Chapter III.

As the empirical models did not specify the range of values for ε_r and σ of the forest from which their measured data from obtained, a reasonable assumption was made on the values to be used in the simulations. Based on [6, 8], the range of ε_r used in the simulation is from 1.01 to 1.5, and the range of σ is from 10^{-5} S/m to 10^{-3} S/m.

In order to generate the loss–distance curve, only the field data inside the dielectric block are considered. Since there is no receiving antenna in the simulation, the Poynting vector at any point in space (coordinates of x, y, z) represents the available power at a receiver located at that point. Hence, the loss L can be represented by

$$L(dB) = 10\log P_t(dB) - 10\log P_r(dB) \tag{25}$$

where P_t is the transmit power in W and P_r is the receive power in W.

Given that the radiated power is 1 W, P_t is 0 dBW and (25) can be simplified to

$$L(dB) = -10\log P_r(dB)\cdot \tag{26}$$

In (25), L ignores the losses incurred in the receiver and represents the path loss between the transmitter and receiver. The MATLAB code to plot the loss–distance curves is given in the Appendix. The loss–distance curve is used to compare against various empirical models to validate the simulation results from CST.

As there is no requirement to examine the fields outside the dielectric block in this section, the background properties are configured as shown in Figure 26.

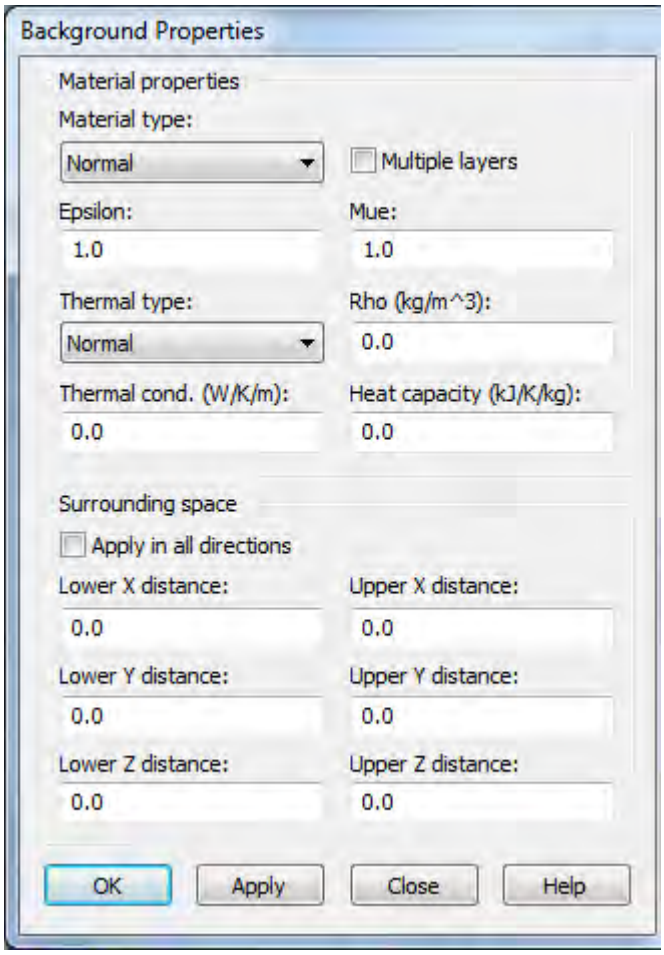

Figure 26. Background properties setting.

Several variations of the simulation model are executed to examine the effects of different variables on the closeness of the simulation results to the empirical models. The variables are electrical properties of dielectric block (i.e., ε_r and σ) and height of transmitting antenna. The general observations for the simulation results are discussed at the end of this section.

1. Simulation Results of Propagation in a Dielectric Block

Test case A1 was constructed using the values shown in Table 4. The transmitter is at a height of 5 m from the ground. In order avoid effects due to reflections from the forest edges, the transmitter is sited at a position such that it is at least 50 m away from all the side walls of the dielectric block.

Table 4. Values used to set up model for test case A1.

	Parameter	Description	Value
1	$\ell 2$	Length of dipole antenna	2.54 m
2	f	Frequency of interest	50 MHz
3	H	Height of dielectric block	20 m
4	L	Length of dielectric block	200 m
5	W	Width of dielectric block	100 m
6	xd	x-coordinate of dipole center	50 m
7	yd	y-coordinate of dipole center	0 m
8	zd	z-coordinate of dipole center	5 m
9	ε_r	Relative permittivity	1.065
10	σ	Conductivity	0.000135 S/m

Based on the values in Table 4, the simulated power flow plot of the fields along the *x*-*z* plane (i.e., $y = 0$ m) in the dielectric block is shown in Figure 27.

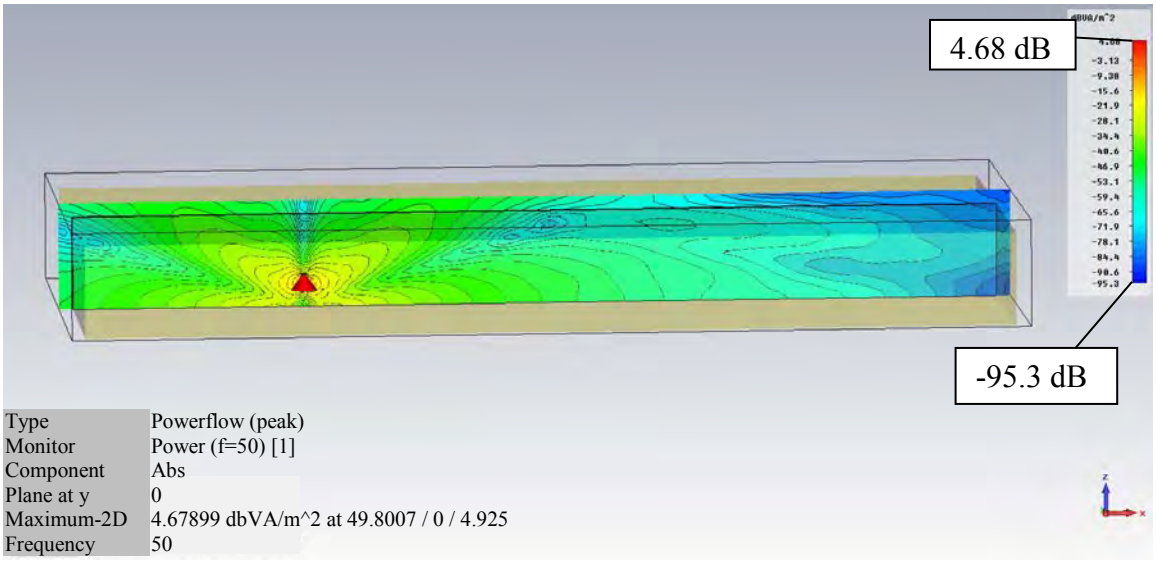

Figure 27. Power flow plot at $y = 0$ m for test case A1.

From the exported data, the loss–distance curves are plotted in MATLAB for different transmitter heights h_t that are parallel to the x-y plane. The height h_r also represents the height of a receiver. The loss–distance curves for different h_r are shown in Figures 28, 29, 30 and 31. In the figures, the Tewari model [9], the Jansky and Bailey model [10] and the LITU-R model curves are plotted for comparison with the simulated results [1].

From Figures 28, 29, 30 and 31, it can be observed that the loss–distance curves for the simulated results are close to those predicted by LITU-R model (19) for low receiver heights (i.e., h_r = 1–5 m). As the receiver height is increased, the loss–distance curves exhibit a downward shift towards the curves predicted by Tewari's model (16) and the Jansky and Bailey model (17).

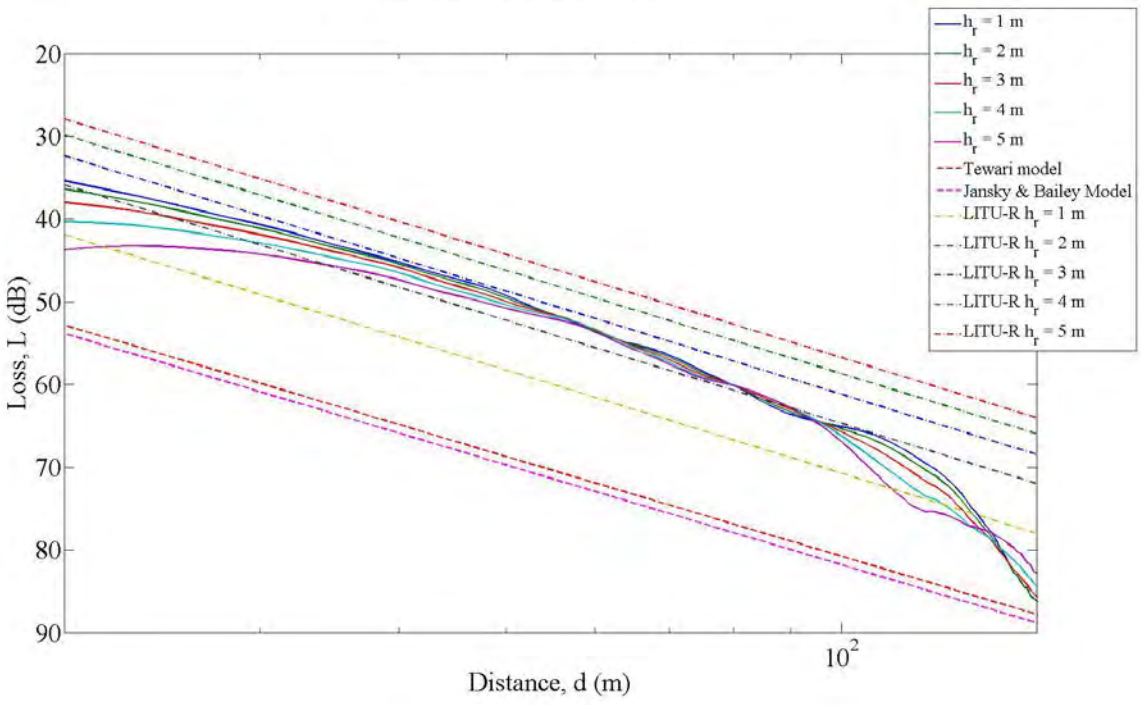

Figure 28. Loss–distance curves for h_r = 1–5 m (test case A1).

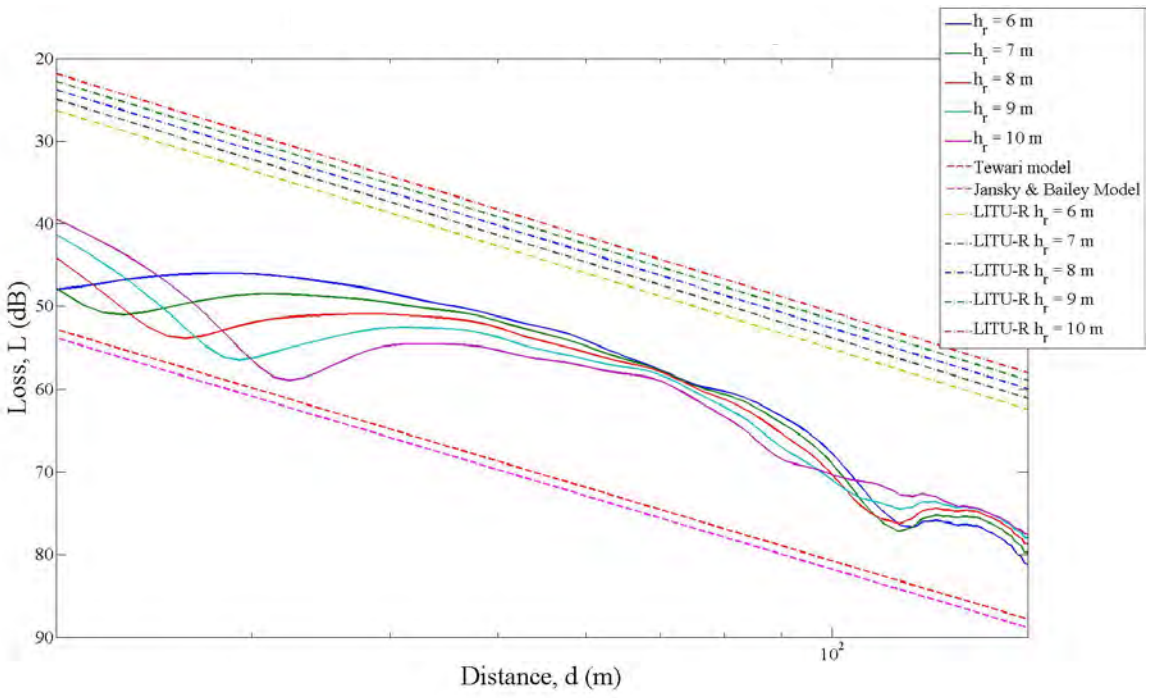

Figure 29. Loss–distance curves for h_r = 6–10 m (test case A1).

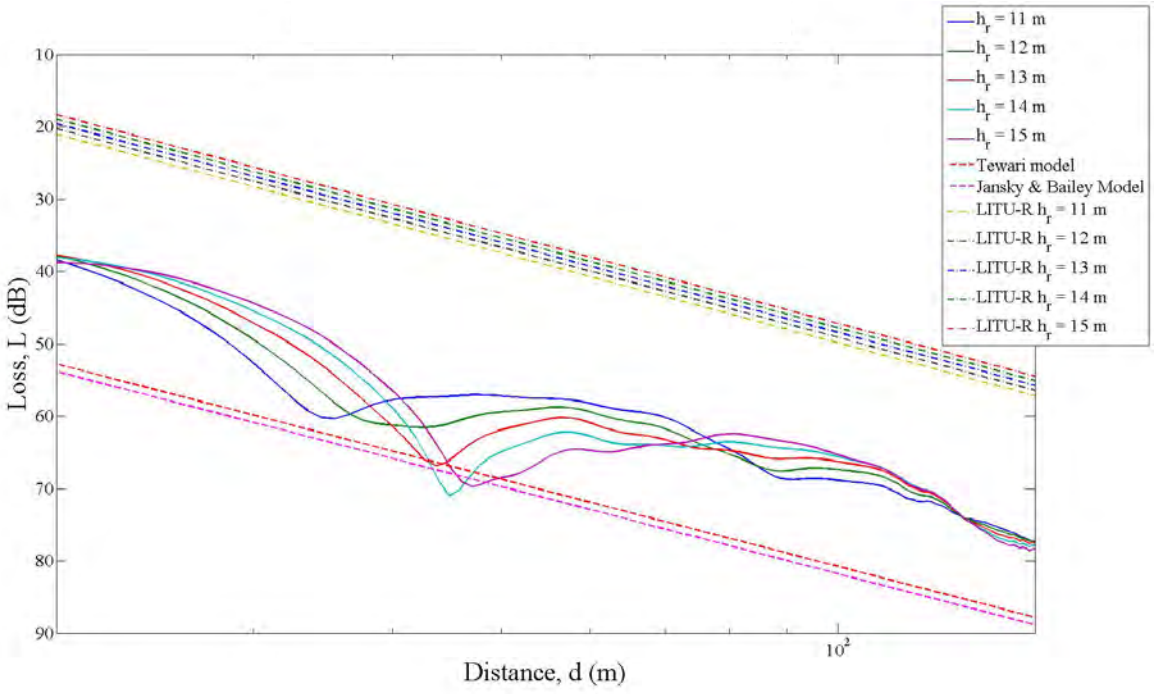

Figure 30. Loss–distance curves for h_r = 11–15 m (test case A1).

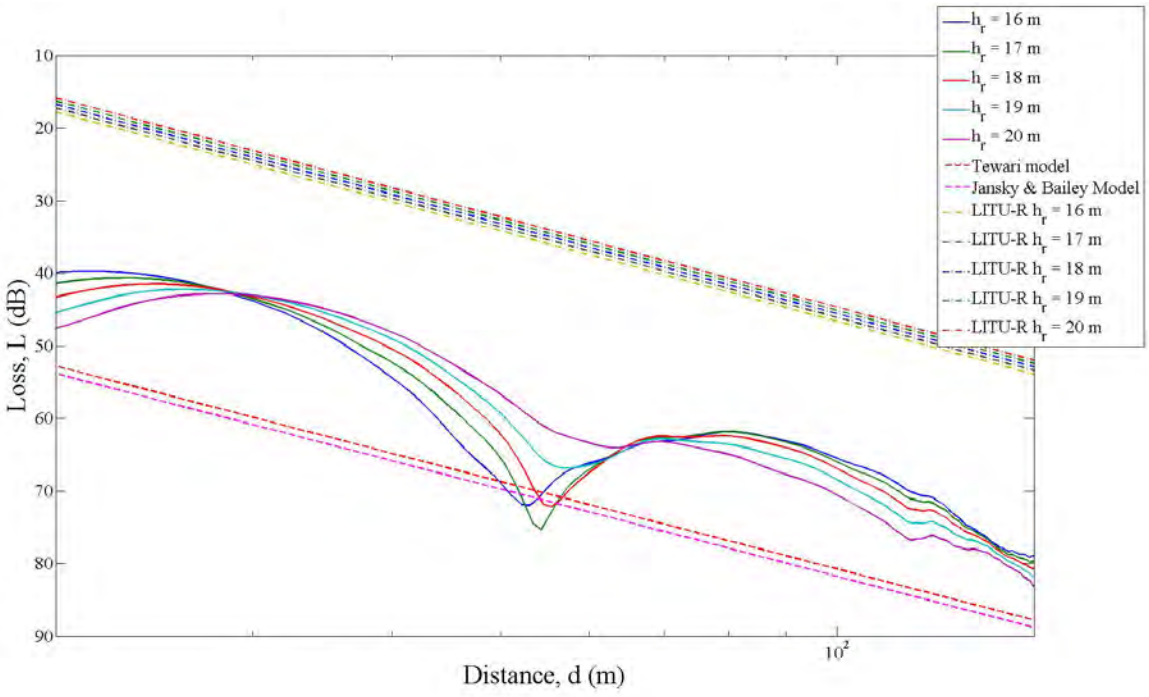

Figure 31. Loss–distance curves for h_r = 16–20 m (test case A1).

2. Effects of Different ε_r and σ values on Simulation Results

In test case B, the effects of different ε_r and σ values on the simulation results with respect to the empirical models are examined. The set-up for the simulation is similar to Table 4. However, in this test case, the pairs of ε_r and σ values as shown in Table 5 are used for each simulation run. In addition, different lengths are used for the dipole antenna so that the antennas are matched at the transmitting frequency. The transmitter antenna is sited at 5 m above the ground.

Table 5. List of ε_r, σ and dipole length $\ell 2$ values used in test case B simulation runs.

Test Case.	ε_r	σ (S/m)	$\ell 2$ (m)
B1	1.01	0.00001	2.6
B2	1.08	0.000135	2.54
B3	1.1	0.000135	2.54
B4	1.5	0.000135	2.54

For test case B1, the simulated power flow plot of the fields along the *x*-*z* plane (i.e., y = 0 m) in the dielectric block is shown in Figure 32. The transmitter antenna is sited at 5 m above the ground.

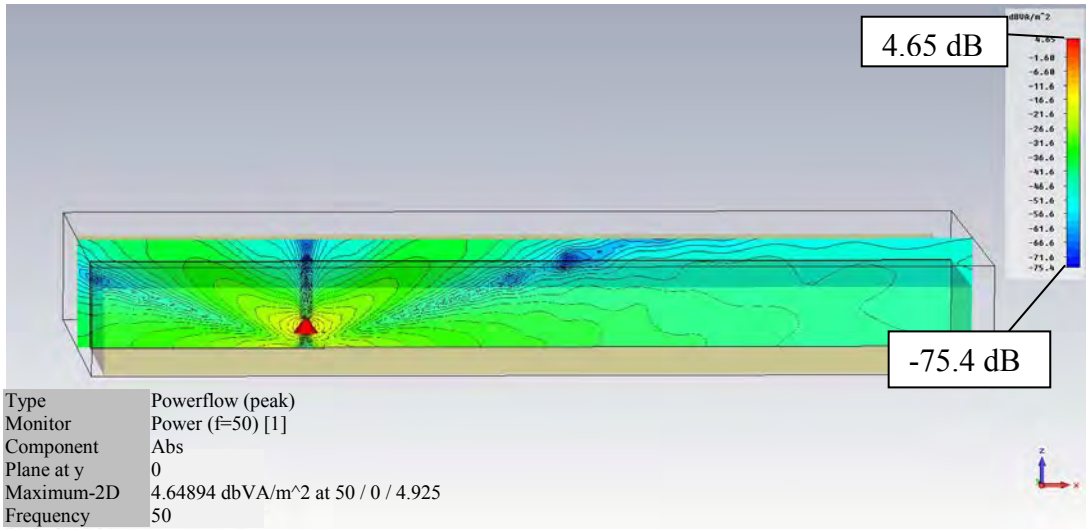

Figure 32. Power flow plot at y = 0 m for test case B1.

The "test case B1" loss–distance curves for different values of h_r are shown in Figures 33, 34, 35 and 36.

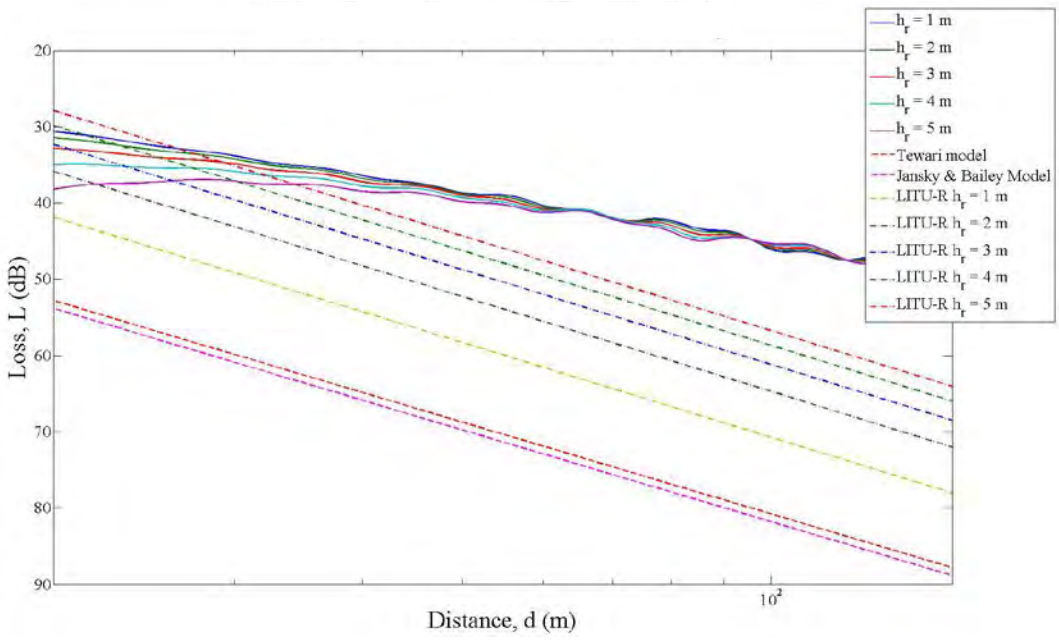

Figure 33. Loss–distance curves for h_r = 1–5 m (test case B1).

In Figure 33 it is observed that the loss–distance curves for the simulated results approximate the LITU-R model at small separation distance from the transmitting antenna.

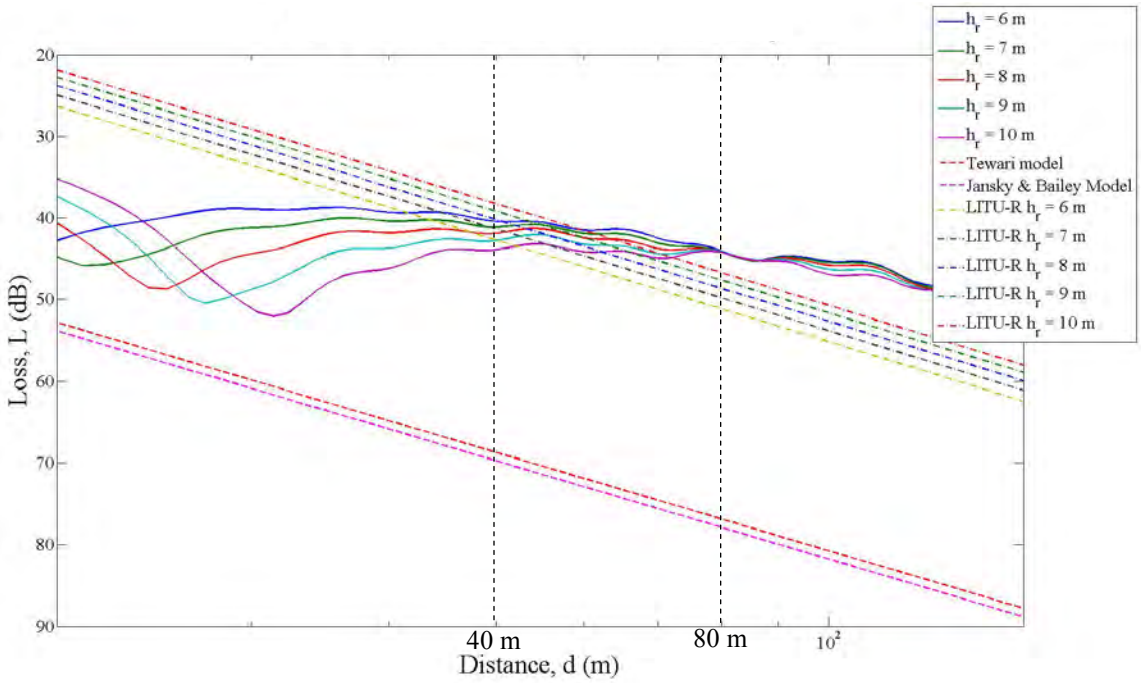

Figure 34. Loss–distance curves for h_r = 6–10 m (test case B1).

In Figure 34, it is observed that the loss–distance curves for the simulated results approximate the LITU-R model at distances of 40–80 m from the transmitting antenna. In this test case, the receiver antennas are sited at heights of 6–10 m from the ground.

In Figure 35, it is observed that the loss–distance curves for the simulated results approximate the LITU-R model at distances of 80–100 m from the transmitting antenna. In this case, the receiver antennas are sited at heights of 11–15 m from the ground.

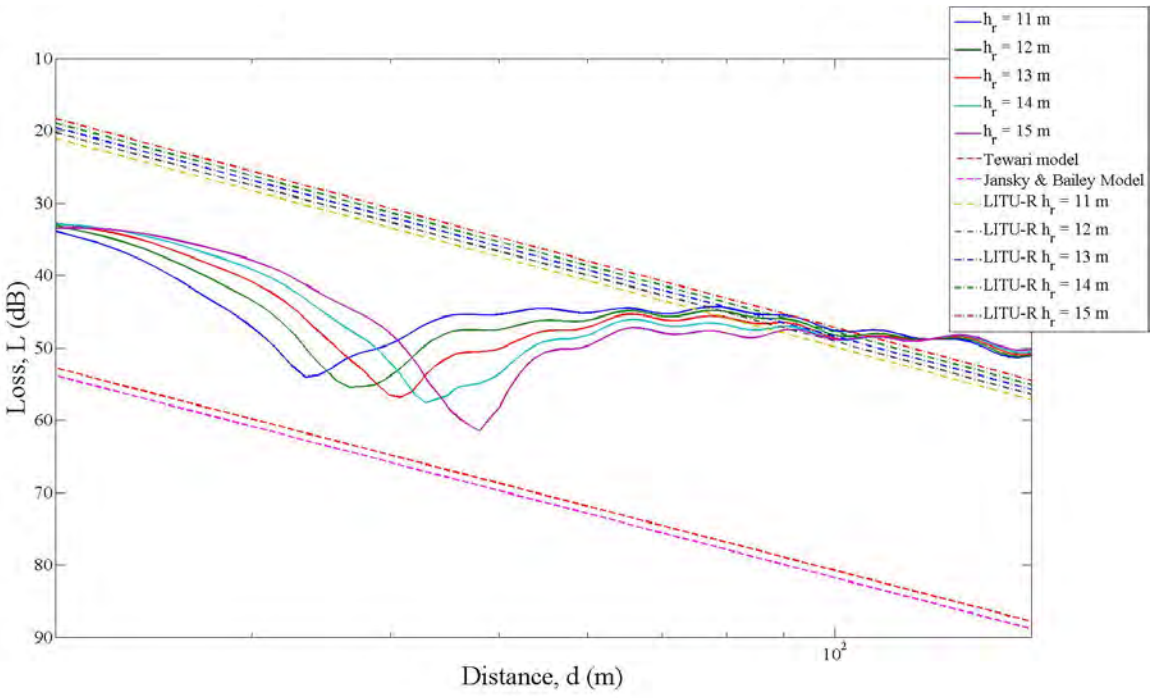

Figure 35. Loss–distance curves for h_r = 11–15 m (test case B1).

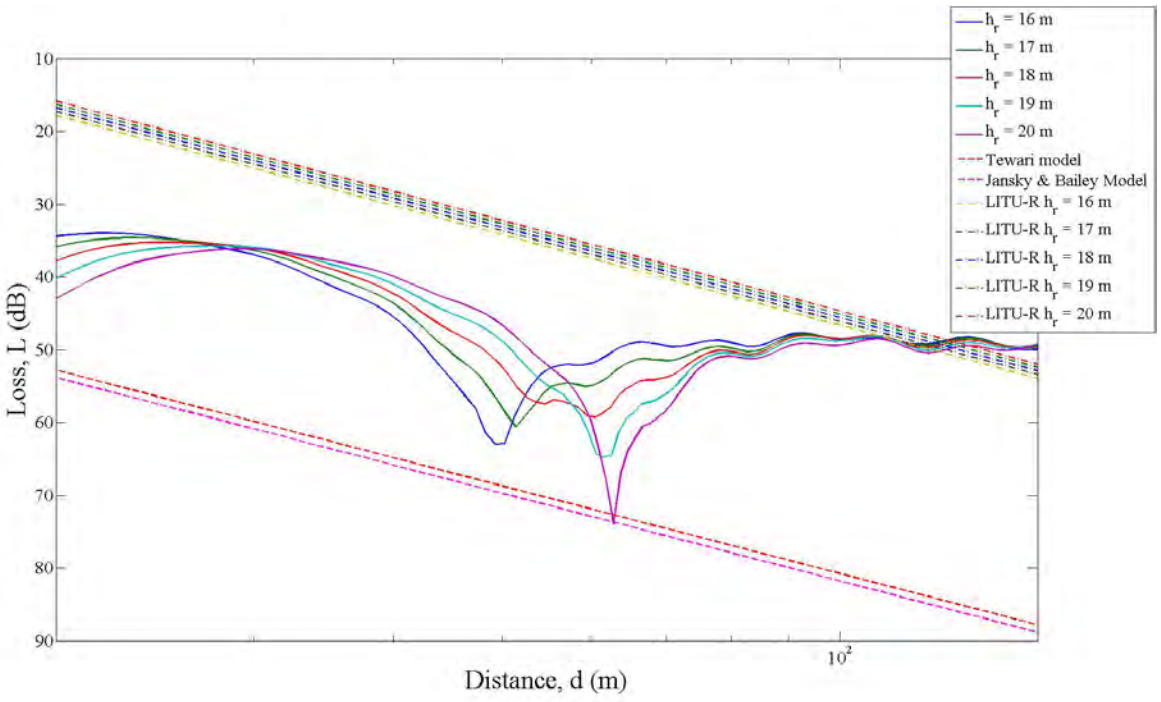

Figure 36. Loss–distance curves for h_r = 16–20 m (test case B1).

In Figure 36, it is observed that the loss–distance curves for the simulated results approximate the LITU-R model at distances of 100–120 m from the transmitting antenna. In this case, the receiver antennas are sited at heights of 16–20 m from the ground.

For test case B2, the simulated power flow plot of the fields along the *x*-*z* plane (i.e., y = 0 m) in the dielectric block is shown in Figure 37. The transmitter antenna is sited at 5 m above the ground.

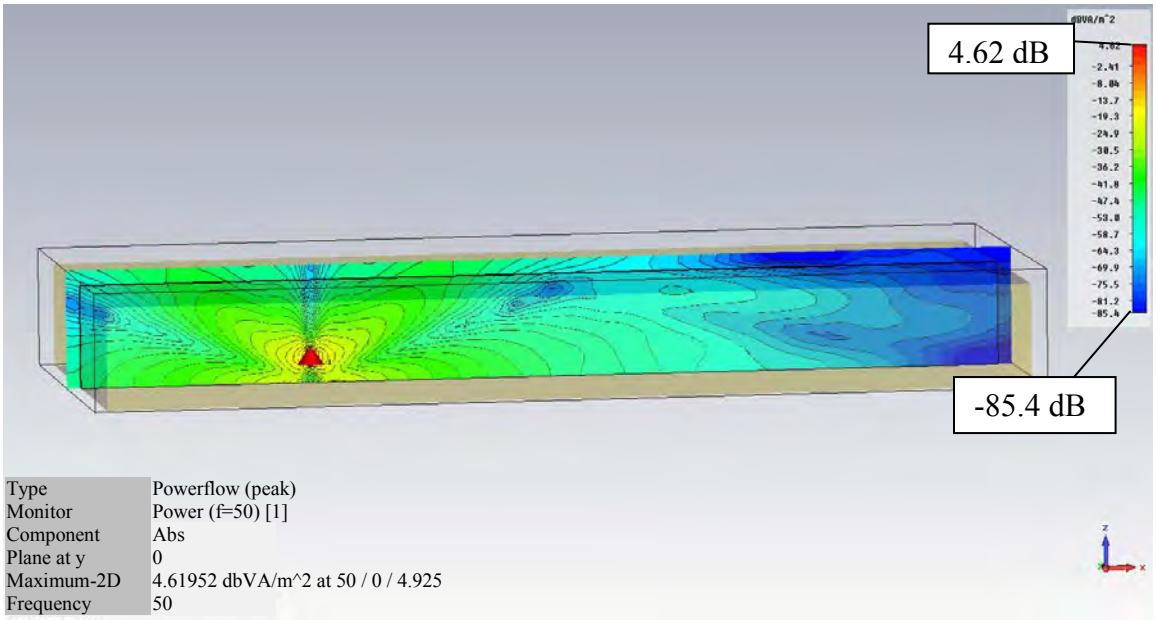

Figure 37. Power flow plot at y = 0 m for test case B2.

The "test case B2" loss–distance curves for different values of h_r are shown in Figures 38 and 39.

In Figure 38, it is observed that the loss–distance curves for the simulated results approximate the LITU-R model at separation distances up to 100 m from the transmitting antenna. In this case, the receiver antennas are sited at heights of 1–5 m from the ground.

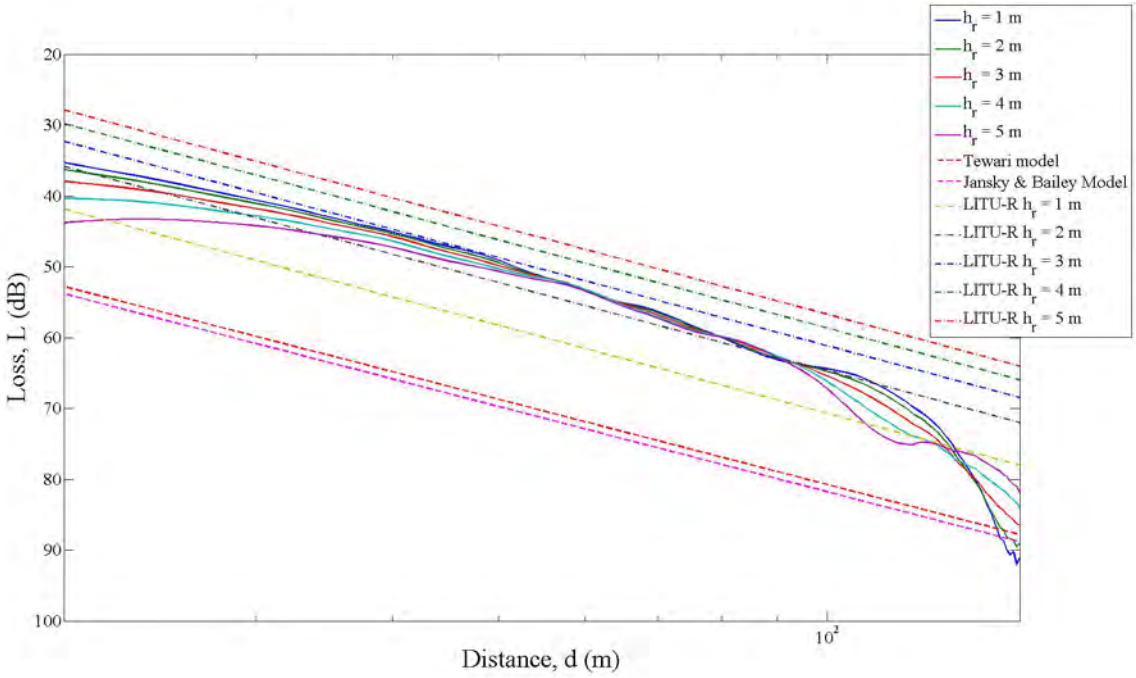

Figure 38. Loss–distance curves for h_r = 1–5 m (test case B2).

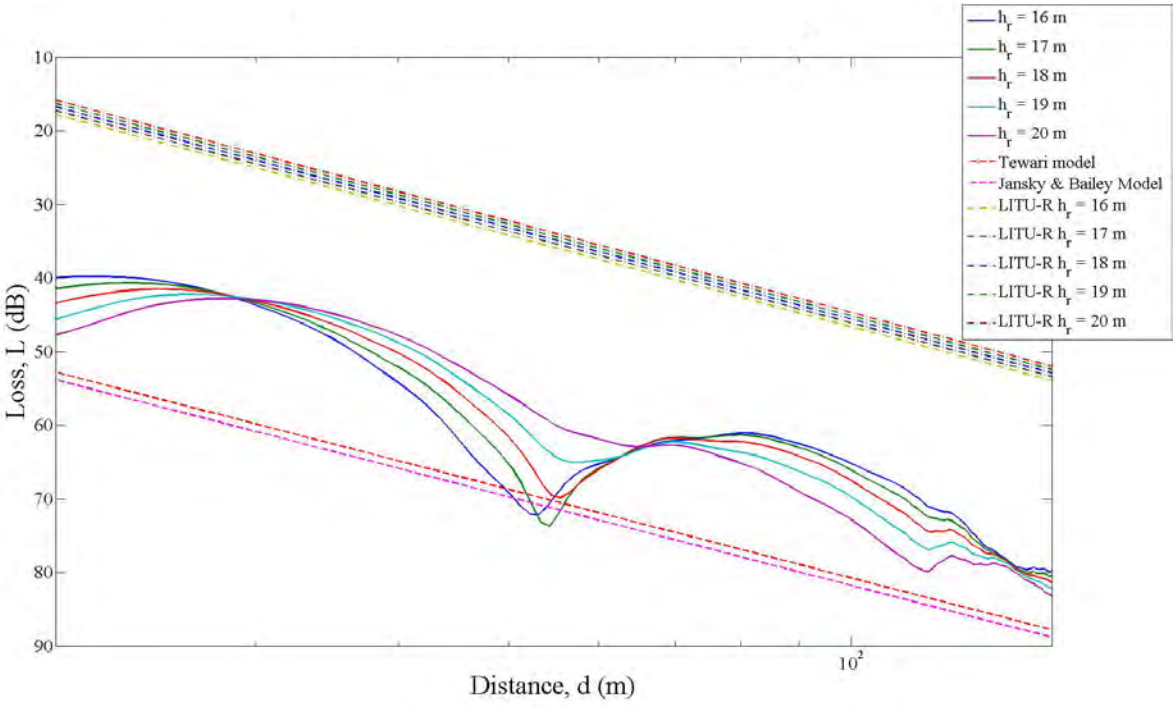

Figure 39. Loss–distance curves for h_r = 16–20 m (test case B2).

Comparing Figure 39 to Figure 38, we observe that as the height of the receiving antenna increases (i.e., from 1 m to 20 m), the loss for a given separation distance increases. At higher receiving antenna heights (i.e., 16–20 m), the loss–distance curves are closer to those predicted by Tewari's model and the Jansky and Bailey model.

For test case B3, the simulated power flow plot of the fields along the *x*-*z* plane (i.e., $y = 0$ m) in the dielectric block is shown in Figure 40. The transmitter antenna is sited at 5 m above the ground.

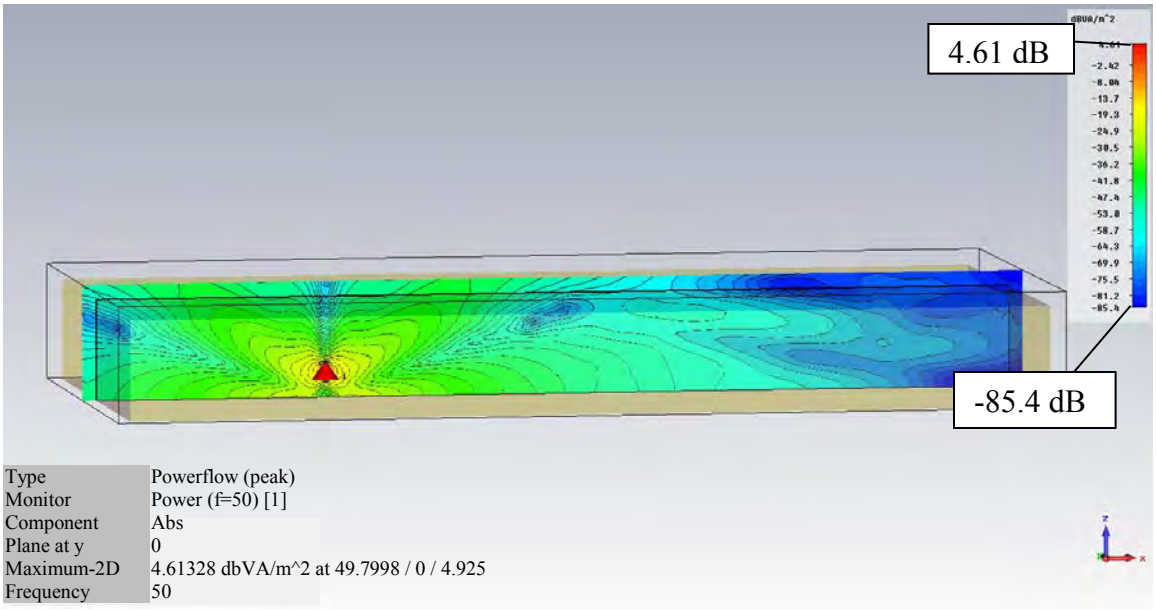

Figure 40. Power flow plot at $y = 0$ m for test case B3.

The "test case B3" loss–distance curves for different values of h_r are shown in Figures 41 and 42.

In Figure 41 it is observed that the loss–distance curves for the simulated results approximate the LITU-R model at separation distances up to 120 m from the transmitting antenna. In this case, the receiver antennas are sited at heights of 1–5 m from the ground.

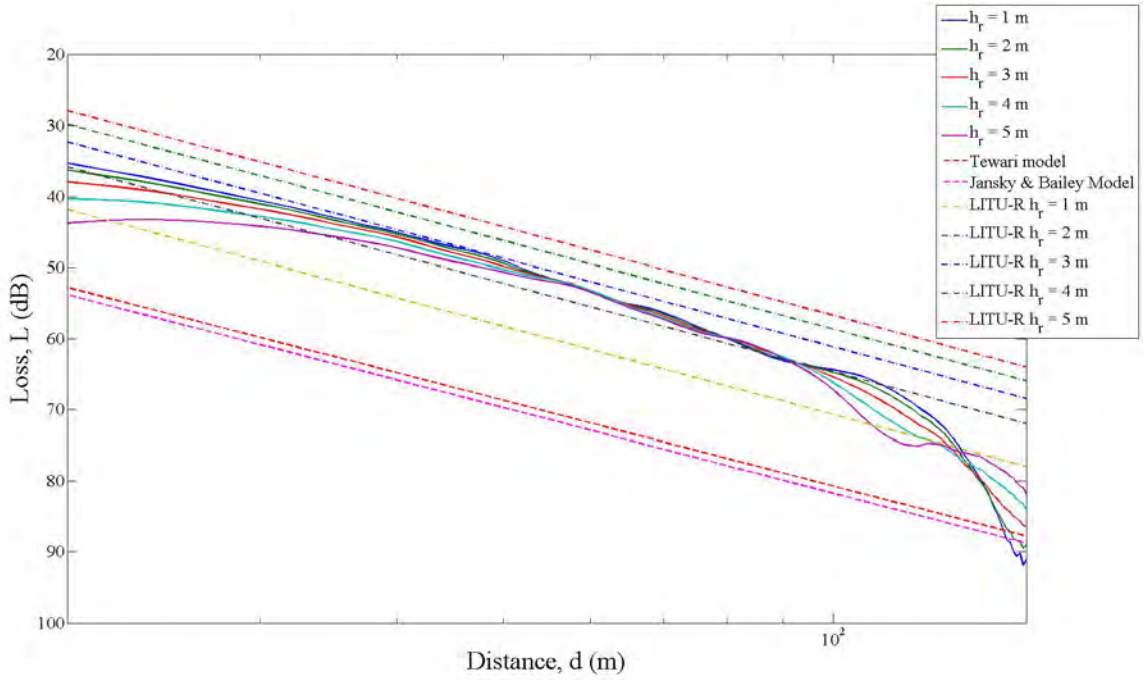

Figure 41. Loss–distance curves for h_r = 1–5 m (test case B3).

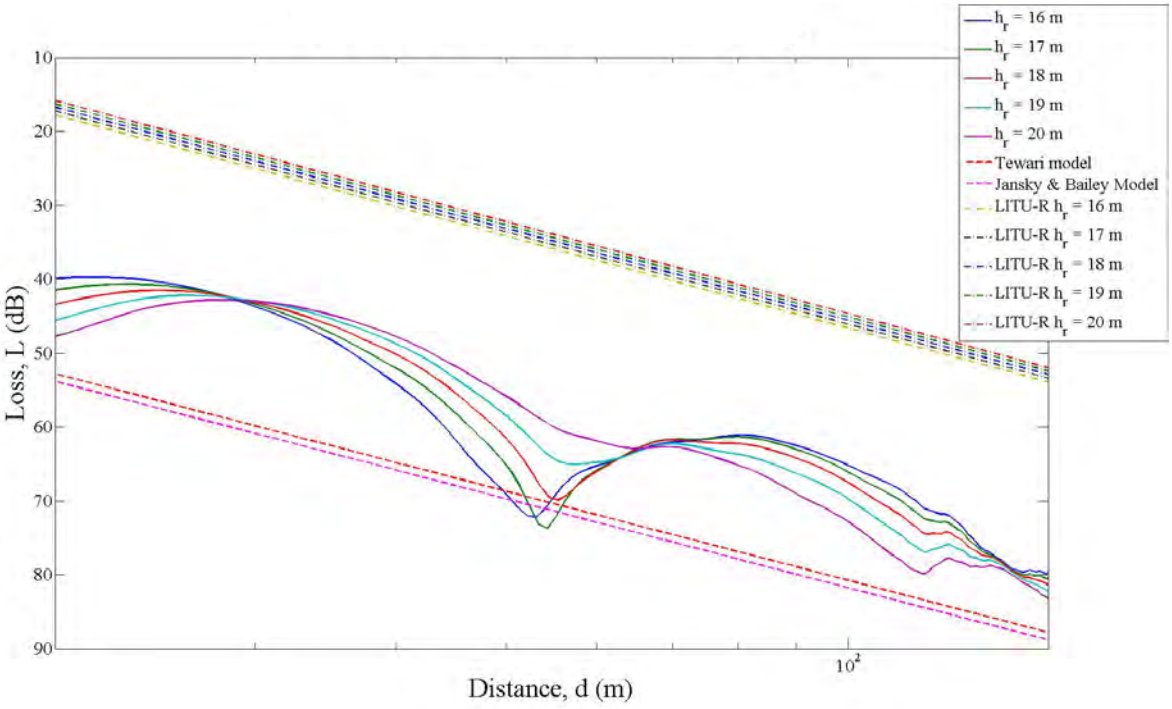

Figure 42. Loss–distance curves for h_r = 16–20 m (test case B3).

Comparing Figure 42 to Figure 41, we observe that as the height of the antennas increases (i.e., from 1 m to 20 m), the loss for a given separation distance increases. At higher antenna heights (i.e., 16–20 m), the loss–distance curves are closer to those predicted by Tewari's model and the Jansky and Bailey model.

For test case B4, the simulated power flow plot of the fields along the *x*-*z* plane (i.e., $y = 0$ m) in the dielectric block is shown in Figure 43. The transmitter antenna is sited at 5 m above the ground.

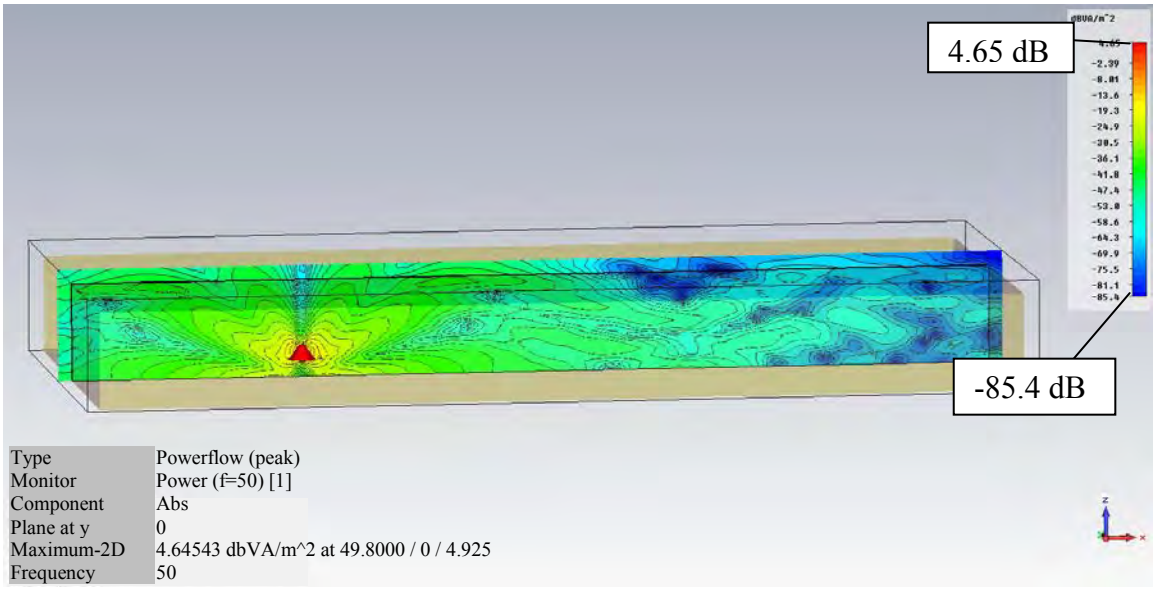

Figure 43. Power flow plot at $y = 0$ m for test case B4.

The "test case B4" loss–distance curves for different values of h_r are shown in Figures 44 and 45.

In Figure 44, it is observed that the loss–distance curves for the simulated results approximate the LITU-R model at separation distances up to 150 m from the transmitting antenna. In this case, the receiver is sited at heights of 1–5 m from the ground.

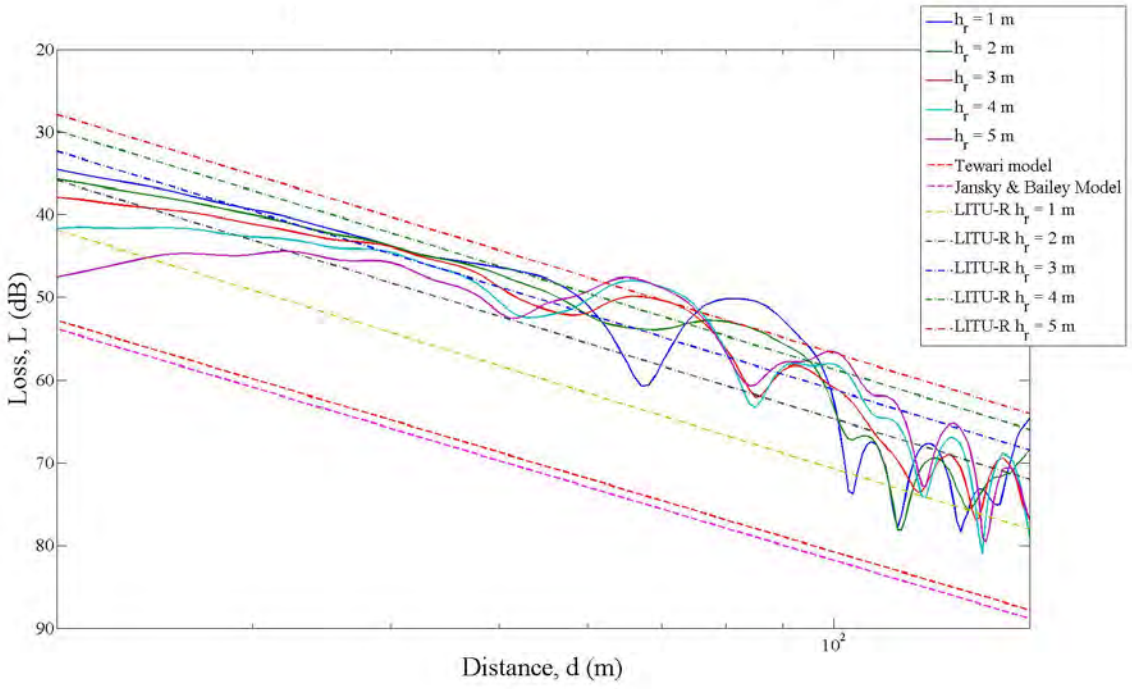

Figure 44. Loss–distance curves for h_r = 1–5 m (test case B4).

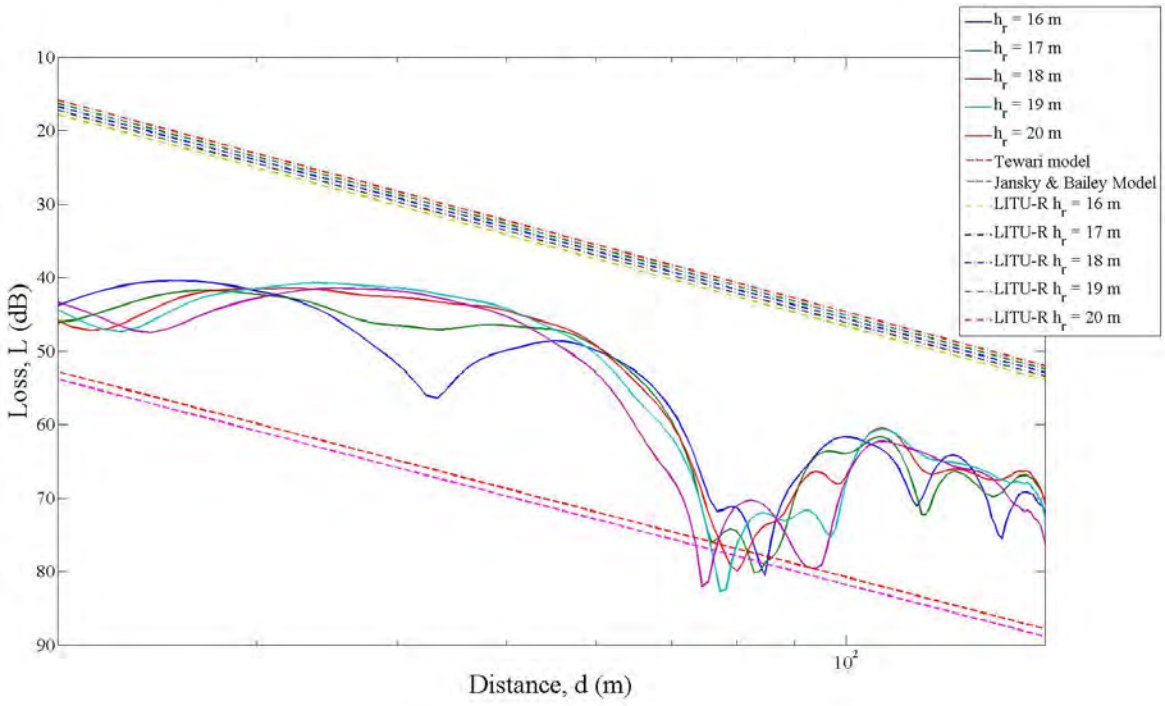

Figure 45. Loss–distance curves for h_r = 16–20 m (test case B4).

Comparing Figure 45 to Figure 44, we observe that as the height of the antennas increases (i.e., from 1 m to 20 m), the loss for a given separation distance increases. At higher receiving antenna heights (i.e., 16–20 m), the loss–distance curves are closer to those predicted by Tewari's model and the Jansky and Bailey model.

In general, for denser forest (i.e., having higher ε_r values of at least 1.08 and σ on the order 10^{-4} S/m and higher), the simulated results approximate those predicted by the LITU-R model when the receiver is sited at low heights (i.e., 1–5 m) in the simulation. At higher antenna heights (i.e., 16–20 m), both Tewari's model and the Jansky and Bailey model provide a closer approximation to the simulated results than the LITU-R model. This is expected as both empirical models were proposed based on measured data obtained in dense forest with similar electrical characteristics (i.e., ε_r values of at least 1.08 and σ of the order 10^{-4} S/m) as that used in the simulation. Conversely, it is observed that the simulated results based on smaller values of ε_r (i.e., 1.01) and σ (i.e., 10^{-5} S/m) do not closely match the three empirical models. This is evidenced by comparing the slope of the loss–distance curves for the simulated results to the curves for the three empirical models. The slope of the curves for the simulated results are much flatter as compared to the empirical models. This is because the smaller ε_r and σ values represent a less dense forest that is very much different from the forests used to obtain both Tewari's model and the Jansky and Bailey model.

3. Effects of Different Transmitter Heights on Simulation Results

In test case C, the effects of different transmitter heights on the simulation results with respect to the empirical models are examined. However, in this test case, different transmitter antenna heights h_t, as shown in Table 6, are used in each simulation run. The height, H, of the dielectric block is 30 m. The values of the other variables needed to set-up the simulation are kept constant for all the simulation runs in this test case and are shown in Table 4.

Table 6. List of difference transmitting antenna heights used in test case C simulation runs.

Test Case.	h_t (m)
C1	2
C2	5
C3	10
C4	20
C5	25

For test case C1, the simulated power flow plot of the fields along the *x*-*z* plane (i.e., y = 0 m) in the dielectric block is shown in Figure 46. The transmitter antenna is sited at 2 m above the ground.

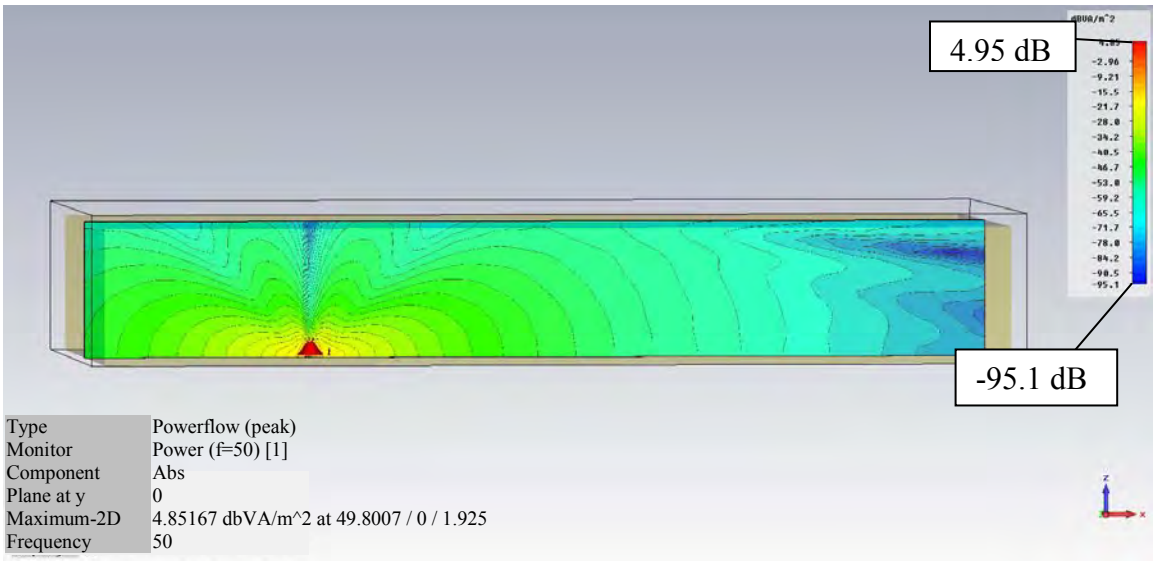

Figure 46. Power flow plot at y = 0 m for test case C1.

For test case C1, the loss–distance curves for different values of h_r are shown in Figures 47, 48 and 49.

From Figures 47, when the receiver is at a height of 1–5 m, it is observed that the loss–distance curves for the simulated results are bunched together. The curves for the simulated results are closer to the curves for the LITU-R model than the curves for both Tewari's model and the Jansky and Bailey model.

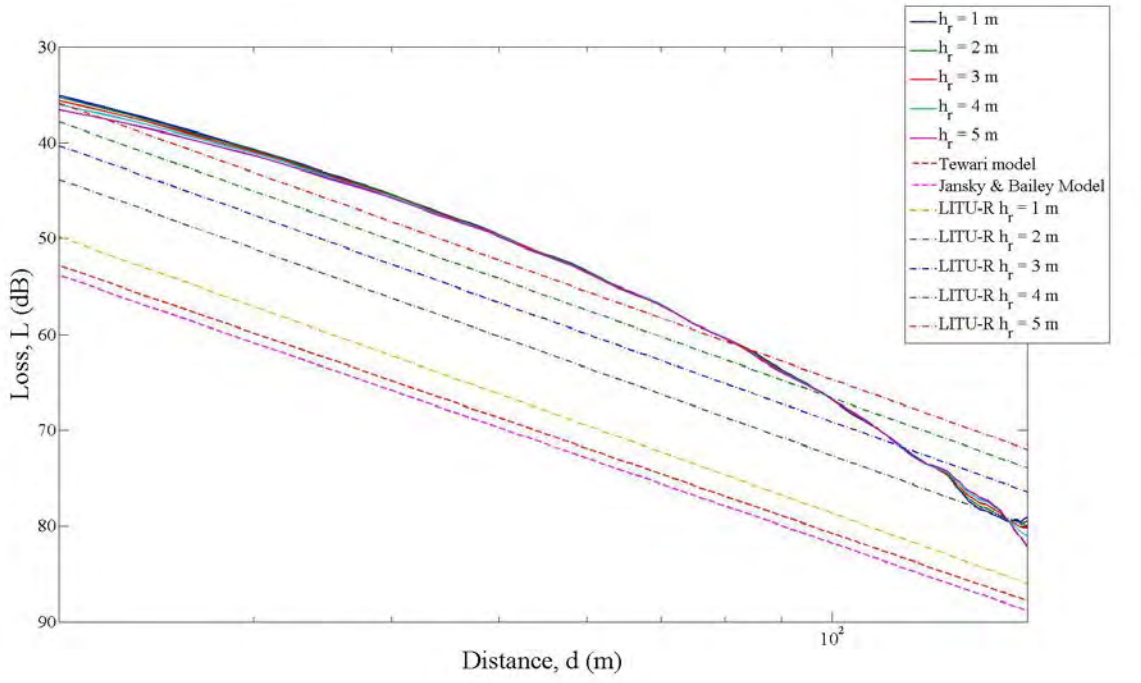

Figure 47. Loss–distance curves for h_r = 1–5 m (test case C1).

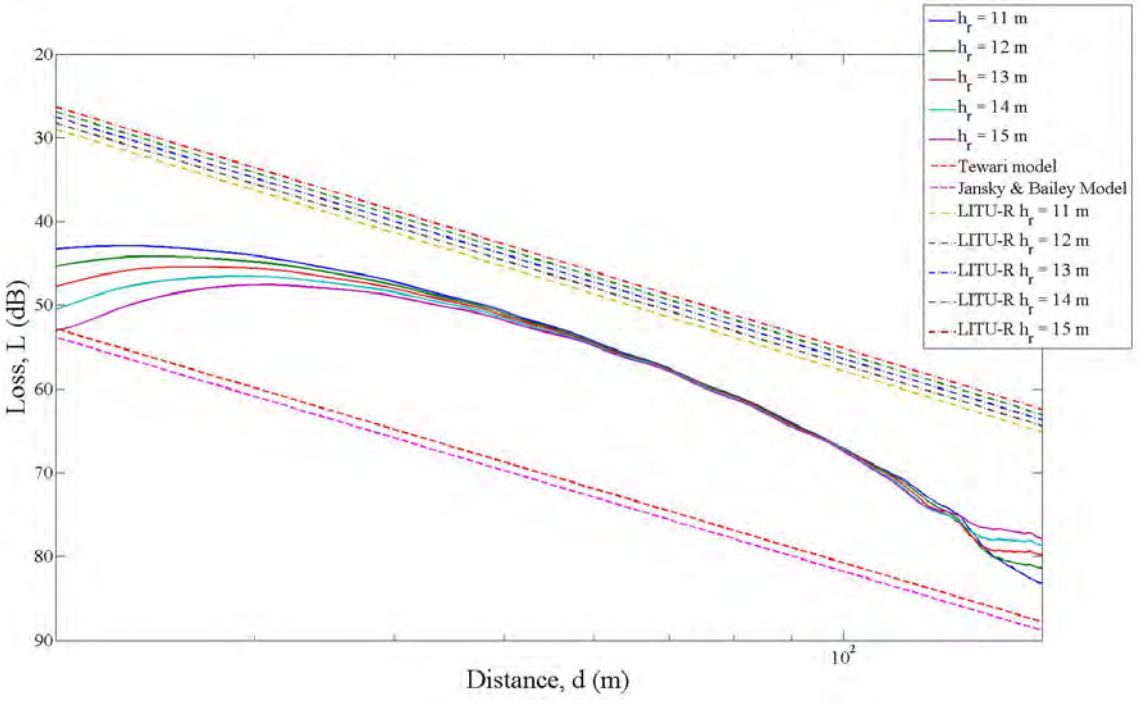

Figure 48. Loss–distance curves for h_r = 11–15 m (test case C1).

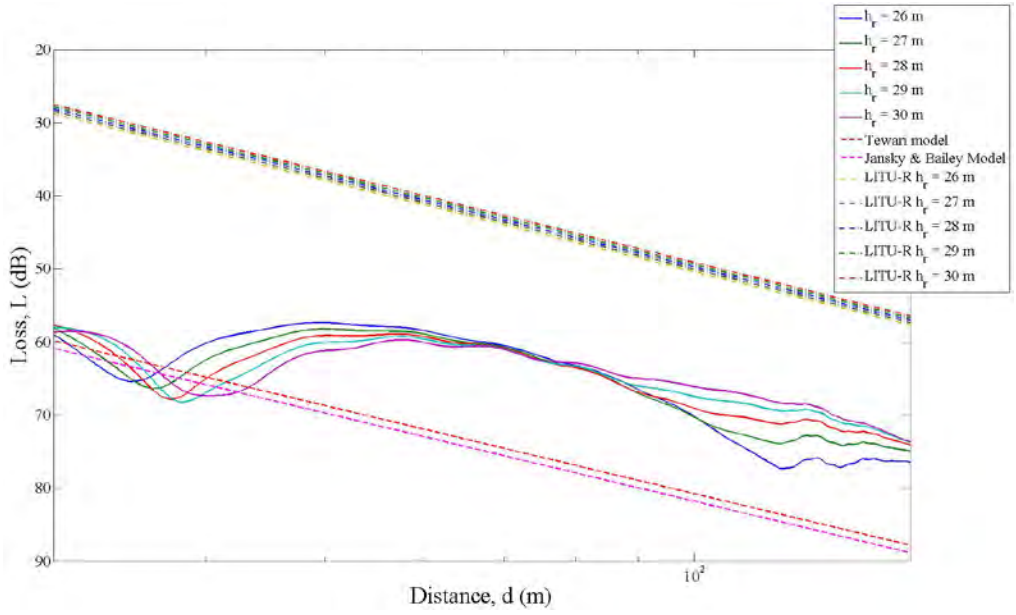

Figure 49. Loss–distance curves for h_r = 26–30 m (test case C1).

From Figures 48 and 49, it is observed that, as the receiver height increases, the loss–distance curves for the simulated results exhibit a downward shift and move closer to the curves predicted by Tewari's model and the Jansky and Bailey model.

For test case C2, the simulated power flow plot of the fields along the *x*-*z* plane (i.e., y = 0 m) in the dielectric block is shown in Figure 50. The transmitter antenna is sited at 5 m above ground.

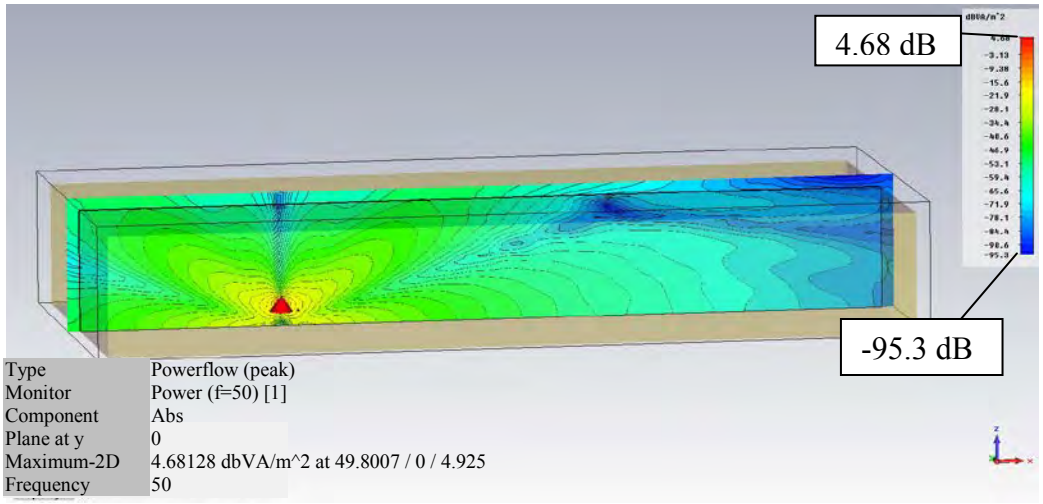

Figure 50. Power flow plot at y = 0 m for test case C2.

For test case C2, the loss–distance curves for different values of h_r are shown in Figures 51–53.

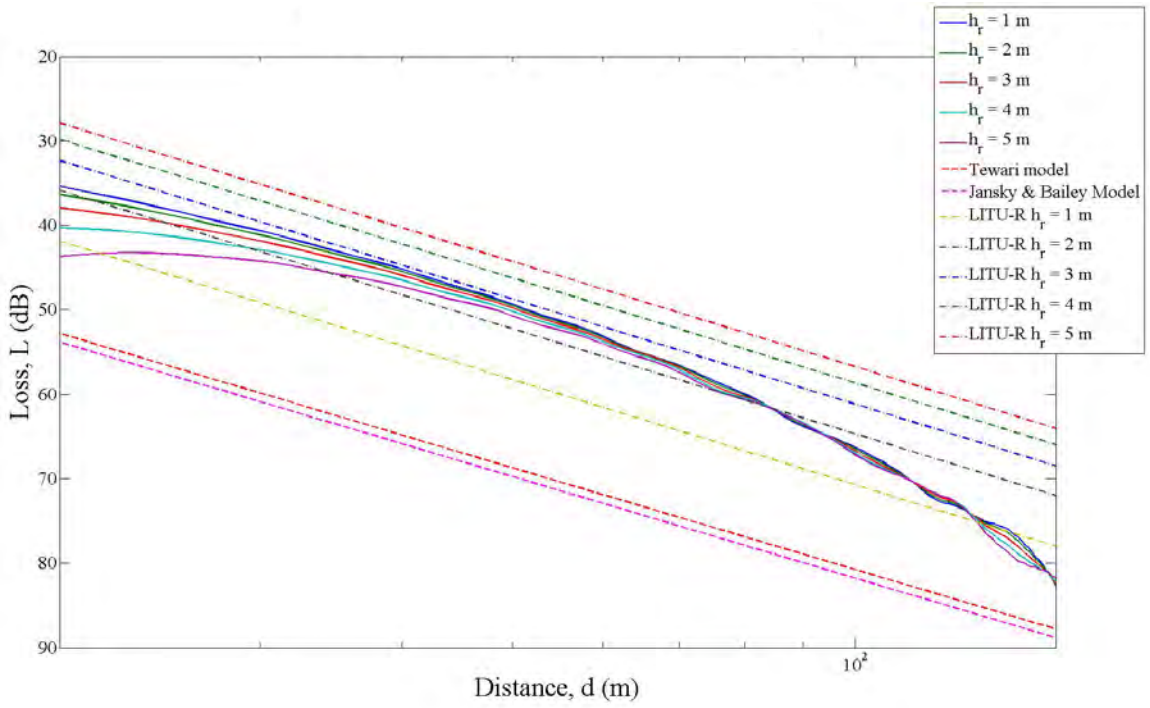

Figure 51. Loss–distance curves for h_r = 1–5 m (test case C2).

From Figure 51, when the receiver is at a height of 1–5 m, it is observed that the loss–distance curves for the simulated results are bunched together. The curves for the simulated results are closer to the curves for the LITU-R model than the curves for both Tewari's model and the Jansky and Bailey model.

From Figures 52 and 53, it is observed that, as the receiver height increases, the loss–distance curves for the simulated results exhibit a downward shift and move closer to the curves predicted by Tewari's model and the Jansky and Bailey model.

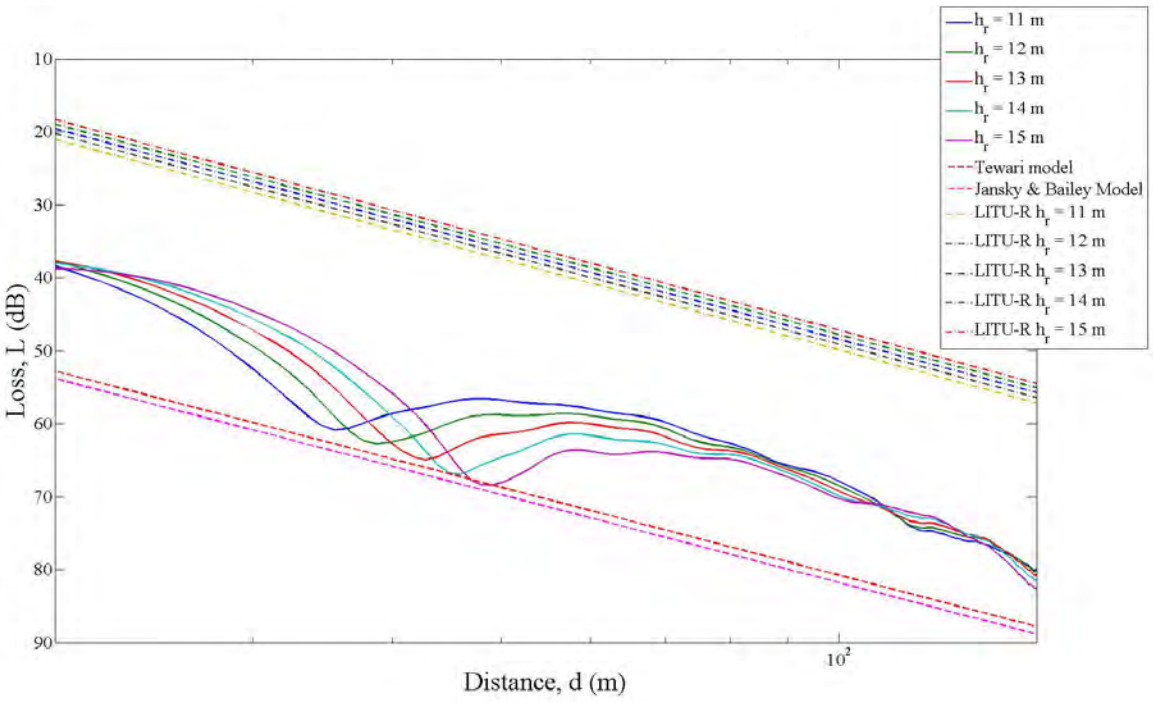

Figure 52. Loss–distance curves for h_r = 11–15 m (test case C2).

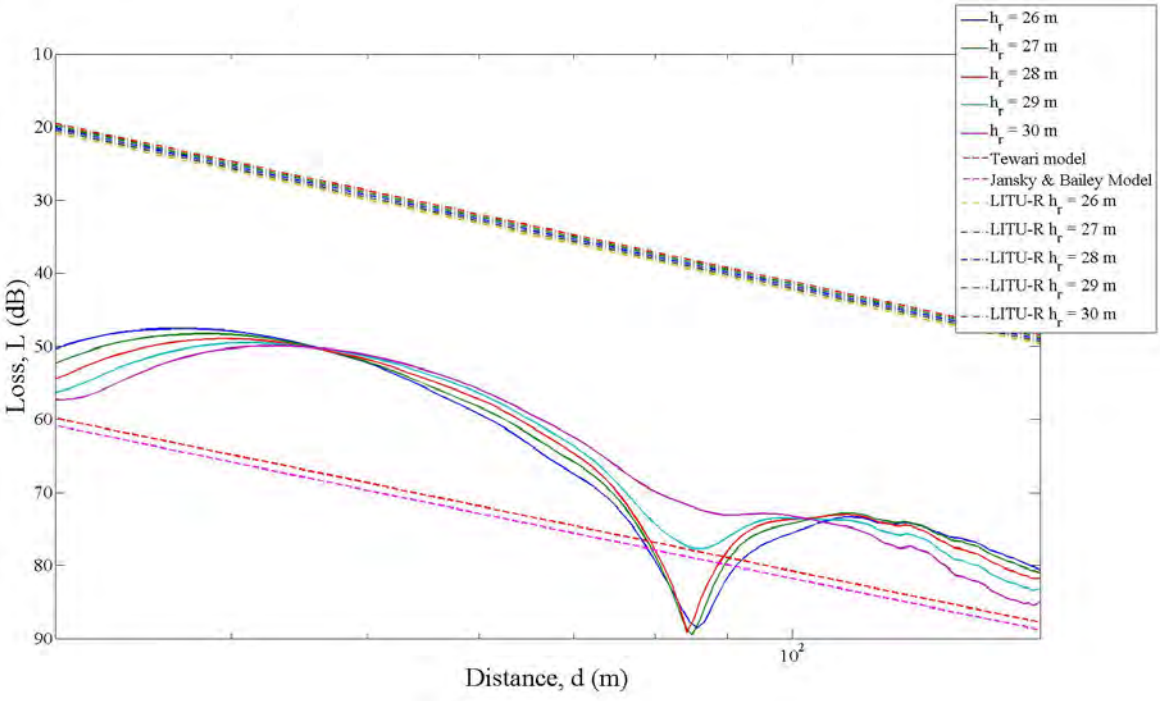

Figure 53. Loss–distance curves for h_r = 26–30 m (test case C2).

For test case C3, the simulated power flow plot of the fields along the *x*-*z* plane (i.e., y = 0 m) in the dielectric block is shown in Figure 54. The transmitter antenna is sited at 10 m above ground.

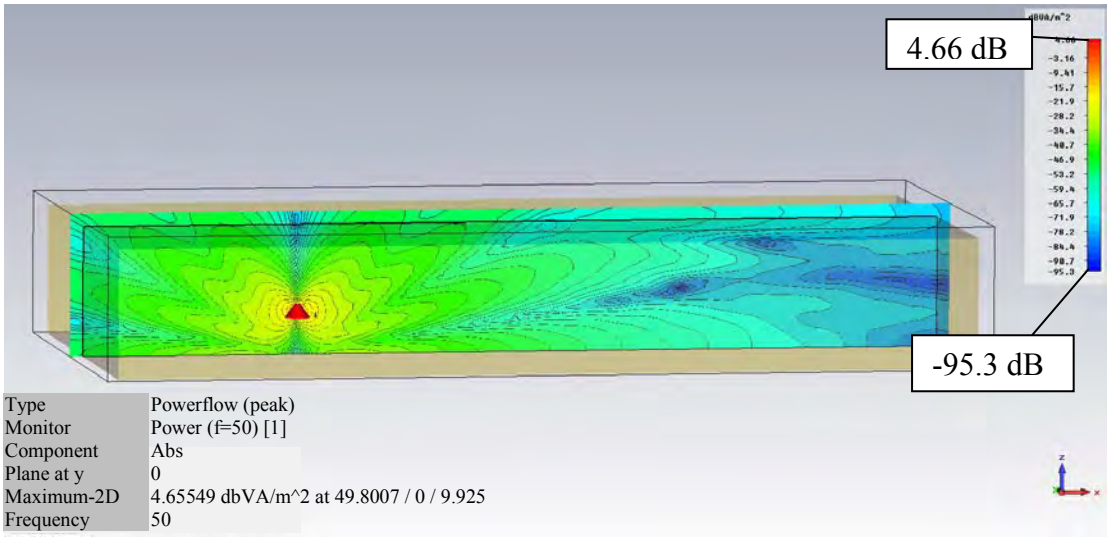

Figure 54. Power flow plot at y = 0 m for test case C3.

For test case C3, the loss–distance curves for different values of h_r are shown in Figures 55–57.

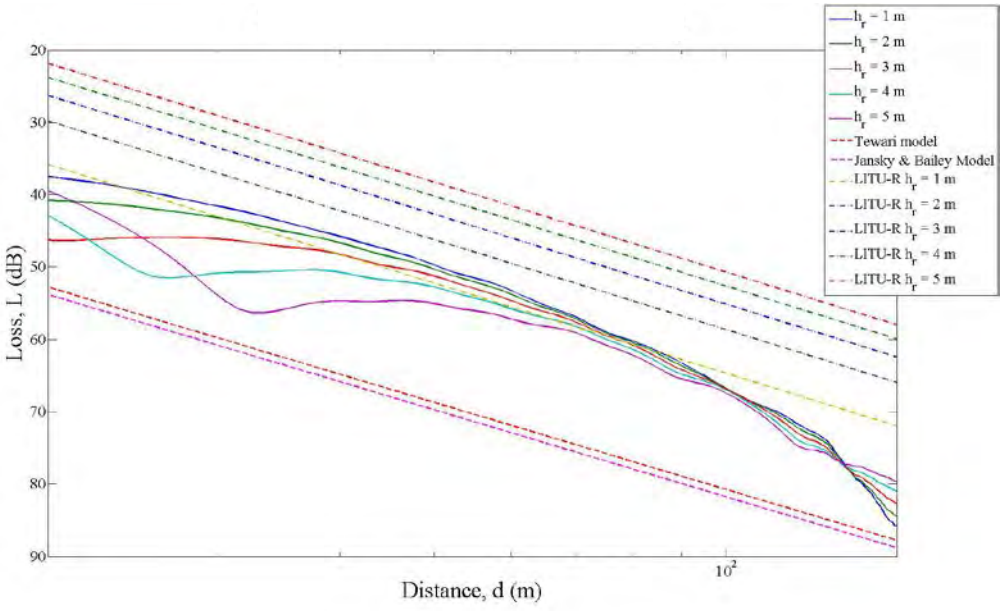

Figure 55. Loss–distance curves for h_r = 1–5 m (test case C3).

From Figure 55, when the receiver is at a height of 1–5 m and separation distance of 40–110 m from the transmitter, it is observed that the loss–distance curves for the simulated results are closer to the curves for the LITU-R model than the curves for both Tewari's model and the Jansky and Bailey model.

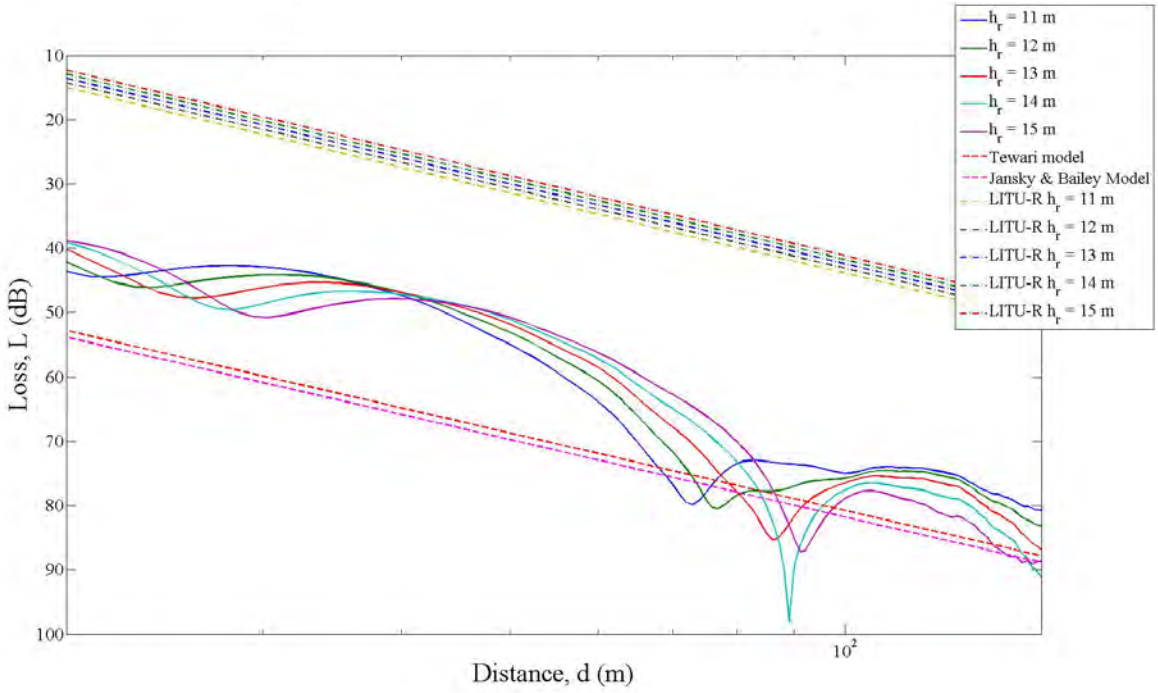

Figure 56. Loss–distance curves for h_r = 11–15 m (test case C3).

From Figures 56 and 57, it is observed that, as the receiver height increases from 11–30 m, the loss–distance curves for the simulated results are fairly similar. The curves are closer to the curves predicted by Tewari's model and the Jansky and Bailey model than the LITU-R model.

For test case C4, the simulated power flow plot of the fields along the *x*-*z* plane (i.e., y = 0 m) in the dielectric block is shown in Figure 58. The transmitter antenna is sited at 20 m above ground.

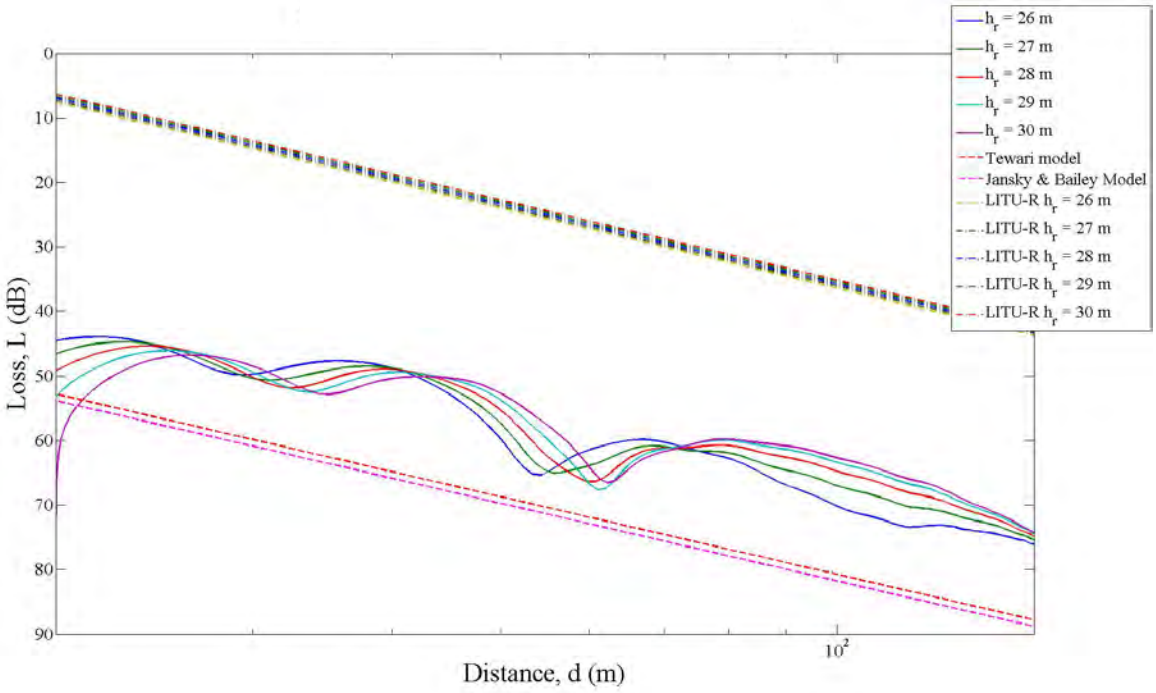

Figure 57. Loss–distance curves for h_r = 26–30 m (test case C3).

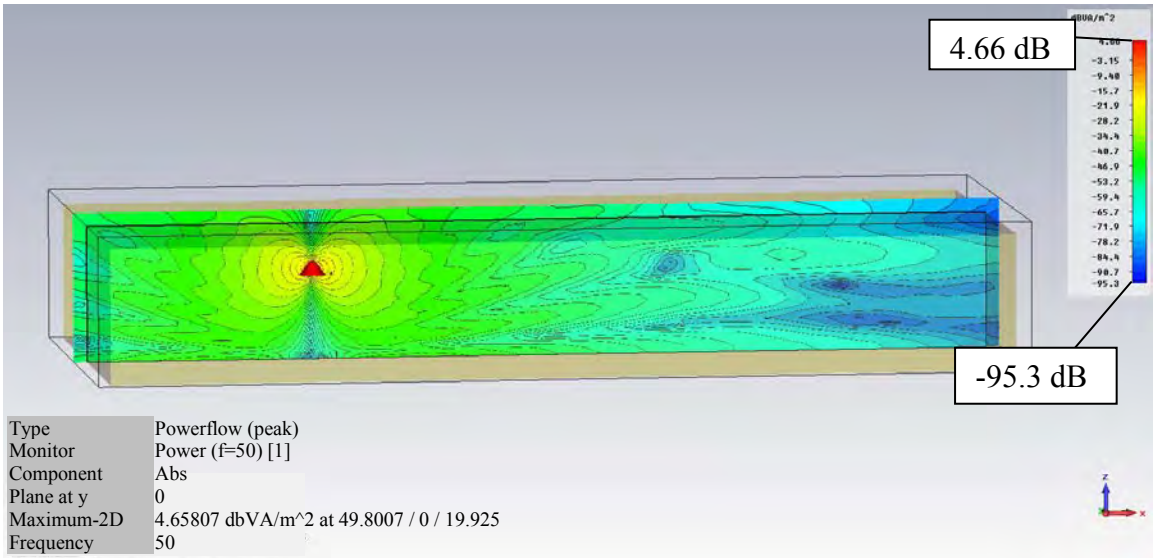

Figure 58. Power flow plot at y = 0 m for test case C4.

For test case C4, the loss–distance curves for different values of h_r are shown in Figures 59–61.

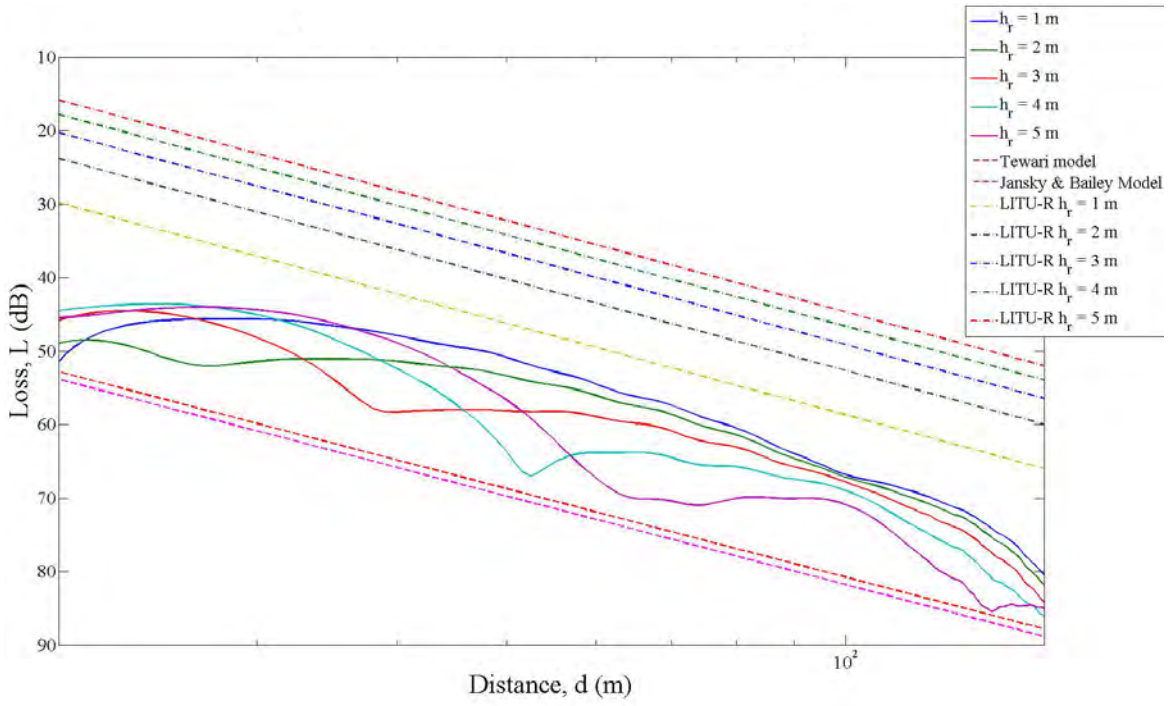

Figure 59. Loss–distance curves for h_r = 1–5 m (test case C4).

From Figure 59, when the receiver is at a height of 1–5 m, it is observed that the loss–distance curves for the simulated results are between the curves for the LITU-R model and both curves for Tewari's model and the Jansky and Bailey model.

From Figures 60 and 61, it is observed that, as the receiver height increases from 11–30 m, the loss–distance curves for the simulated results are fairly similar. The curves are closer to the curves predicted by Tewari's model and the Jansky and Bailey model than the LITU-R model.

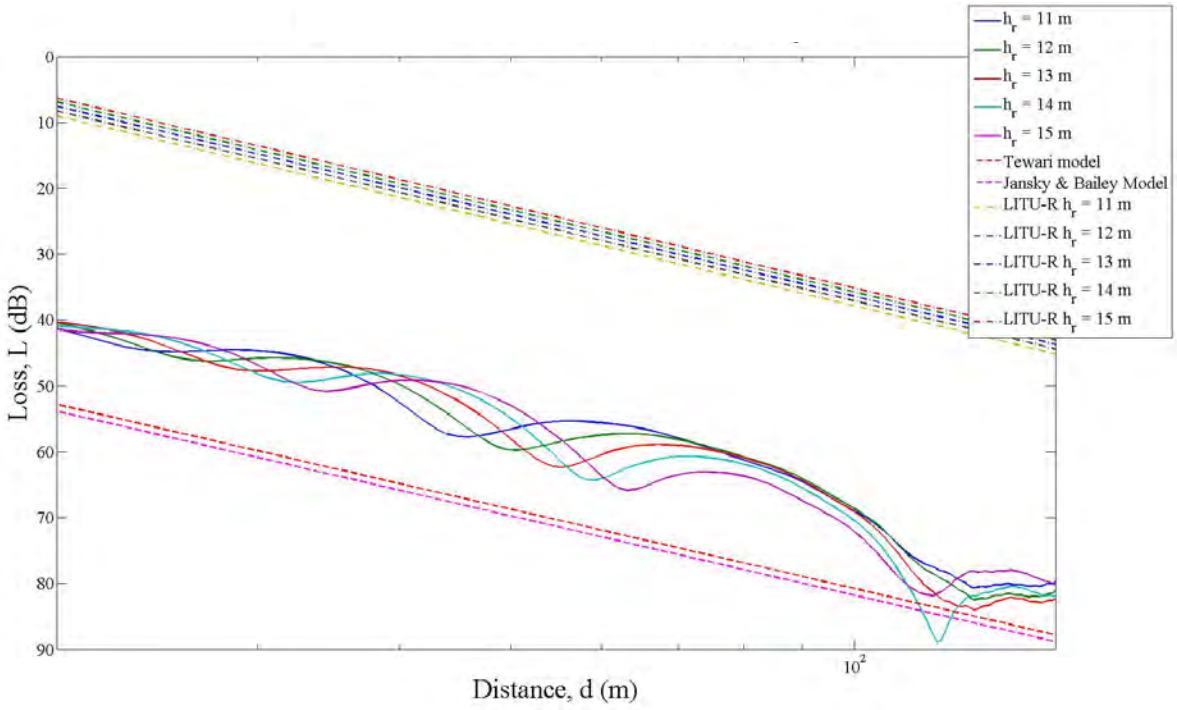

Figure 60. Loss–distance curves for h_r = 11–15 m (test case C4).

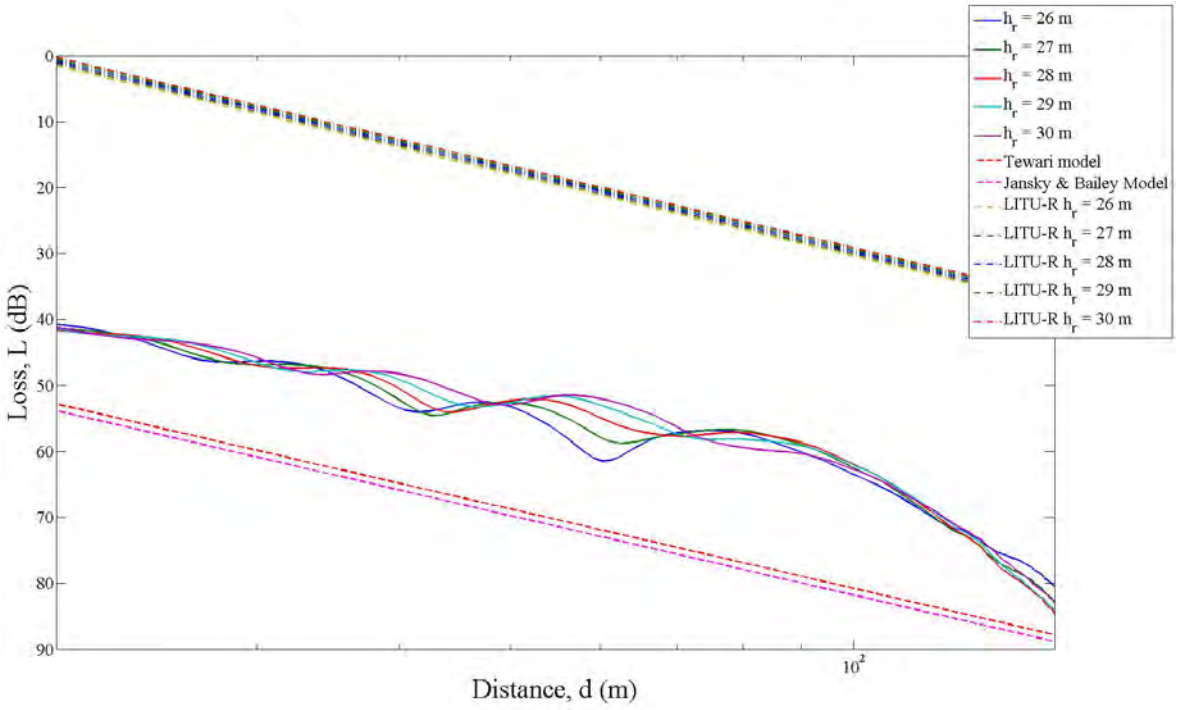

Figure 61. Loss–distance curves for h_r = 26–30 m (test case C4).

For test case C5, the simulated power flow plot of the fields along the *x*-*z* plane (i.e., y = 0 m) in the dielectric block is shown in Figure 62. The transmitter antenna is sited at 25 m above ground.

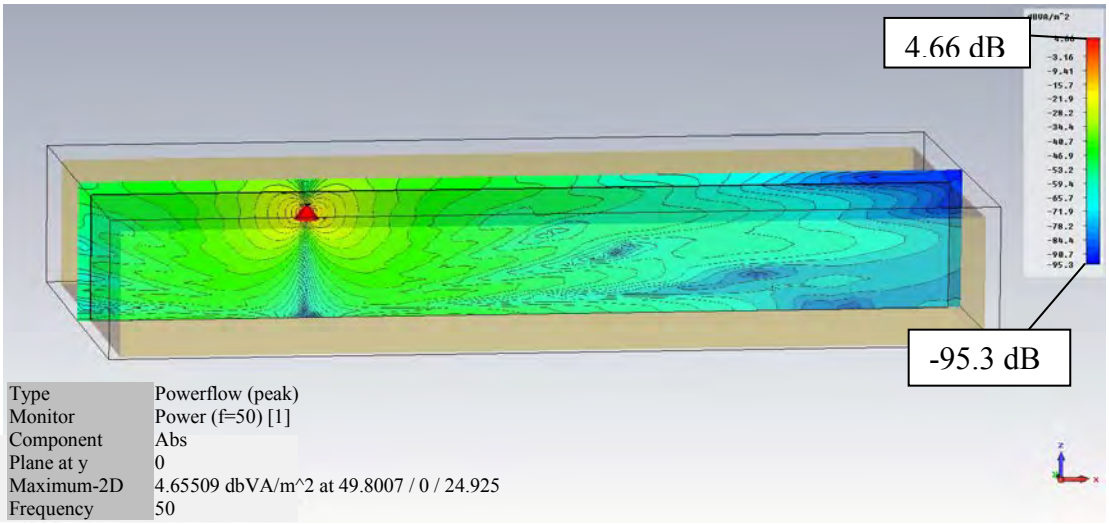

Figure 62. Power flow plot at y = 0 m for test case C5.

For test case C5, the loss–distance curves for different values of h_r are shown in Figures 63–65.

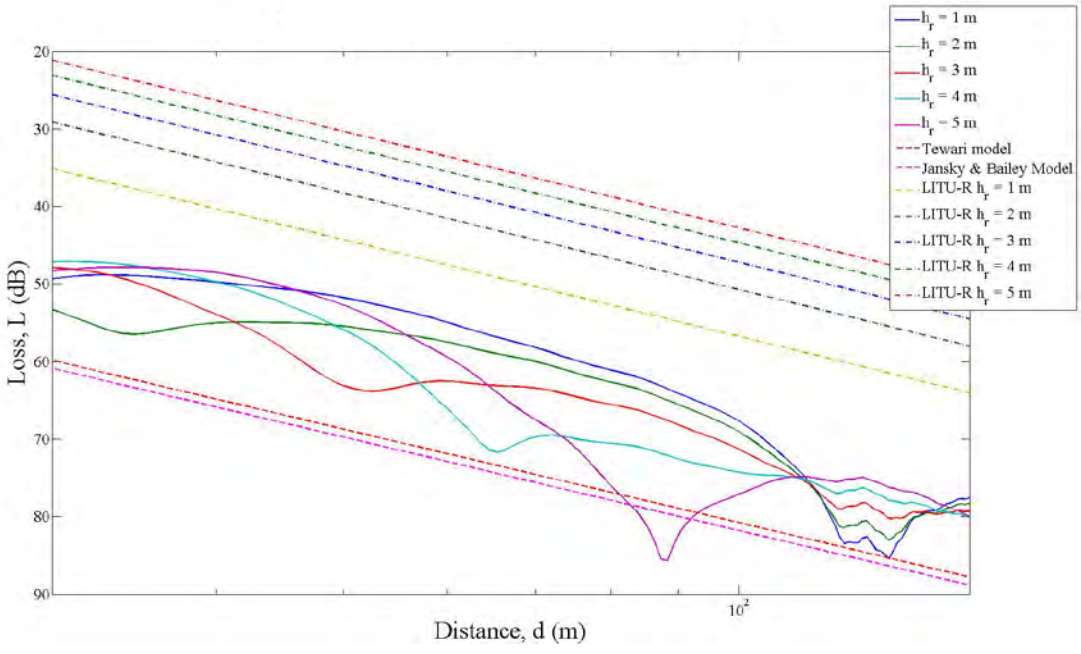

Figure 63. Loss–distance curves for h_r = 1–5 m (test case C5).

From Figure 63, it is observed that, as the receiver height increases from 1–5 m, the loss–distance curves for the simulated results exhibit a downward shift and move closer to the curves predicted by curves Tewari's model and the Jansky and Bailey model.

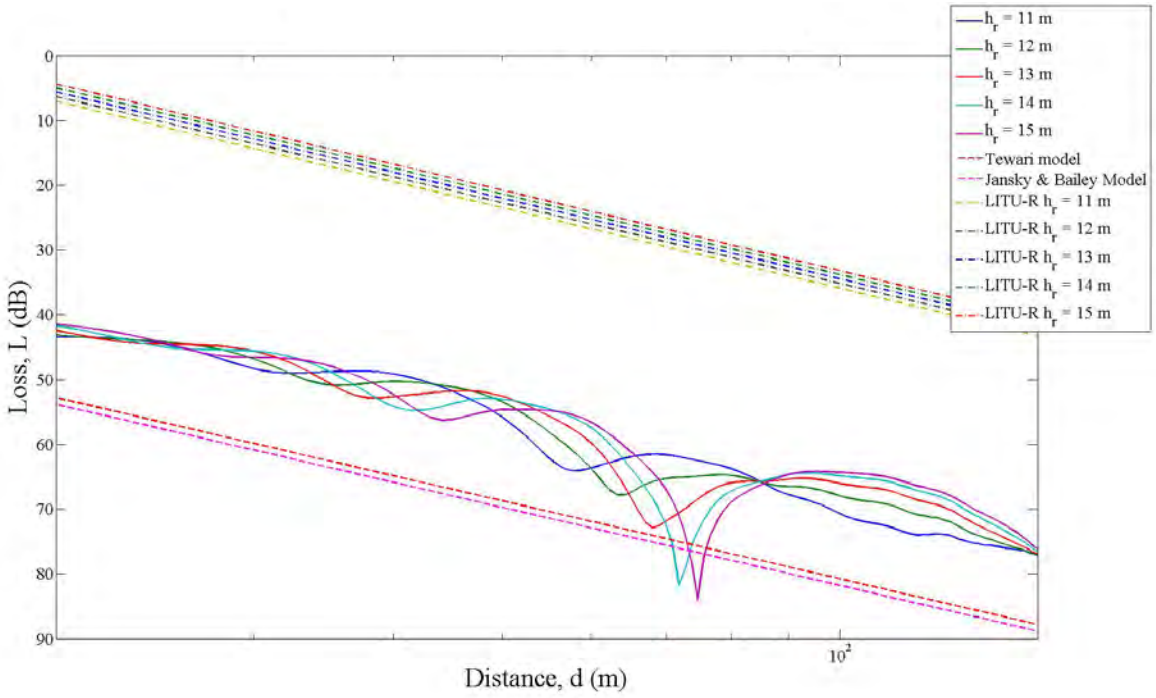

Figure 64. Loss–distance curves for h_r = 11–15 m (test case C5).

From Figures 64 and 65, it is observed that, as the receiver height increases from 11–30 m, the loss–distance curves for the simulated results are fairly similar. The curves are closer to the curves predicted by Tewari's model and the Jansky and Bailey model than the LITU-R model.

At any given point inside the foliage, the field is the sum of a direct wave and reflected wave and is given by (24). When the receiver is in foliage, the point P (as shown in Figure 8) is in foliage, and the path length for the direct wave R_0 is given by

$$R_0 = \sqrt{d^2 + \Delta h^2} \tag{27}$$

where Δh is the difference between the transmitter height, h_t (defined by the variable zd in the simulation setup) and receiver height, h_r and is expressed as

$$\Delta h = \left| h_t - h_r \right| \cdot \tag{28}$$

The path length of the reflected wave R_{12} is given

$$R_{12} = R_1 + R_2 \cdot \tag{29}$$

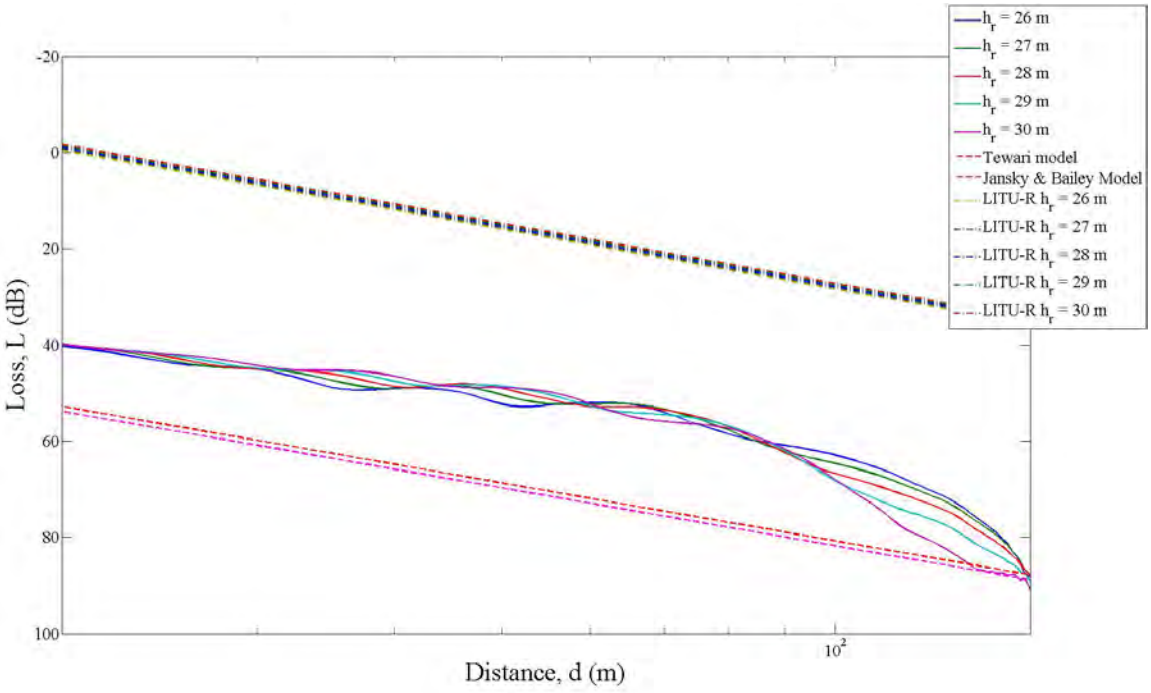

Figure 65. Loss–distance curves for h_r = 26–30 m (test case C5).

From (24), the total field at P, $E(P)$ is related to R_0 and R_{12}. In addition, a higher $E(P)$ results in a lower path loss, L. The effect of h_t and h_r on $E(P)$ and L is shown in Table 7.

From Table 7, when the transmitter and receiver at sited near the ground, the path loss is the lowest. This is substantiated by Figure 47 that represents the simulation run with both transmitter and receiver near the ground, and the loss–distance curves for the simulation results show the lowest L as compared to other simulation runs. This occurs because the direct and reflected waves are nearly in phase for a vertical dipole.

Table 7. Effect of h_t and h_r on $E(P)$ and L.

Case	h_t and h_r	R_0	R_1, R_2	R_{12}	$E(P)$	L
1	High h_t High h_r	Smaller	Larger R_1 Larger R_2	Larger	Lower	Higher
2	Low h_t Low h_r	Smaller	Smaller R_1 Smaller R_2	Smaller	Highest	Lowest
3	High h_t Low h_r	Larger	Larger R_1 Smaller R_2	Larger	Lower	Higher
4	Low h_t High h_r	Larger	Smaller R_1 Larger R_2	Larger	Lower	Higher

For the scenarios described by cases 3 and 4 in Table 7, the path loss is approximately the same since the effect of a smaller R_1 is negated by a larger R_2 or vice versa. Similarly for case 1, the effect of a larger path length for the reflected wave is compensated by a smaller path length for the direct wave and results in a path loss comparable to cases 3 and 4. This is evidenced from the simulation results in test cases C2, C3, C4 and C5.

4. Observations

From the various simulation runs, it is observed that the simulated results for sparse foliage (i.e., $\varepsilon_r = 1.01$ and $\sigma = 10^{-5}$ S/m) does not closely follow the three empirical models, i.e., Tewari's model, the Jansky and Bailey model or the LITU-R model. Generally, for denser foliage (i.e. $\varepsilon_r \geq 1.05$ and $\sigma \geq 10^{-5}$ S/m), both Tewari's model and the Jansky and Bailey model are better approximations to the simulation results than the LITU-R empirical model for receiver situated at higher heights. Generally, the LITU-R model gives a better approximation to the simulation results for both transmitter and

receiver situated near the ground. While the simulated path losses do not exactly match those given by the three empirical models, the difference between the simulated result and empirical result is approximately 10 dB in most cases. This could be due to various factors. While the empirical models were proposed to be an approximation to the loss experienced for foliage propagation, it should be noted that these models were formulated based on measured data from foliage in a particular geographical location. Given the lack of knowledge on the electrical properties (ε_r and σ) of the actual foliage, assumed values of the electrical properties were used in the simulations. Hence, it was expected that there would be difference between the simulated results and empirical figures. Nevertheless, given the observed difference, the simulation models can only be considered as a rough approximation to actual foliage propagation.

B. COVERAGE DIAGRAMS

In this section, the effects of the forest on the coverage of a transmitting antenna immersed in foliage are examined. The coverage diagram for a transmitting antenna can be obtained from the electric field plots of a CST simulation. A simulation is first carried out for the transmitting antenna in free space. This is to establish a baseline for comparison purposes. Subsequent simulation runs are carried out to examine the effects of the forest on radiowave propagation with respect to height of the transmitter in foliage and forest's electrical properties. The general observations for the simulation results are discussed at the end of this section.

1. Transmitter in Free Space

A dipole antenna is set up as the transmitting antenna. The antenna's height is very close to the ground. The ground is represented by the *x*-*y* plane ($z_{\min} = 0$) with the boundary condition configured as "*electric (Et = 0)*". The simulation is carried out with the antenna at four different heights. The heights h_t are 2 m, 5 m, 10 m and 20 m. The values used to set up the test case in CST are summarized in Table 8. Due to practical reasons, an adjacent volume of space is defined as free space to define the computational domain for the simulation of fields in free space. This is achieved via the background

properties in CST, and the settings are shown in Figure 66. *E-field* and *Power* monitors are added to monitor the fields at a frequency of 50 MHz.

Table 8. Values used to set-up dipole antenna transmitting in free space.

	Parameter	Description	Value
1	$\ell 2$	Length of dipole antenna	2.6 m
2	f	Frequency of interest	50 MHz
3	xd	x-coordinate of dipole center	50 m
4	yd	y-coordinate of dipole center	0 m
5	zd	z-coordinate of dipole center	2, 5, 10 or 20 m

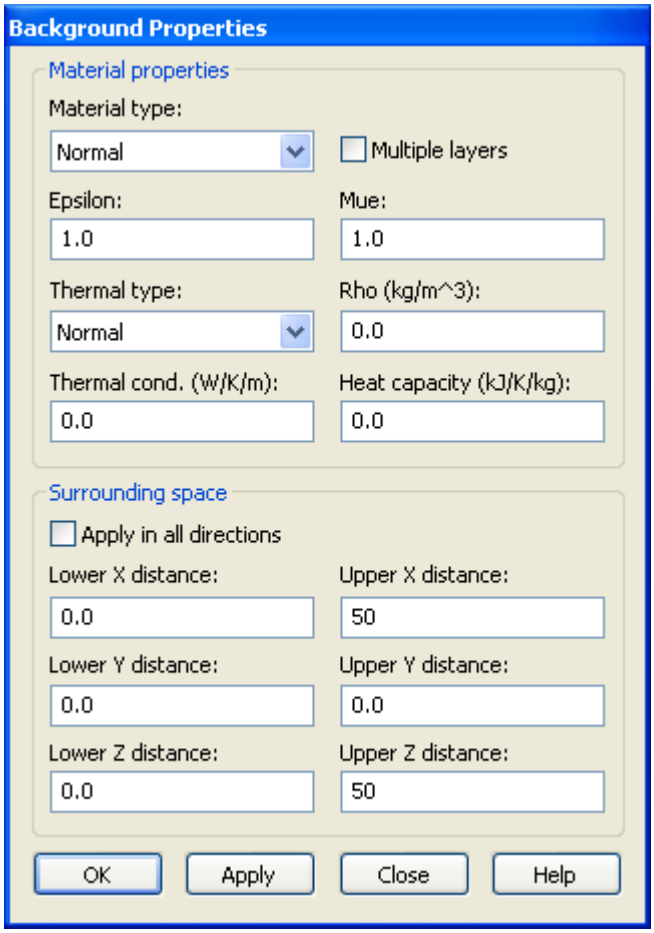

Figure 66. Setting for background properties (for coverage diagram test cases).

The generated E-fields for the dipole antenna at heights of 2 m, 5 m, 10 m and 20 are shown in Figures 67, 68, 69 and 70, respectively.

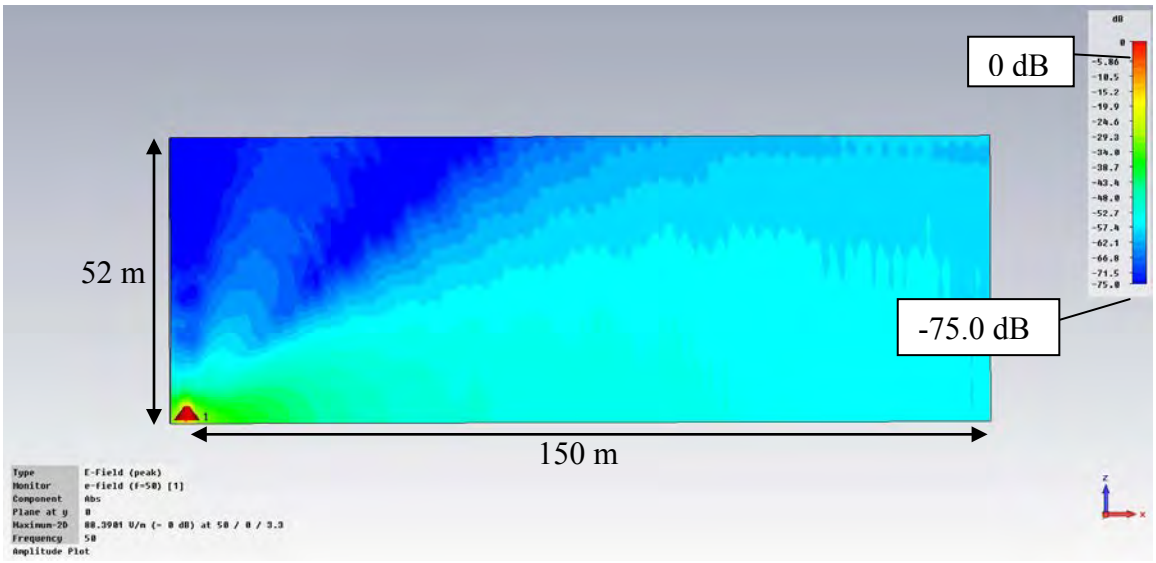

Figure 67. Coverage diagram for a dipole antenna in free space (height 2 m).

In Figure 67, the transmitting antenna is at a height of 2 m. It can be observed that there is only one main lobe radiating out from the antenna.

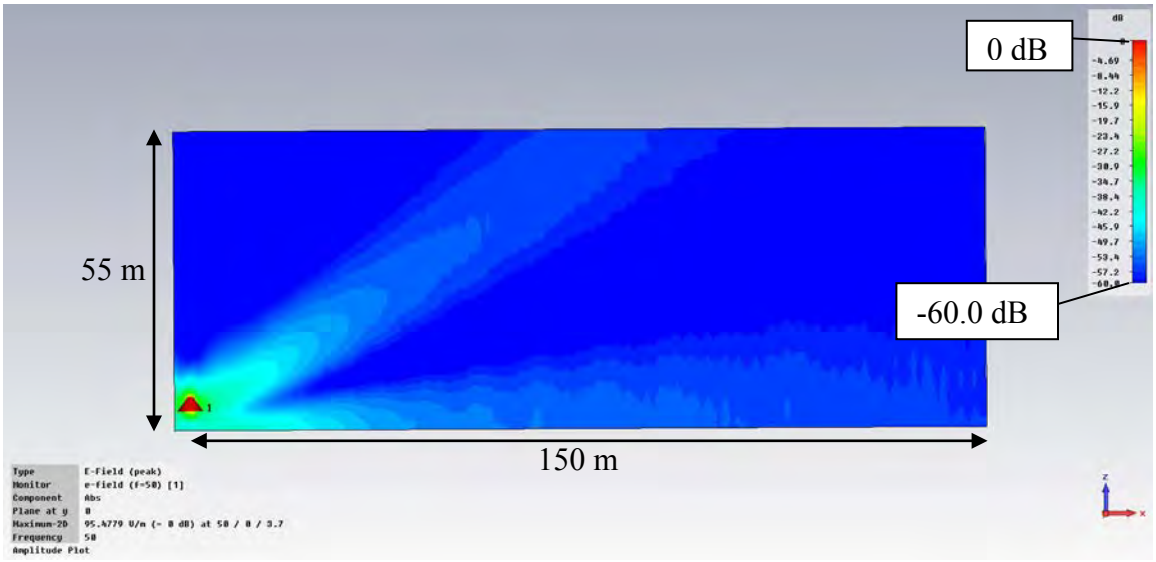

Figure 68. Coverage diagram for a dipole antenna in free space (height 5 m).

In Figure 68, the transmitting antenna is at a height of 5 m. It can be observed that there are two main lobes radiating out from the antenna. One of the lobes is

seemingly along the ground, while the other is at an angle of approximately 30^{o} from the ground.

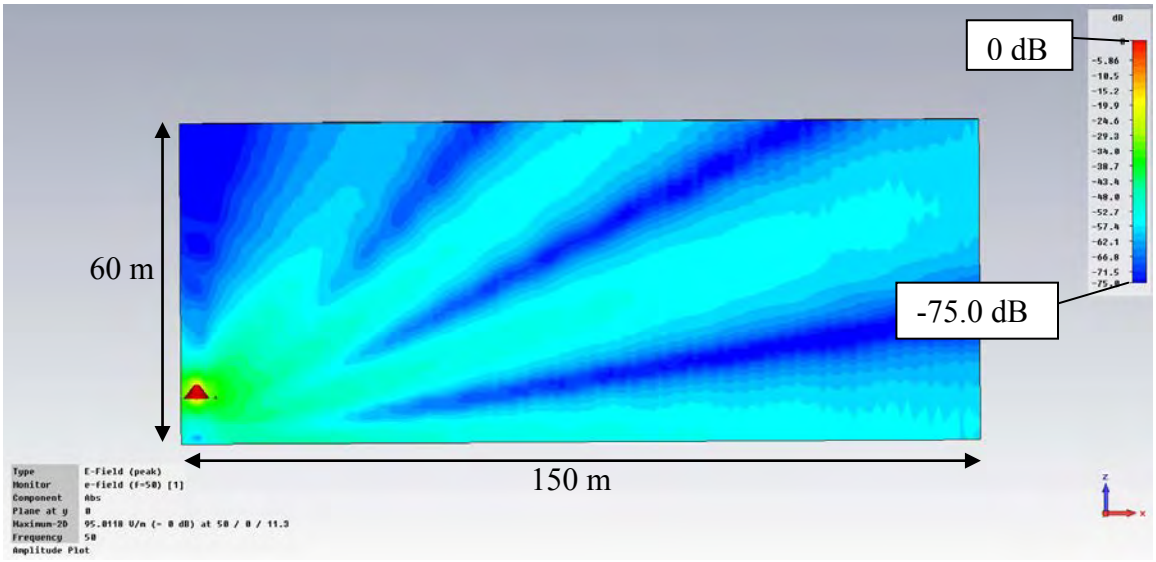

Figure 69. Coverage diagram for a dipole antenna in free space (height 10 m).

In Figure 69, the transmitting antenna is at a height of 10 m. Compared to Figure 28, it can be observed that the number of lobes increases as the antenna height increases. In this case, three main lobes can be observed.

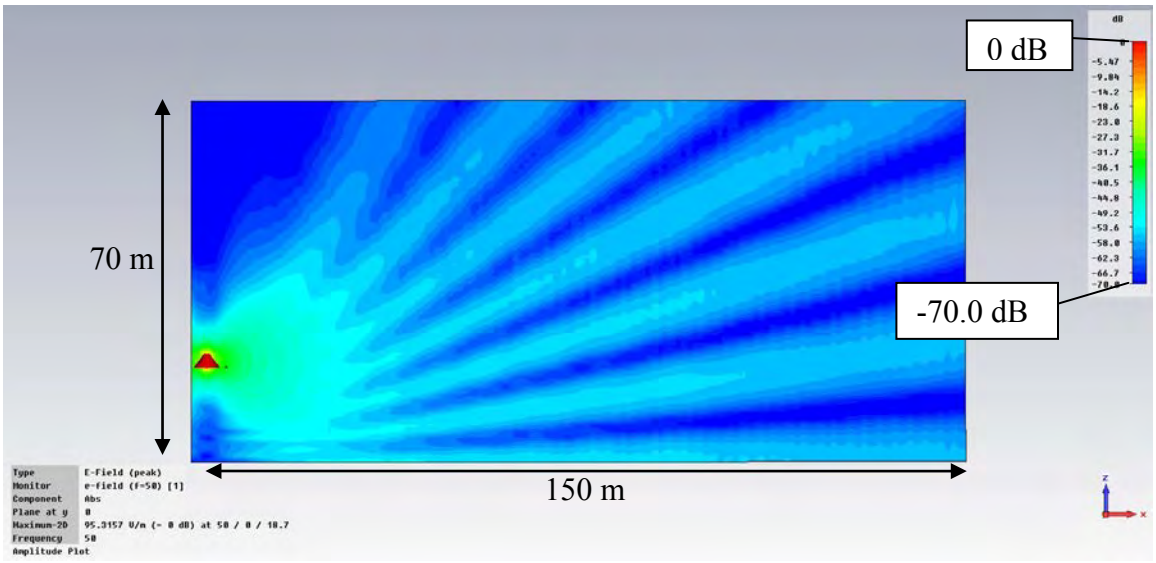

Figure 70. Coverage diagram for a dipole antenna in free space (height 20 m).

In Figure 70, the transmitting antenna is at a height of 20 m. Compared to Figures 28 and 29, there are more lobes and the lobes are also narrower.

2. Transmitter in Forest (ε_r = 1.065 and σ = 0.000135 S/m)

In this test case, the objective is to examine the coverage diagram with the transmitting dipole antenna immersed in foliage. The antenna is set up in the same manner as the free space test case. A rectangular dielectric block is added to the model. The antenna and forest are created using the values shown in Table 9. Free space is defined around the dielectric block using the settings in Figure 66. The amount of free space added is 50 m above the forest (i.e., along the positive *z*-direction) and 50 m to the right of the forest (i.e., along the positive *x*-direction). The constructed model in CST is shown in Figure 71.

Table 9. Values used to set up model for examining coverage diagram with transmitting antenna immersed in foliage.

	Parameter	Description	Value
1	$\ell 2$	Length of dipole antenna	2.54 m
2	f	Frequency of interest	50 MHz
3	H	Height of dielectric block	25 m
4	L	Length of dielectric block	300 m
5	W	Width of dielectric block	100 m
6	xd	x-coordinate of dipole center	50 m
7	yd	y-coordinate of dipole center	0 m
8	zd	z-coordinate of dipole center	2, 5, 10 or 20 m
9	ε_r	Relative permittivity	1.065
10	σ	Conductivity	0.000135 S/m

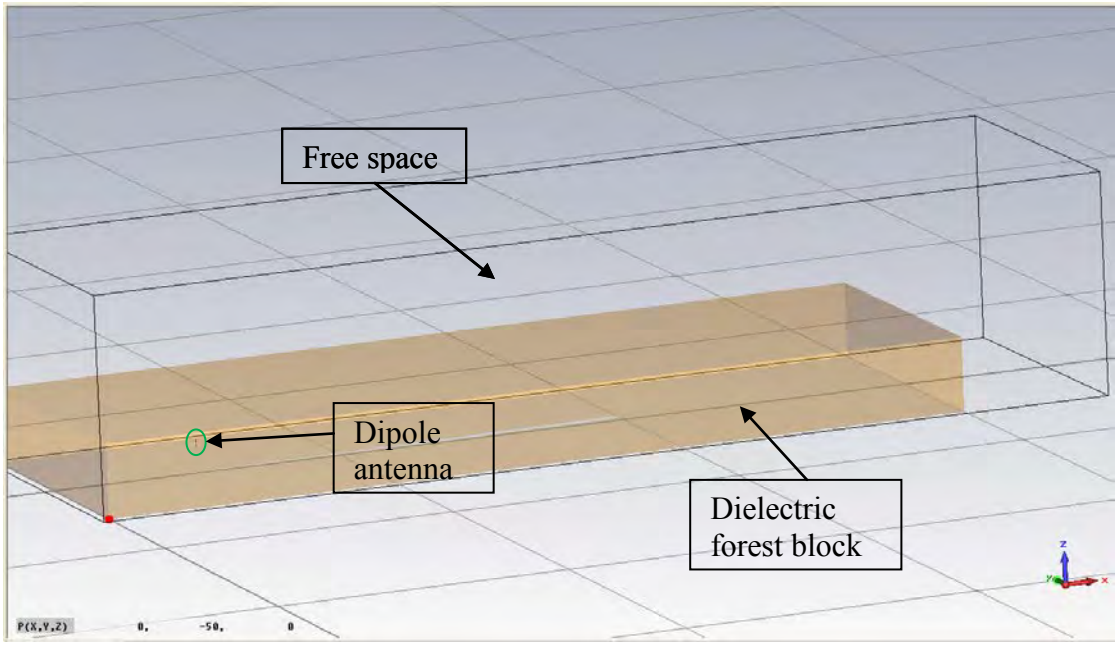

Figure 71. Dipole antenna immersed in dielectric forest block and free space outside the block.

The simulation is executed for varying antenna heights of 2, 5 , 10 and 20 m with the corresponding E-field plots (generated by CST) shown in Figures 72, 73, 74 and 75, respectively.

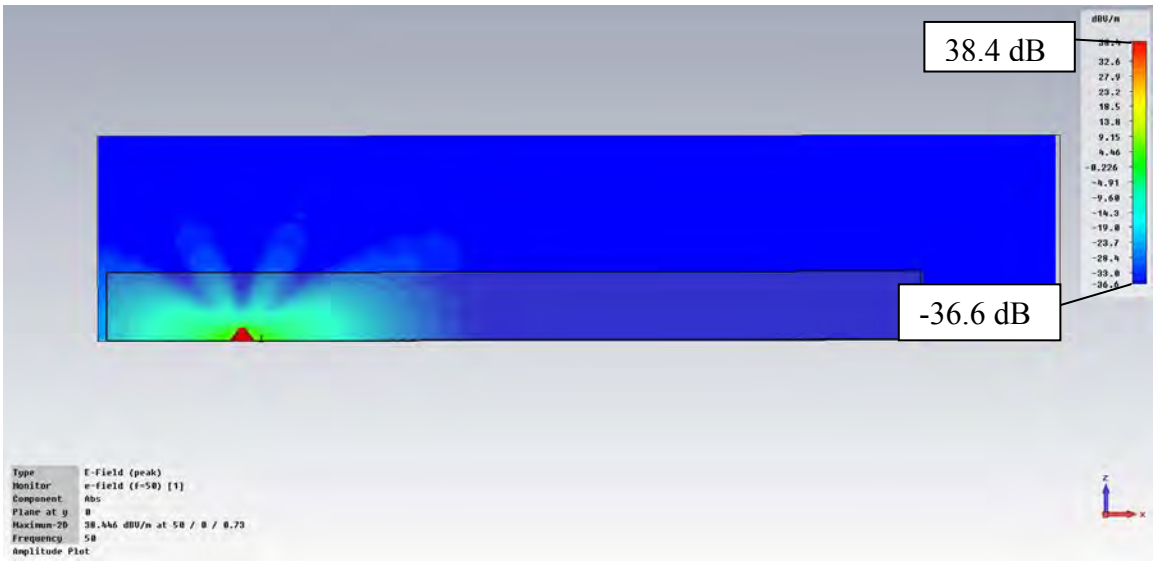

Figure 72. Coverage diagram for dipole antenna in foliage (height 2 m).

Comparing Figure 72 and Figure 67, we observe that the addition of the forest dielectric block causes the main lobe (i.e. maxima) along the ground to be shorter. For a point located at a separation distance of 50 m from the transmitter and just above the ground, the E-field strength is −24.5 dBV/m in Figure 72 versus −13.7 dBV/m in Figure 67. This is due to the attenuation as the EM wave propagates through the lossy dielectric media.

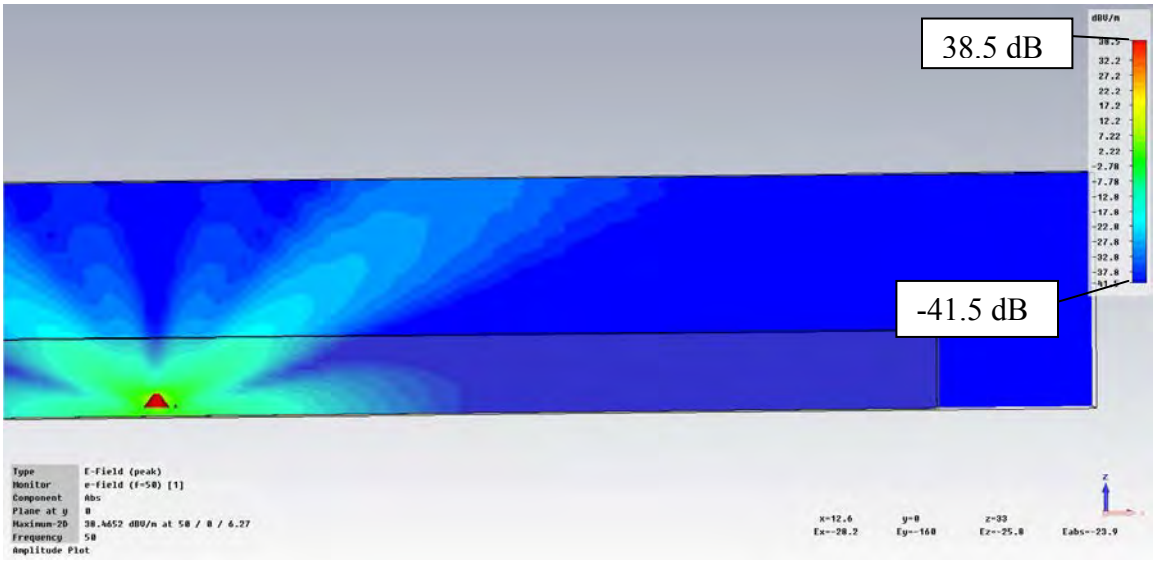

Figure 73. Coverage diagram for dipole antenna in foliage (height 5 m).

Comparing Figure 73 with Figure 68, we observe that there are still two main lobes in the coverage diagram. However, for the case of the transmitter immersed in foliage, the maximum of each lobe is reduced. At a point given by the coordinates x = 100 m, y = 0 m and z = 35 m just above the foliage block along one of the maxima, the E-field strength is −25.1 dBV/m in Figure 73 versus −15.4 dBV/m in Figure 68. This is because the EM waves experience a higher attenuation when travelling through the lossy dielectric media as compared to free space.

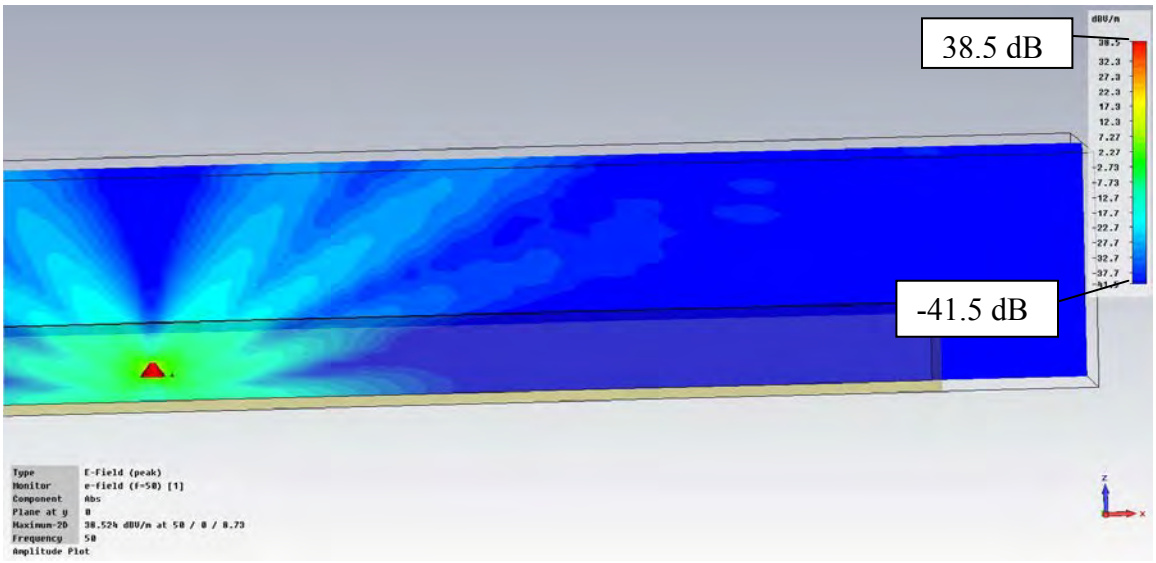

Figure 74. Coverage diagram for dipole antenna in foliage (height 10 m).

Comparing Figure 74 with Figure 69, we observe that there are still two main lobes in the coverage diagram. However, for the case of the transmitter immersed in foliage, the maximum of each lobe is reduced. At a point given by the coordinates x = 100 m, y = 0 m and z = 38 m above the foliage block along one of the maxima, the E-field strength is −24.7 dBV/m in Figure 74 versus −15.6 dBV/min Figure 69. This is because the EM waves experience a higher attenuation when travelling through the lossy dielectric media as compared to free space.

In Figure 75, the main lobes can be faintly observed. While the number of main lobes is comparable to the free space case (Figure 70), the maxima of the main lobes are greatly reduced. At a point given by the coordinates x = 100 m, y = 0 m and z = 28 m above the foliage block along one of the maxima, the E-field strength is −22.4 dBV/m in Figure 75 versus −15.4 dBV/m in Figure 70. The lobes are due to the reflections of EM waves by the ground. As the antenna is sited higher, the path length that the reflected wave has to travel becomes longer. When the transmitter is sited in the lossy dielectric media, the reflected waves experience higher attenuation as compared to the free space case. This results in much shorter lobes (as evidenced in Figure 75).

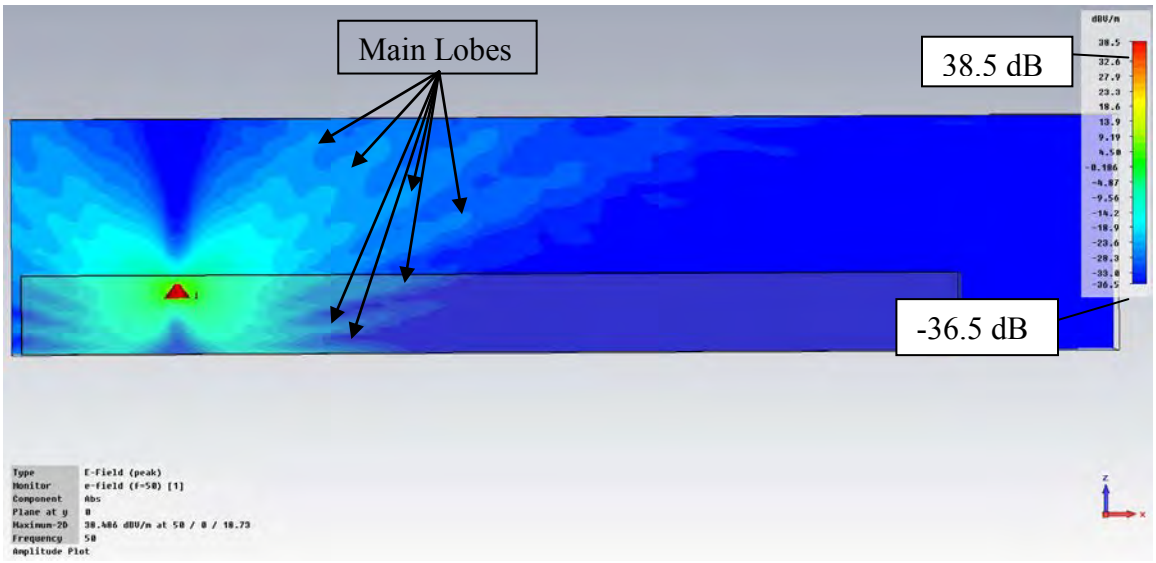

Figure 75. Coverage diagram for $\lambda/2$ dipole antenna in foliage (height 20 m).

3. Transmitter in Forest ($\varepsilon_r = 1.15$ *and* $\sigma = 0.00015$ *S/m)*

In this test case, the coverage diagram is examined with higher ε_r and σ values, which represent denser foliage. The antenna is set up in the same manner as the free space test case. A rectangular dielectric block is added to the model. The antenna and forest are created using the values shown in Table 10. Free space is defined around the dielectric block using the settings in Figure 76. The amount of free space added is 50 m above the forest (i.e., along the positive z-direction) and 50 m to the right of the forest (i.e., along the positive x-direction). The constructed model in CST is similar to that shown in Figure 71.

The simulation is executed for varying antenna heights of 2, 5 , 10 and 20 m with the corresponding E-field plots (generated by CST) shown in Figures 76, 77, 78 and 79, respectively.

Table 10. Values used to set up model for examining coverage diagram with transmitting antenna immersed in foliage.

	Parameter	Description	Value
1	$\ell 2$	Length of dipole antenna	2.54 m
2	f	Frequency of interest	50 MHz
3	H	Height of dielectric block	25 m
4	L	Length of dielectric block	300 m
5	W	Width of dielectric block	100 m
6	xd	x-coordinate of dipole center	50 m
7	yd	y-coordinate of dipole center	0 m
8	zd	z-coordinate of dipole center	2, 5, 10 or 20 m
9	ε_{r_C}	Relative permittivity	1.15
10	σ	Conductivity	0.00015 S/m

Comparing Figure 76 and Figure 72, we observe that the main lobe (i.e., maxima) along the ground is slightly shorter in the denser foliage block. For a point located at a separation distance of 50 m from the transmitter and just above the ground, the E-field strength is −25 dBV/m in Figure 72 versus −24.5 dBV/m in Figure 72. This is due to the increased attenuation of the wave in the denser foliage with higher values of ε_r and σ.

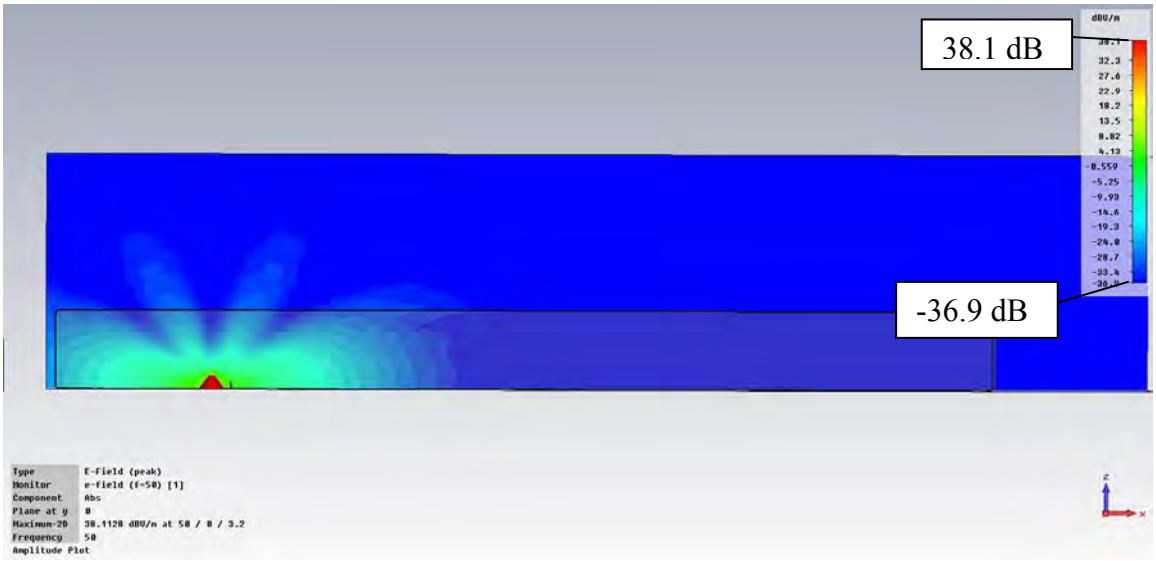

Figure 76. Coverage diagram for a dipole antenna in foliage (height 2 m).

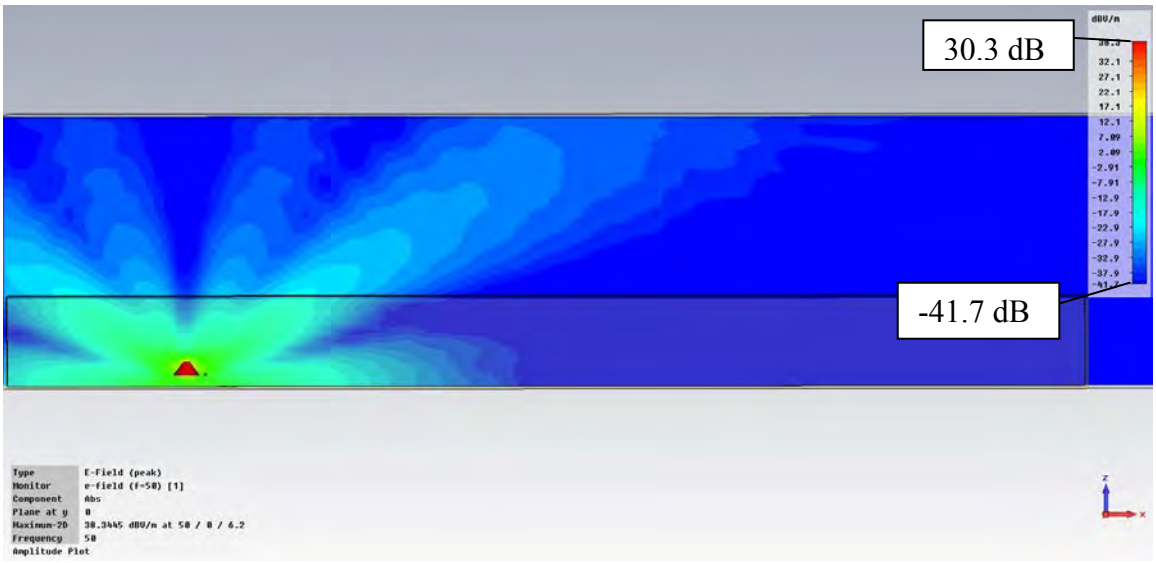

Figure 77. Coverage diagram for a dipole antenna in foliage (height 5 m).

Comparing Figure 77 with Figure 73, we observe that there are still two main lobes in the coverage diagram. However, the maximum of each lobe is reduced in the denser foliage block. At a point given by the coordinates x = 100 m, y = 0 m and z = 35 m above the foliage block along one of the maxima, the E-field strength is −25.9 dBV/m in Figure 77 versus −25.1 dBV/m in Figure 73. This is due to the increased attenuation of the wave in the denser foliage with higher values of ε_r and σ.

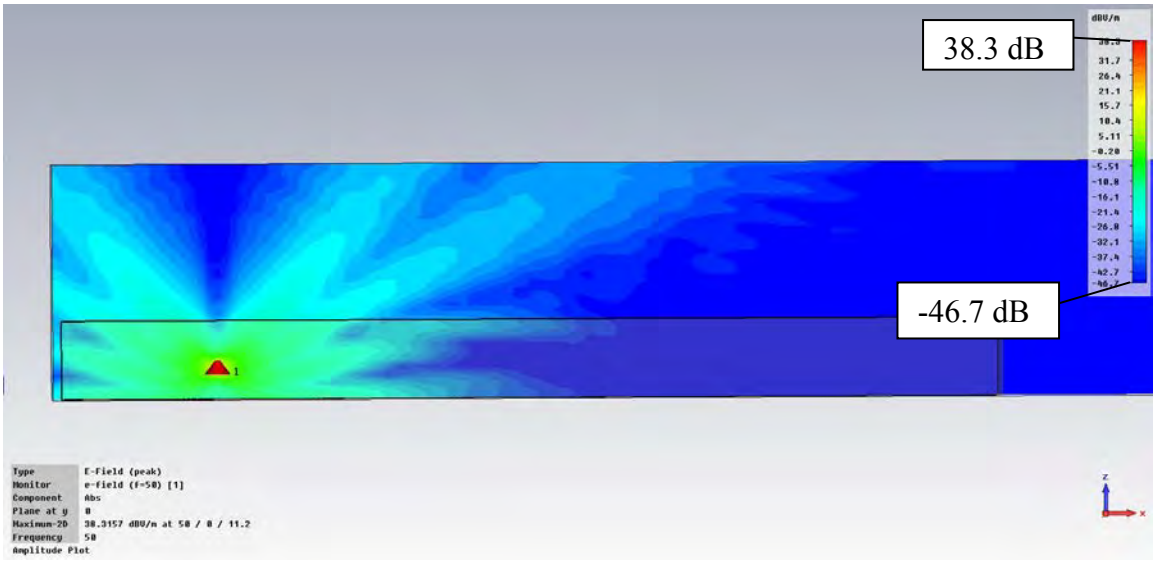

Figure 78. Coverage diagram for a dipole antenna in foliage (height 10 m).

Comparing Figure 78 with Figure 74, we observe that there are still two main lobes in the coverage diagram. However, the maximum of each lobe is reduced for the case of the denser foliage block. At a point given by the coordinates x = 100 m, y = 0 m and z = 38 m above the foliage block, the E-field strength is −27.3 dBV/m in Figure 78 versus −24.7 dBV/m in Figure 74. This is due to the increased attenuation of the wave in the denser foliage with higher values of ε_r and σ. It is also observed that the point (x = 100 m, y = 0 m, z = 38 m) does not lie exactly on the maxima. From Figure 74, the E-field strength at point (x = 101 m, y = 0 m, z = 33 m) along one of the maxima is −25 dBV/m.

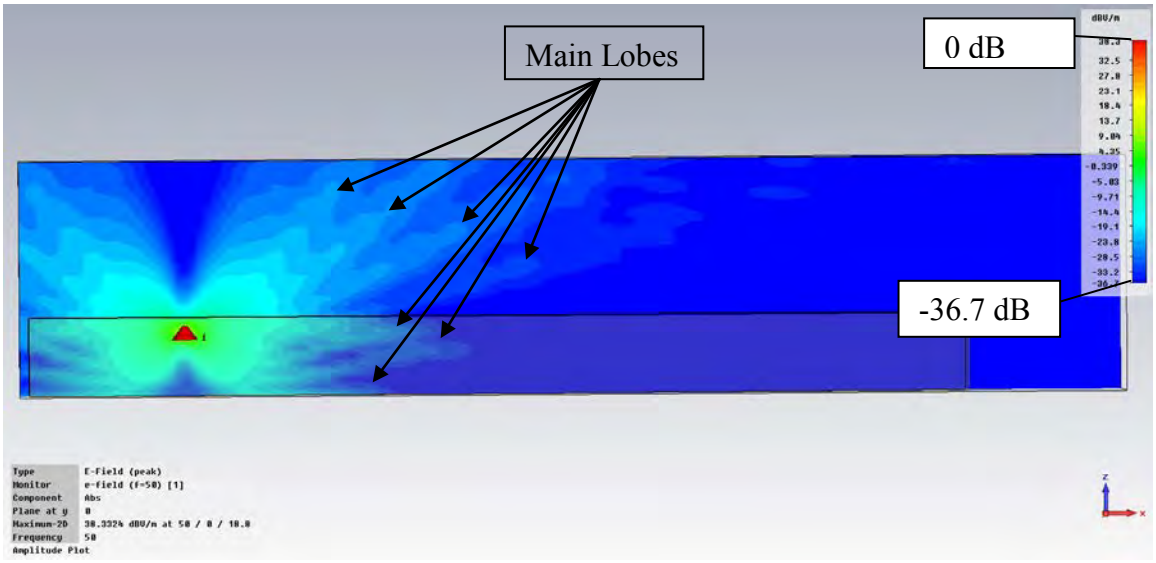

Figure 79. Coverage diagram for a dipole antenna in foliage (height 20 m).

In Figure 79, the difference between the maxima and nulls is much smaller. Hence, the lobes in Figure 79 are not easily discernible. Comparing Figure 79 with Figure 75, we observe that the number of lobes is the same. However, the maximum of each lobe is reduced for the case of the denser foliage block. At a point given by the coordinates x = 100 m, y = 0 m and z = 28 m above the foliage block, the E-field strength is −28.3 dBV/m in Figure 79 versus −22.4 dBV/m in Figure 75. This is due to the increased attenuation of the wave in the denser foliage with higher values of ε_r and σ.

4. Observations

In general, it is observed that an increase in the height of the transmitter inside the foliage results in more maxima (or lobes). In addition, the angular difference between the maxima and nulls becomes smaller as the antenna height is increased until near the canopy of the foliage. As the transmitter is sited higher up in foliage, the path length of the reflected wave in foliage becomes longer and results in a lower E-field strength. For a transmitter sited inside a denser forest with higher ε_r and σ values, the lobes are shortened as compared to ones sited in a less dense forest. This is due to the increased attenuation in denser foliage, which is a result of higher ε_r and σ values.

C. COMMENTS ON SIMULATION USING CST

General comments on using CST for the simulation of radiowave propagation in foliage are made in this section. During the conduct of the various simulation runs, we made several observations on the limitations of CST with respect to foliage simulation. The simulations are run on a personal computer (PC) equipped with Intel Xeon Quad-Core 2.53 GHz processor and 4 GB RAM memory. The PC is running on the Windows 7 Professional operating system. One main limitation on the simulation with respect to total simulation time is the maximum frequency used. In order for a simulation run to be completed within 12 hours, the frequency used should not exceed 75 MHz for a dielectric block of size 200 m by 100 m by 25 m. An increase in the maximum frequency results in an exponential increase in the number of mesh cells generated by CST. A larger number of mesh cells requires more computer resources and leads to an increase in simulation time.

D. SUMMARY

In summary, the feasibility of using a single dielectric block to model foliage propagation at the HF/VHF frequency band was examined. It was found that the proposed simulation model using CST provides a rough approximation to actual foliage propagation. From the simulation results, it was also shown that the path loss in foliage is affected by transmitter height, receiver height and foliage electrical characteristic (ε_r

and σ). The effect of foliage on a transmitter (located inside the foliage) was also examined. Compared to free space, the lobes from a transmitter in foliage is shorter due to the increased attenuation experienced by radiowave propagating in foliage. Increasing the height of a transmitter in foliage leads to a smaller difference between the maxima and nulls in the coverage diagram. In a practical application such as radar, this would improve consistency in tracking a target flying at a constant height. However, the detection range is also reduced due to the increased attenuation through foliage.

V. SUMMARY AND CONCLUSION

A. SUMMARY

The main objective of this thesis was to investigate the various simulation models for radiowave propagation in foliage environments. The simulation models are built upon the concept of representing the forest as a single dielectric block. The model is valid for frequencies up to 100 MHz. There are two important parameters that represent the forest electrical characteristics. They are ε_r and σ. These parameters affect the radiowave propagation in foliage. The values used for ε_r and σ in the simulation models are obtained from literature that document the values derived from measured data in real forest.

The EM simulation application, CST Studio Suite, is used for the simulation. After the simulation is completed, MATLAB was used to process the field data and display the loss–distance curves. The contour plots for the E-field strength are given directly by CST.

In order to examine the suitability of the proposed simulation models, three empirical models are selected for comparison with the simulated results. The models are Tewari's model, the Jansky and Bailey model and the LITU-R model. The effect of the foliage's characteristic (ε_r and σ), height of transmitter and height of receiver were also examined in this thesis.

The coverage diagram for a transmitter located inside foliage was also examined in this thesis. Different values for the foliage electrical characteristics and height of transmitter were used in the simulation runs to examine their effects on the coverage diagram

B. CONCLUSIONS

The results and data analysis from the simulation show that the proposed simulation models provide a rough approximation to radiowave propagation in an actual rainforest environment. It is feasible to model foliage using EM simulation applications.

From the simulation technique proposed in this thesis, an RF engineer could model an RF system (especially the antenna) that is being developed for operations in foliage in CST. The performance of the system could then be examined during the design phase. This would allow the designer to change the design before the actual system was built and available for actual field tests.

Based on the simulation results, it can be concluded that different values of ε_r, σ, height of transmitter and height of receiver affect the path loss in foliage. The coverage diagram for a transmitter immersed in foliage is also similarly affected by ε_r, σ and the height of the transmitter. For a transmitter located near the foliage canopy, the resulting coverage diagram has maxima and nulls closer to each other.

C. FUTURE WORK

1. Model the Forest as Multiple Smaller Blocks

Further investigation work should be carried out to determine the usefulness of higher fidelity physical model of the forest. Instead of representing the forest as a single dielectric block, the forest could be decomposed into smaller blocks. This "small block" structure would be useful for conducting foliage propagation studies at a higher frequency, where the smaller wavelength is considered to be significant compared to the dimensions of the leaves and branches. The forest could also be further sub-divided into multiple layers to represent the undergrowth layer, tree trunks and canopy layer. Different ε_r and σ could be assigned to the different layers.

As actual trees in a forest are not uniform in height, the smaller blocks could have different heights. The heights are randomly generated. This is a model of the roughness of the air-canopy interface. Simulation could be conducted to investigate the effect of the roughness (i.e., non-uniform canopy heights) on the propagation of lateral waves along the air-canopy interface.

2. Perform the Simulation using FEKO

Another possibility for future work is to conduct the simulation with another EM simulation application such as FEKO. FEKO is an EM simulation software tool, based on computational electromagnetics (CEM) techniques. The objectives would be to determine the suitability of other EM simulation application for conducting propagation studies in foliage environment as well as to validate the results obtained in CST. Another objective is to also find an application which could simulate foliage propagation at higher frequencies in a more efficient manner than CST.

THIS PAGE INTENTIONALLY LEFT BLANK

APPENDIX A MATLAB CODE

This MATLAB code was used to plot the loss–distance curves for the empirical models, i.e., Tewari's model, the Jansky and Bailey model and the LITU-R model.

```
%Plot Empirical Models of Propagation in Foliage

clear all
close all

%Tewari's model model
%Vertical Polarization
f = [50 200 500 800];
A = [0 0.4989 0.3658 0.2661];
alpha = [0 0.0125 0.0135 0.0140];
B = [1.917 1.8358 0.9040 0.5331];
c = ['b', 'g', 'r', 'm'];
set(gca,'YDir','reverse');

for x=1:4
   for i = 10:200
      Lb(i-9)=-27.57+20*log10(f(x))-20*log10((A(x)*exp(-alpha(x)*i)/i)+(B(x)/(i^2)));
      d(i-9)=i;
   end
   plot(d,Lb,c(x));
   set(gca,'YDir','reverse','FontName','Times New Roman','FontSize',18);
   hold all;
   xlabel('Distance, d (m)','FontName','Times New Roman','FontSize',18)
   ylabel('Loss, L_b (dB)','FontName','Times New Roman','FontSize',18)
end
legend('50 MHz','200 MHz','500 MHz','800 MHz');

clear d;
clear f;

%Jansky and Bailey model
f = [25 50 100 250 400];
A = [0 0 0.615 0.759 1.02];
alpha = [0 0 0.045 0.050 0.055];
B = [0.00212 0.00106 0.000529 0.000443 0.000523];
c = ['b', 'g', 'r', 'm','k'];
set(gca,'YDir','reverse');
figure;
```

```
for x=1:5
   for i = 10:200
      z = i/1609;
      LJ(i-9)= 36.57+20*log10(f(x))-20*log10((A(x)*exp(-
1609*alpha(x)*z)/z)+(B(x)/(z^2)));
      d(i-9)=i;
   end
   plot(d,LJ,c(x));
   set(gca,'YDir','reverse','FontName','Times New Roman','FontSize',18);
   hold all;
   xlabel('Distance, d (m)','FontName','Times New Roman','FontSize',18)
   ylabel('Loss, L_b (dB)','FontName','Times New Roman','FontSize',18)
end
legend('25 MHz','50 MHz','100 MHz','250 MHz','400 MHz');

clear d;
clear f;

%Lateral ITU-R (LITU-R) model
%VHF bands
clear d;
clear f;
f = [30 50 100 300];
T = 5;
R = 5;
c = ['b' 'g' 'r' 'm'];
figure;
for x = 1:4
   for i = 20:200
      Litur(i-19)=40*log10(i)-20*log10(T)-20*log10(R)+0.48*f(x)^0.43*i^0.13;
      d(i-19)=i;
   end
   plot(d,Litur,c(x));
   set(gca,'YDir','reverse','FontName','Times New Roman','FontSize',18);
   hold all;
end
xlabel('Distance, d (m)','FontName','Times New Roman','FontSize',18)
ylabel('Loss, L (dB)','FontName','Times New Roman','FontSize',18)
legend('30 MHz H_t=H_r=5m','50 MHz H_t=H_r=5m','100 MHz H_t=H_r=5m','300
MHz H_t=H_r=5m');

xlim([0 200]);
```

This MATLAB code was used to plot the loss–distance curves for the simulated results in Chapter IV.

```
% Plot Loss versus Seperation Distance Curves
% Using ASCII file of powerflow data (absolute values) exported from CST Studio
% Only for fields projected onto the X-Z plane in CST
% created by Chan Chung Wei, ECE Dept, Naval Postgradute School

clear all
close all

% Import data from Ascii file into Matlab
filename = input('Enter file name: ','s');
file = importdata(filename);
len = length(file.data);

L = input('max x coord of block (len): ');
W = input('max y coord of block (wt): ');
H = input('max z coord of block (ht): ');
L0 = input('x origin of block: ');
W0 = input('y origin of block: ');
H0 = input('z origin of block: ');
x0 = input('dipole centre,x: ');
y0 = input('dipole centre,y: ');
z0 = input('dipole centre,z: ');
zoffset = input('Enter offset of z steps in data file: ');
%offet obtained by looking at z data in ASCII file
% e.g. offset for z = 3.1 is 0.1

% Calculate separation distance and poynting vector at each point (x,y,z)
j = 0;
for i=1:len-L0
   x(i)=single(file.data(i,1));   %import x
   y(i)=single(file.data(i,2));   %import y
   z(i)=single(file.data(i,3));   %import z
   PxRe(i)=single(file.data(i,4));   %import Px Re
   PyRe(i)=single(file.data(i,5));   %import Py Re
   PzRe(i)=single(file.data(i,6));   %import Pz Re
   PxIm(i)=single(file.data(i,7));   %import Px Imag
   PyIm(i)=single(file.data(i,8));   %import Py Imag
   PzIm(i)=single(file.data(i,9));   %import Pz Imag

   if (x(i)<=L && x(i)>=x0) && (y(i)<=W && y(i)>=W0) && (z(i)<=H && z(i)>=H0)
      j = j+1;
```

```
        r(j) = sqrt((x(i)-x0)^2+(y(i)-y0)^2+(z(i)-z0)^2);   %calculate distance
        Px(j) = sqrt(PxRe(i)^2+PxIm(i)^2);
        Py(j) = sqrt(PyRe(i)^2+PyIm(i)^2);
        Pz(j) = sqrt(PzRe(i)^2+PzIm(i)^2);
        Pr(j) = -10*log10(sqrt(Px(j)^2+Py(j)^2+Pz(j)^2)); %calculate magnitude of
Poinyting vector
        %loss(j) = 0-Pr(j);  Transmit Power is 1 W = 0 dBW
        ht(j)=z(i);
    end
end


hl=input('lower height limit to plot: ');
hu=input('upper height limit to plot: ');

for disph=hl:hu
    clear dispr;
    clear dispPr;
    clear index;

    dht = disph+zoffset;

    j = 0;
    for i=1:length(ht)
        if ht(i)==dht
            j=j+1;
            index(j) = i;
        end
    end

    for i=1:j
        dispr(i)=r(index(i));
        dispPr(i)=Pr(index(i));
    end
    semilogx(dispr,dispPr);
    set(gca,'YDir','reverse','FontName','Times New Roman','FontSize',18);
    hold all
end


title('Plot of Loss vs Distance at different Height, Ht');
xlabel('Distance, r (m)')
ylabel('Loss, L (dB)')

%plot Tewari Basic Transmission Loss Model
```

```
f = 50;
A = 0;
alpha = 0;
B = 1.917;
for i = 10:300
   Lb(i-9)=-27.57+20*log10(f)-20*log10((A*exp(-alpha*i)/i)+(B/(i^2)));
   d(i-9)=i;
end
semilogx(d,Lb,'--r');

%Jansky and Bailey Model
clear d;
f = 50;
A = 0;
alpha = 0;
B = 0.00106;

for i = 10:300
   z = i/1609;
   LJ(i-9)= 36.57+20*log10(f)-20*log10((A*exp(-1609*alpha*z)/z)+(B/(z^2)));
   d(i-9)=i;
end
semilogx(d,LJ,'--m');

%lateral ITU-R model
clear d;
f=50;
% plot curve for receiver height from hu to hl
for x = 1:hu-hl+1
   hr = hl-1+x+offset;
   for i = 20:300
      Litur(i-19)=40*log10(i)-20*log10(z0)-20*log10(hr)+0.48*f^0.43*i^0.13;
      d(i-19)=i;
   end
   semilogx(d,Litur,'-.')
end

xlim([20 150]);
%legend('Ht = 20','Ht = 21','Ht = 22','Ht = 23','Ht = 24', 'Ht = 25','Tewari model','Jansky
& Bailey Model','Lateral ITU-R');
```

THIS PAGE INTENTIONALLY LEFT BLANK

LIST OF REFERENCES

[1] Yu Song Meng, Yee Hui Lee and Boon Chong Ng, "Empirical near ground path loss modeling in a forest at VHF and UHF bands," *IEEE Transactions on Antennas and Propagation*, vol. 57, No. 5, pp. 1461–1468, May 2009.

[2] Wikipedia, "Tropical Forest," October 25, 2011, http://en.wikipedia.org/wiki/Tropical_rainforest.

[3] Rhett A. Butler, "Tropical Rainforest, November 1, 2011" http://rainforests.mongabay.com.

[4] David C. Jenn, "Radiowave Propagation," Notes for EC3630, Naval Postgraduate School, 2011.

[5] Curt A. Lewis, Joel T. Johnson and Fernando L. Teixeira, *Radiowave Propagation*, John Wiley & Sons, Hoboken, New Jersey, 2010.

[6] Theodor Tamir, "On radio-wave propagation in forest environments," *IEEE Transactions on Antennas and Propagation*, vol. AP-15, no. 6, pp. 806–817, November 1967.

[7] Mauro S. Assis and Rafael C. Pinto Filho, "Measurements of the electrical characteristics of vegetation in a dense jungle," *Proceedings Fourth European Conference on Antennas and Propagation (EuCAP)*, pp. 1–4, 2010.

[8] R.K.Tewari, S. Swarup and M. N. Roy, "Evaluation of relative permittivity and conductivity of forest slab from experimentally measured data on lateral wave attenuation constant," *International Journal of Electronics*, vol. 61, pp. 597–605, Nov 1996.

[9] R.K.Tewari, S. Swarup and Manujendra N. Roy, "Radio wave propagation through rain forests of India," *IEEE Transactions on Antennas and Propagation*, vol. 38, pp. 433–449, April l990.

[10] Mark A. Weissberger, "An initial critical summary of models for predicting the attenuation of radio waves by trees," Electromagnetic Compatibility Analysis Center, Annapolis, Maryland, Rep. ESD-TR-81-101, July 1982.

[11] CST Studio Suite™, October 26, 2011, http://www.cst.com/Content/Products/CST_S2/Overview.aspx.

[12] FEKO, October 26, 2011, http://www.feko.info/product-detail/overview-of-feko.

THIS PAGE INTENTIONALLY LEFT BLANK

INITIAL DISTRIBUTION LIST

1. Defense Technical Information Center
   Ft. Belvoir, Virginia

2. Dudley Knox Library
   Naval Postgraduate School
   Monterey, California

3. Chairman, Department of Electrical and Computer Engineering
   Naval Postgraduate School
   Monterey, CA

4. Professor David C. Jenn
   Naval Postgraduate School
   Monterey, CA

5. Professor Ric Romero
   Naval Postgraduate School
   Monterey, CA

6. Professor Yeo Tat Soon
   Chairman, Temasek Defense Systems Institute
   National University of Singapore
   Singapore

7. Tan Lai Poh
   Senior Manager, Temasek Defense Systems Institute
   National University of Singapore
   Singapore

8. LCDR Chan Chung Wei
   Republic of Singapore Navy
   Singapore